DEVELOPMENT OF A DESIGN METHOD FOR CENTRIFUGAL COMPRESSORS

By

Kangsoo Im

A DISSERTATION

Submitted to
Michigan State University
in partial fulfillment of the requirements
for the degree of

DOCTOR OF PHILOSOPHY

Mechanical Engineering

2012

ABSTRACT

Development of a Design Method for Centrifugal Compressors

by

Kangsoo Im

This dissertation is the development of a centrifugal compressor design and analysis code that can be used to inexpensively design and analyze the performance of a centrifugal compressor. It can also be used to match the components of centrifugal compressor and to integrate and optimize system performance. The design system is being developed also with the intent to reduce the time taken to experimentally match a centrifugal compressor with the operational environment, a task that is key to process industry application. The design and analysis code will use both one and two-dimensional thermo-fluid equations to analyze the compressor and its components. For each compressor component, the tool calculates the velocities, pressures, temperatures, pressure losses, energy transfer and transformation, and efficiencies for a specified set of compressor geometry, atmospheric conditions, rotational speed, and fluid mass flow rate. The design-tool will be based on and include established loss models found in literature and extensive industrial experimental data. The other main feature of the design-tool will be its ready and easy integration and interaction with other CFD, CAM, and Stress Analysis commercial packages.

ACKNOWLEDGEMENTS

I wish to express my gratitude to my advisor Dr. Abraham Engeda, who has supported and guided me in my study and personal life. I specially thank him for encouragement whenever I was discouraged. Sincere thanks to Professors Craig Somerton, Norbert Mueller, Wei Liao for their advice, discussion, and interest in this work.

I would like to express my sincere appreciation to The Solar Turbines Incorporated. I also want to express my gratitude to Mike Cave for support and advice during internships and other research. In addition I am also thankful to Min Ji and Russ Marechale for experiment data and advice.

Finally, I am very thankful to my lovely wife, Hye-Young, and my family, parents, parents in law, Su-Kyoung, Jung-Min and Yu-Kyoung for support and pray. And I would like to express special thanks to my friend, Hyun-Jin and his family. Most of all, I greatly give thanks to God for all I am. I am Yours.

TABLE OF CONTENTS

LIST OF TABLES

LIST OF FIGURES

Nomenclature

B	Blockage
BL	Blade loading coefficient
b	Blade height [in]
C	Absolute fluid velocity
C_M	Disk torque coefficient
C_P	Pressure recovery coefficient
D_{eq}	Equivalent diffusion factor
d	Diameter
d_H	Hydraulic diameter
DR	Diffusion ratio
H	Head
h	Enthalpy
I	Work input coefficient
K	Blade angle design parameter
L	blade mean streamline meridional length
L_B	Length of blade mean camberline
M	Mach number
m	Meridional distance
$\dot{m}$	Mass flow rate [lb/s]
N	Impeller rotational speed [rpm]
P_v	Velocity pressure

p	pressure
R	Gas constant
Re	Reynolds number
t	Seal fin thickness
Q	Volume flow rate [cfm]
r	Radius [in]
U	Blade speed [ft/s]
v	Fluid velocity [ft/s]
W	Relative fluid velocity [ft/s]
Z	Number of blades dimensionless
α	Absolute velocity angle, measured from radial direction [degrees]
β	Relative velocity angle, measured from tangential direction [degrees]
δ	Incidence angle [degrees]
φ	Inlet flow coefficient dimensionless
φ_2	tip flow coefficient
κ	blade angle with respect to meridional angle
κ_m	streamline curvature
λ	impeller tip distortion factor
ξ	distance along the blade mean camberline
ρ	gas density
η	Isentropic efficiency dimensionless
ψ	Isentropic head coefficient dimensionless
ω	Rotational speed [rad/s]

$\bar{\omega}$ total pressure loss coefficient

Subscripts

1 Impeller inlet

2 Impeller exit

3 Diffuser inlet

4 vaneless diffuser exit

5 diffuser exit

B a blade parameter

C cover parameter

D disk parameter

h Hub

imp Impeller

isen Isentropic

L leakage parameter

LE Blade leading edge

M Meanline

m meridional direction

p primary flow

ps Pressure side

r radial direction

s Shroud, secondary flow

ss Suction side

sta Stage

TE	Blade trailing edge
t	Blade tip, total thermodynamic condition
z	axial direction
θ	theta direction

1. *FUNDAMENTALS OF CENTRIFUGAL COMPRESSOR*

1.1. INTRODUCTION

Flows in the impellers of radial flow centrifugal compressor are among the most complex in turbomachinery. These flows occur in twisted trapezoidal passages. They are often transonic, with shocks in the inducer section that could be accompanied by significant viscous and secondary flow effects with the possibility of regions of separation. The complexities, however, did not deter many researchers in the last fifty years from tackling very important problem areas such as flow visualization using the laser Doppler anemometry and the production of highly sophisticated computerized techniques that can handle the analysis of both a viscous and non-viscous, three-dimensional flow picture.

In spite of the above mentioned advancements, however, the aero-thermodynamic design methodologies for radial flow centrifugal impellers do not appear to have kept pace with these important developments, open literatures dealing with the design methodologies particularly from industrial sources are still very scarce. It can be generally stated, however, that the primary objective of the centrifugal impeller designer is to produce a detailed impeller geometry that operates at a given rotational speed and can handle the design mass flow as efficiently as possible. Effective modeling procedures, however, must also take into account the physical conditions imposed on the working fluid as it passes through the passage such as diffusion levels, relative inlet flow angles, relative outlet flow angles, etc. All of these parameters and their effects on other dependent design parameters should be taken into account in any comprehensive design method.

A single stage centrifugal compressor consists of an impeller (the rotating part), a diffuser (non-rotating), and a volute. Inlet guide vanes are sometimes used in front of the rotor to direct

1. FUNDAMENTALS OF CENTRIFUGAL COMPRESSOR

1.1. INTRODUCTION

Flows in the impellers of radial flow centrifugal compressor are among the most complex in turbomachinery. These flows occur in twisted trapezoidal passages. They are often transonic, with shocks in the inducer section that could be accompanied by significant viscous and secondary flow effects with the possibility of regions of separation. The complexities, however, did not deter many researchers in the last fifty years from tackling very important problem areas such as flow visualization using the laser Doppler anemometry and the production of highly sophisticated computerized techniques that can handle the analysis of both a viscous and non-viscous, three-dimensional flow picture.

In spite of the above mentioned advancements, however, the aero-thermodynamic design methodologies for radial flow centrifugal impellers do not appear to have kept pace with these important developments, open literatures dealing with the design methodologies particularly from industrial sources are still very scarce. It can be generally stated, however, that the primary objective of the centrifugal impeller designer is to produce a detailed impeller geometry that operates at a given rotational speed and can handle the design mass flow as efficiently as possible. Effective modeling procedures, however, must also take into account the physical conditions imposed on the working fluid as it passes through the passage such as diffusion levels, relative inlet flow angles, relative outlet flow angles, etc. All of these parameters and their effects on other dependent design parameters should be taken into account in any comprehensive design method.

A single stage centrifugal compressor consists of an impeller (the rotating part), a diffuser (non-rotating), and a volute. Inlet guide vanes are sometimes used in front of the rotor to direct

the flow to the impeller inducer. The impeller is used to impart energy to the flow by increasing the velocity and pressure of the fluid. The diffuser is used to convert the kinetic energy available at the impeller exit into static pressure by decelerating the fluid. The diffuser is followed by a volute, which collects the fluid from the periphery of the diffuser. Usually an exit cone is connected to the volute exit to delivery the compressed fluid to the pipeline of desired application. The exit cone is essentially a divergent device where the fluid is further diffused. Figure below a typical configuration of a single stage centrifugal compressor.

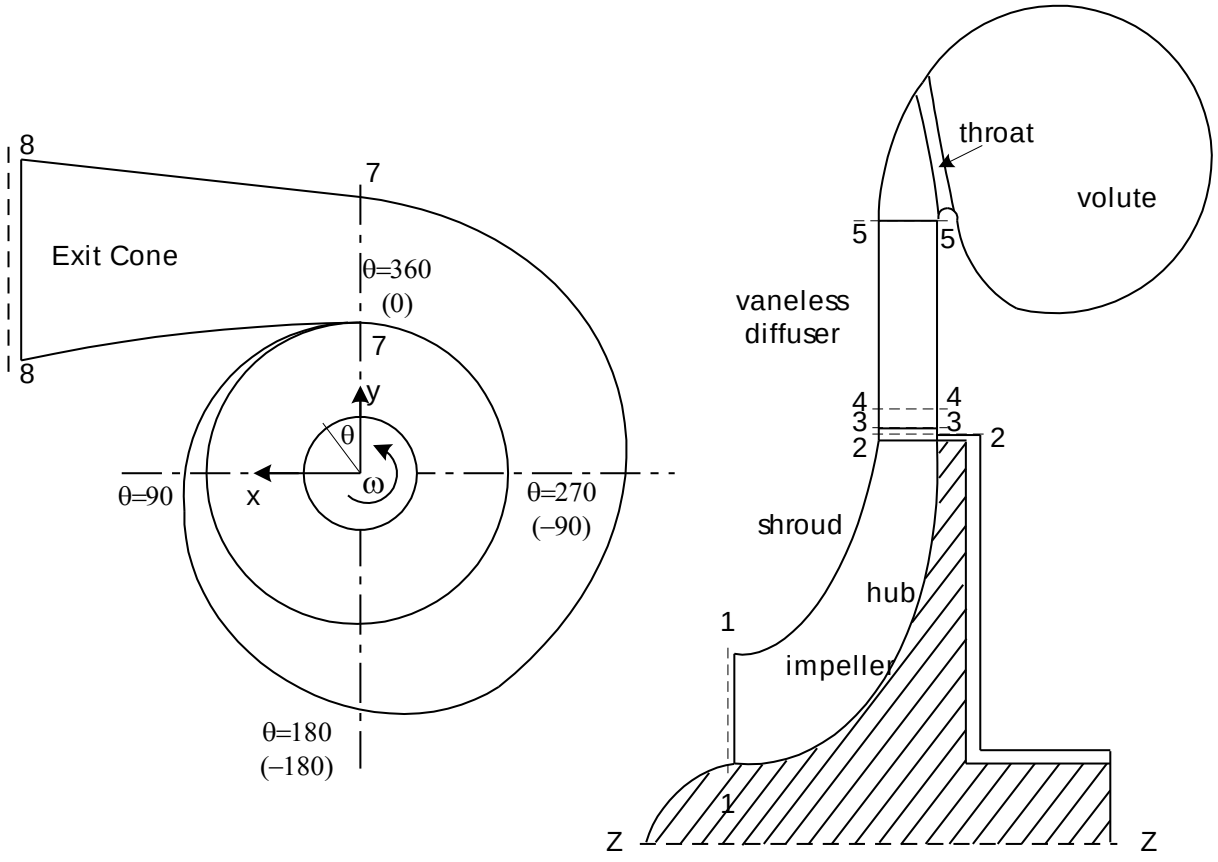

Fig. 1- 1 Configuration of a single stage centrifugal compressor

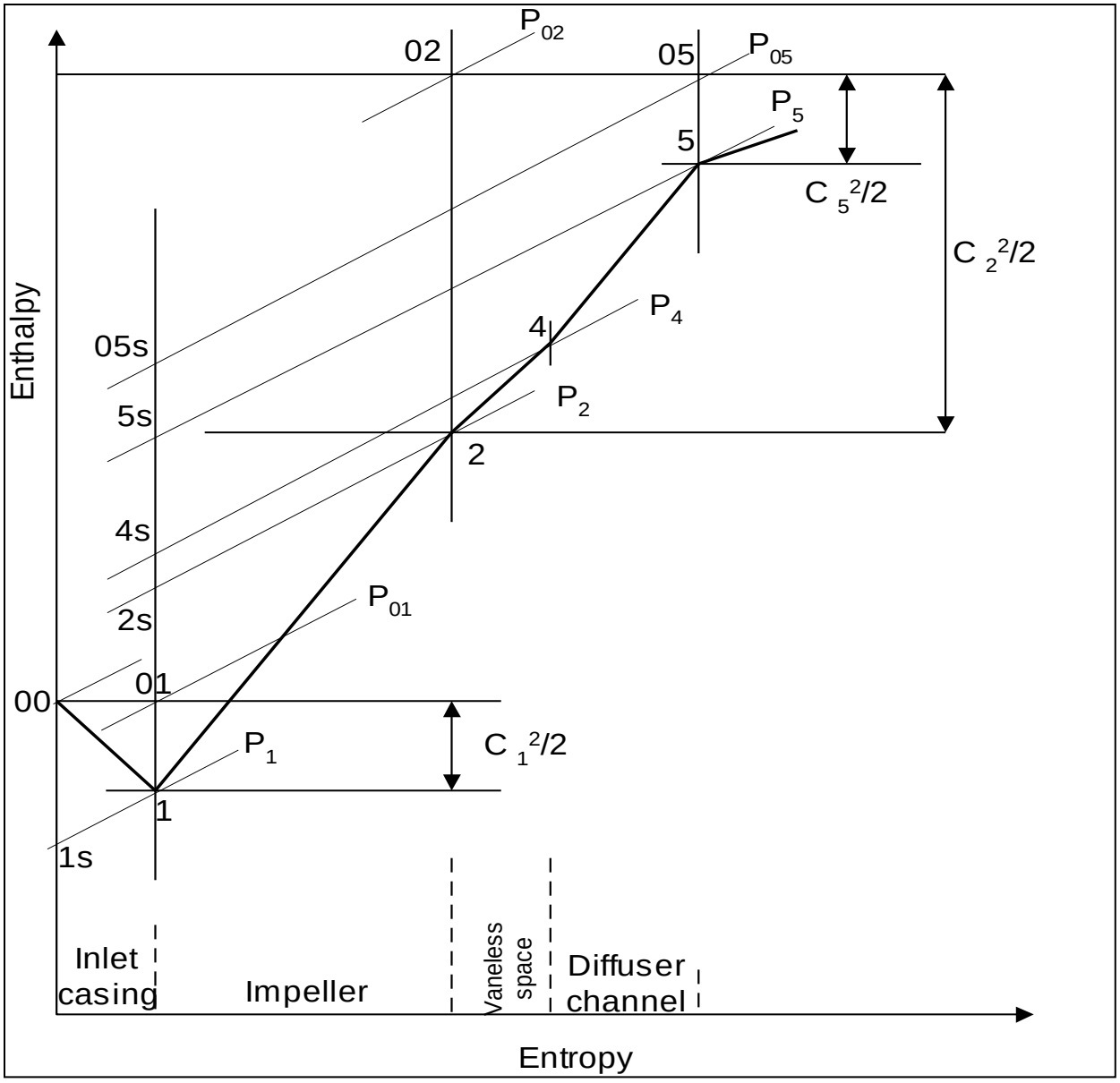

Fig. 1- 2 h-s diagram for the centrifugal compressor stage

1.2. THE IMPELLER

The impeller is the rotating component of the centrifugal compressor stage, where energy transfer of the compressor stage occurs.

$$\Delta h_{0c} = h_{05} - h_{01} = h_{02} - h_{01} \tag{1-1}$$

The specific energy transfer can be derived from the velocity triangle at inlet and outlet from the impeller. The rate of change of angular momentum will equal the sum of the moments of the external forces, TQ. When the angular momentum theorem applied to an impeller, the torque, TQ, is given by

$$TQ = \dot{m}(r_2 C_{u2} - r_1 C_{u1}) \tag{1-2}$$

The energy transfer is given by the product of the angular velocity and the torque, given by the Euler equation

$$\dot{m}\Delta h_{0c} = -\dot{W} = \omega TQ = \dot{m}(U_2 C_{u2} - U_1 C_{u1}) \tag{1-3}$$

Applying the law of trigonometry to the velocity triangles of exit and inlet of the impeller yields

$$U_2 C_{u2} = \tfrac{1}{2}(U_2^2 + C_2^2 - W_2^2) \tag{1-4}$$

$$U_1 C_{u1} = \tfrac{1}{2}(U_1^2 + C_1^2 - W_1^2) \tag{1-5}$$

Combining (1-3), (1-4), and (1-5) results in the enthalpy rise in terms of velocity relations

$$\Delta h_{0c} = \tfrac{1}{2}\left[(U_2^2 - U_1^2) + (W_1^2 - W_2^2) + (C_2^2 - C_1^2)\right] \tag{1-6}$$

The sum of the first and the second terms on the right hand side represents the increase in static pressure; and the kinetic energy increase is shown in the last term. In an axial compressor machine, there is no impeller tip speed variation (U_2=U_1=constant) explaining a higher enthalpy rise in a radial compressor.

If we neglect inlet angular momentum, which is generally acceptable, the theoretical enthalpy reduces to

$$\Delta h_{0c} = \frac{\dot{W}}{\dot{m}} = U_2 C_{u2} \tag{1-7}$$

Then the effect of the impeller exit blade angle, β_{2b} on the theoretical enthalpy rise becomes

$$\frac{\dot{W}}{\dot{m}} = U_2^2 (1 - \frac{C_{r2}}{U_2} \cot \beta_{2b}) \tag{1-8}$$

For a given value of impeller exit blade angle, β_{2b} there is a linear relationship between specific energy transfer and flow rate Theoretical enthalpy of impeller backward-curved blades decreases as the flow rate increases, while that of impeller with the radial blades remains constant The positive-slope condition can be unstable and cause surge. For this reason a backward-curved blade impeller is generally preferred.

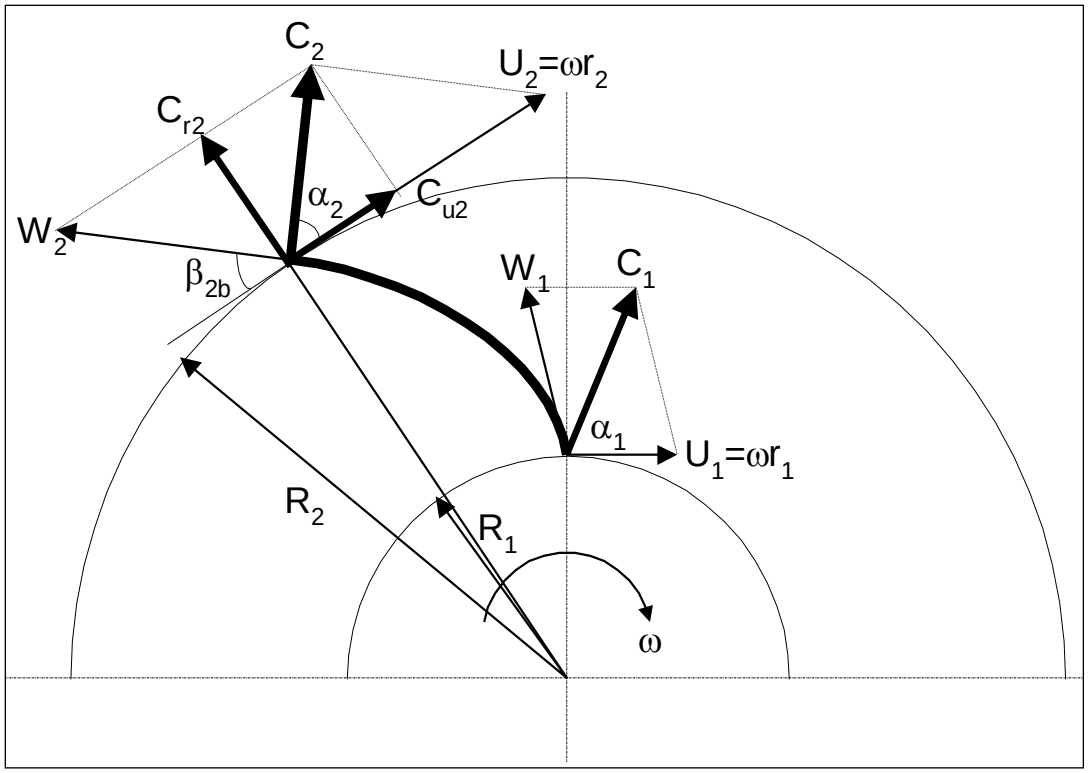

Fig. 1-3 (a) Velocity triangles for an idealized impeller

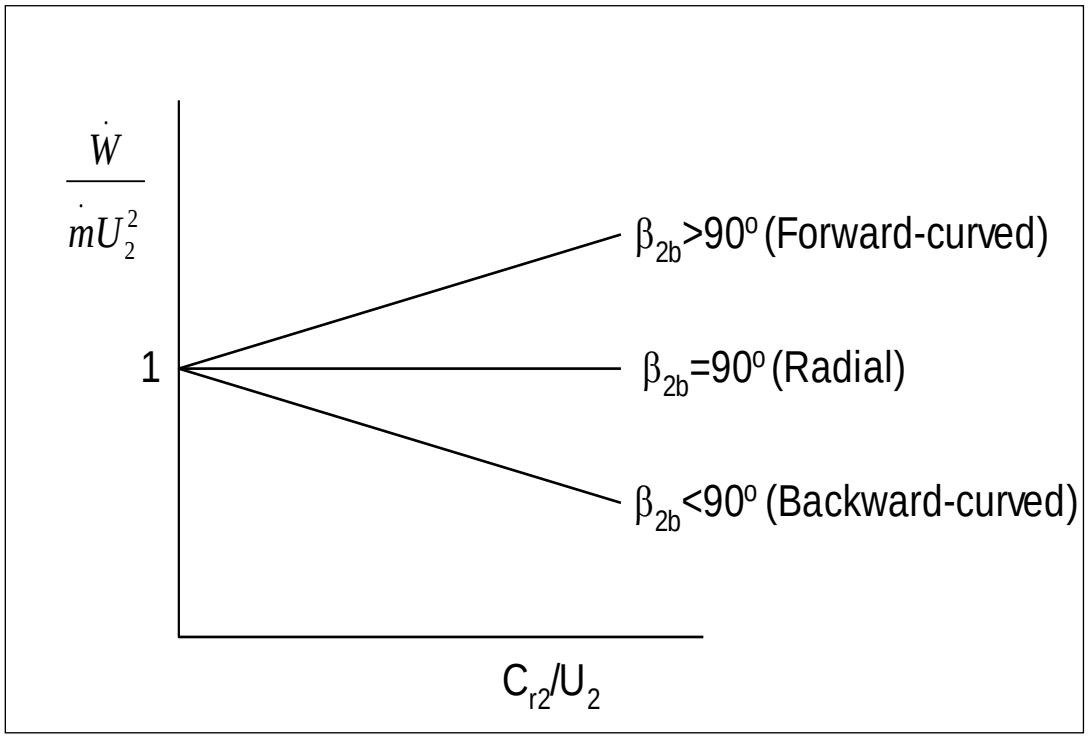

Fig. 1- 3 (b) Effect of the impeller exit blade angle

1.3. THE RADIAL DIFFUSER

Diffusion occurs where velocity reduction occurs. Velocity is a vector quantity having both magnitude and direction. In other words, diffusion can occur on an isolated surface or in a duct.

In centrifugal compressors, energy is transferred to the fluid by the impeller. Even though centrifugal impellers are designed for good diffusion within the blade passage, approximately half of the energy imparted to the fluid remains as kinetic energy at the impeller exit. Therefore, for an efficient centrifugal stage, this kinetic energy must be efficiently converted into the static pressure. Thus, a diffuser, which is stationary and is located downstream of the impeller, is a very important component in a centrifugal compressor.

Since over the years the demands on the centrifugal compressors increased for higher pressure ratios and efficiency, different types of radial diffusers have been developed. These different types of radial diffusers can be classified as the vaneless diffusers, the vaned diffusers, and the low solidity vaned diffusers.

VANELESS DIFFUSERS

Vaneless diffusers consist of two radial walls that may be parallel, diverging, or converging. The flow entering a vaneless diffuser has a large amount of swirl; the swirl angle $[\alpha = \tan^{-1}(C_r / C_u)]$ is typically between 10^o - 30^o. Thus, the tangential component of momentum at low flow rates can be more than twice the radial component. The radial component of the flow diffuses due to the area increase (conservation of mass), and the tangential component diffuses inversely proportional to the radius (conservation of angular momentum). However, the radial component has to surmount the radial pressure gradient for the tangential

component to diffuse continuously. When reverse flow of the radial boundary layer occurs, it is not possible for the tangential component to continue diffusing, as this would imply a pressure increase in one component and not in the other. Therefore, in such cases the breakdown of flow occurs, and this can cause the diffuser to stall and produce other flow instabilities such as surge or stall. However, backflow into the impeller is less frequent with vaneless diffusers than with vaned diffusers where local pressure disturbs caused by vane pressure loading.

The vanelsess diffuser is widely used in automotive turbochargers because of the broad operating range it offers. It is also cheaper to manufacture and more tolerant to erosion and fouling than the vaned diffusers. However, the vaneless diffuser needs a large diameter ratio because of its low diffusion ratio. The flow in a vaneless diffuser follows an approximate logarithmic spiral path. The flow in a vaneless diffuser with a radius ratio of 2 and an inlet flow angle of 6^{o} makes a full revolution before leaving the diffuser. This will result in high friction loss due to viscous drag on the walls and accordingly its pressure recovery is significantly lower than is found with vaned diffusers.

Generally, the vaneless diffuser demonstrates lower pressure recovery by as much as 20% and lower stage efficiency by 10% compared to a vaned diffuser.

VANED DIFFUSERS

The role of the vane in a vaned diffuser is to shorten the flow path by deswirling the flow, allowing a smaller outlet diameter to be used. A vaneless space precedes the vaned diffuser to help reduce flow unsteadiness and Mach number at the leading edge of the vanes so as to avoid shock waves. A boundary layer develops and generates appreciable blockage at the vane leading edge. In order to reduce this blockage, the vaneless space should be minimized until it doesn’t give any unfavorable effects such as increase in noise level or pressure fluctuations due to

interaction of the impeller and diffuser. The flow exiting the impeller follows an approximate logarithmic spiral path to the vane leading edge and is guided by the diffuser channels. The semi-vaneless space follows the vaneless space, ending in a passage throat, which may limit the maximum flow rate in a compressor. The number of diffuser vanes has a direct bearing on the efficiency. With a large number of vanes, the angle of divergence is smaller and the efficiency rises until friction and blockage overcomes the advantage of more gradual diffusion.

Although the vaned diffuser typically exhibits higher pressure recovery, the flow range is limited at a low flow rate due to vane stall. At high flow rates, flow choking at the throat may also limit flow range.

1.4. OBJECTIVE OF THE CURRENT WORKING

The objective of this study is to develop an integrated environment to design and analysis centrifugal compressors. 1D sizing, 1D analysis, and 2D analysis of the centrifugal compressor code, used to design centrifugal compressor, usually work independently. Generally, the design and analysis procedure of centrifugal compressors includes 1D sizing, 1D analysis, determining blade shape, 2D analysis, and 3D CFD. And this procedure is repeated until satisfying the requirement of the customer or finding the optimized geometry. Many aero designers spend their time to making centrifugal impellers since they have many variables dealing with. And they use convenient commercial tools such as COMPAL or CENCOM to make design easy. The programs use different 1d analysis code, Two Zone modeling [1], and Ron Aungier's method [2]. Two Zone modeling is based on the jet and wake model, Dean and Senoo [3], as shown in Fig 1.4, which explains the impeller exit flow velocity profile. The Two Zone model is mostly based on physics equations, although it uses loss models in friction and leakage. The Two Zone model

has high accuracy in the flow characteristics at the impeller exit. However, it requires variables (deviation angle, mass fraction between jet, and wake and pressure recovery coefficients) to calculate properties in impeller flow. And in the other method, Ron Aungier's method, most of the equations explain loss models and he uses empirical correlations for work coefficients. It explains relative pressure loss models that are based on the entropy rise resulting in various loss models. But this method must assume 3D path line for 1D analysis. The deviation angle is only variable for the 1D analysis. Both of the two methods are mostly depend on slip factor commonly. In order to design a high efficiency or maximum performance impeller, there are variables the designer consider, impeller blade exit angle, impeller exit width and impeller exit diameter, etc. And to get an impeller that work properly according to its goal, it is necessary to determine these variables.

To determine 3D shape of an impeller, these 1D analysis and sizing has to be conducted to reduce cost for 3D CFD works, which is taking long time or making prototype. It is efficient to integrate design procedure, which are 1D sizing, 1D analysis, and 2D analysis. Although there are already existing programs, such as COMPAL and CENCOM, house code is good for accessibility to the other users.

For 1D analysis code, this study focuses on Two Zone modeling and Ron Aungier's method, used in COMPAL and CENCOM respectively. And both methods or selectively can be used in 1D analysis code in this study.

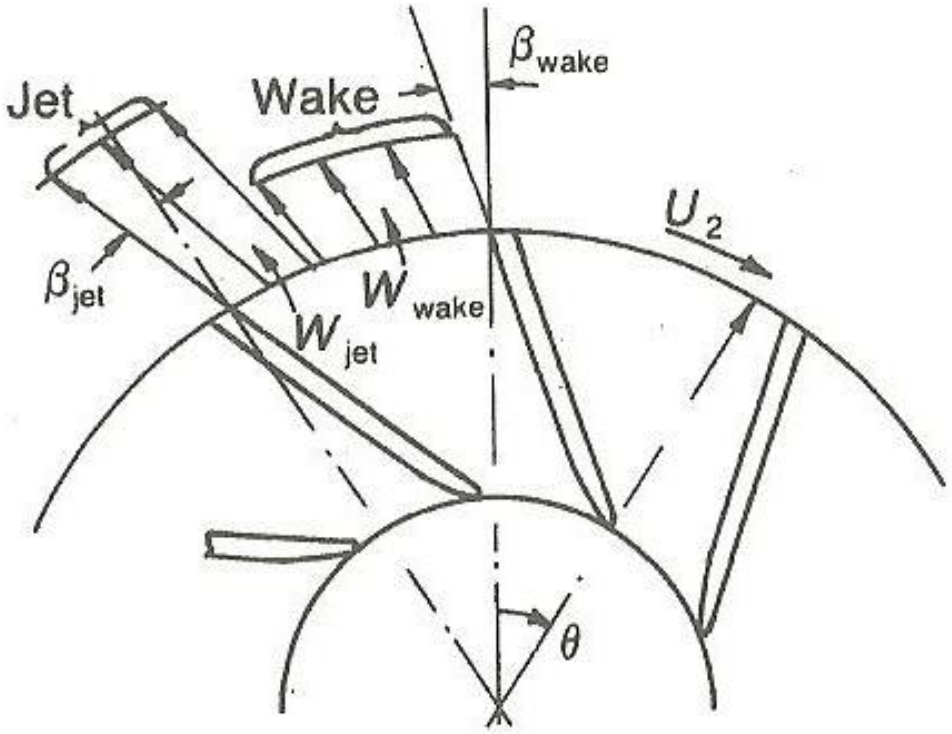

Fig. 1- 4 The idealized jet-wake model (Dean and Senoo) [3]

1.5. THE NEED FOR DESIGN METHOD IN CENTRIFUGAL COMPRESSORS

When designing a centrifugal impeller, 1D analysis gives the approximate 1d sizing results and a chance to reduce the cost for experiments. There are two 1d analysis methods that are well known in the world, Two Zone modeling and Ron Aungier's method. They are verified through many experiments and other's research about them. And they have their own characteristics. There are basically two ways to do 1d analysis on an impeller: flow physics based and empirical based. While the Two Zone model usually depends on flow physics, Ron Aungier's method uses both of them. Most 1D analysis usually depends on empirical formulations because of the complicated impeller 3D shape. Although the Two Zone model uses flow physics using 1D geometry condition, and effectiveness, it makes more accurate analysis

results. This can be explained in Two Elements In Series (TEIS) [1]. The TEIS model can make more accurate performance predictions. It is composed of two elements: blade inlet to throat and throat to blade exit. A first element may be used for the diffuser or nozzle according to high or low flow and the second element is mostly a diffuser in character. According to the inlet portion and the passage portion, the overall diffusion ratio can be made. And it is necessary to assume the effectiveness for accurate performance prediction.

Ron Aungier's 1D analysis method can be said to be more empirical then the Two Zone model. Ron Aungier's method starts with a fundamental thermodynamic relation for entropy. Ron Aungier's method calculates entropy rise in relative total pressure loss in flow within the impeller. It uses various empirical equations about relative pressure loss for normal shock wave, incidence loss at blade inlet, entrance diffusion loss, chocking loss at the impeller throat, blade loading loss, hub to shroud loading loss, skin friction loss, distortion loss for mixing at the impeller exit, clearance gap loss for open impeller and mixing loss at the impeller exit and, supercritical Mach number loss. And it can calculate all thermodynamic conditions at the impeller exit. The loss models used in the Ron Aungier's method are mostly based on relative velocity and geometry conditions. Although this method has high accuracy, some of the loss models cannot be used in the case of approximate blade 3D geometry. In order to use Ron Aungier's model, a blade length and axial length should be assumed.

2. PROCEDURES AND MATHEMATICAL FORMULATIONS USED IN DEVELOPING THE DESIGN METHOD FOR CENTRIFUGAL COMPRESSORS

2.1. TWO ZONE MODELING

The Jet and Wake model, the origin of the Two Zone model, is proposed first by Eckardt [4]. Dean and Senoo[3] explain first that Jet flow is isentropic and wake flow contains all flow losses and very low momentum as shown in Fig 1-4. After that Johnson and Moore[5] show that while jet is almost isentropic, wake has a little mass flow. Japikse develops Two Zone modeling supported by the Jet and Wake model [1]. Two Zone modeling has high accuracy and contains equations about flow physics. Two Zone modeling refer to the Jet flow as a primary isentropic core flow or primary flow and Wake flow as secondary flow. Before introducing Two Zone modeling equations there are basic assumptions in the Two Zone modeling [1].

1. The primary flow is nearly isentropic and deviates from the impeller blade.
2. The secondary flow contains all the impeller losses and is perfectly guided by the impeller blade.
3. The impeller tip static pressure is the same for the primary and secondary zone, which is the unloaded condition.
4. The primary flow and secondary flow do not mix in the impeller passage but mix very rapidly after leaving the impeller exit.
5. The secondary mass flow fraction of the through-flow is in the range of about 0.15 and 0.25.

The following equations are written in ideal gas form for the primary flow.

$$T_{2p} = T_{1t}\left(\frac{p_{2p}}{p_{1t}}\right)^{(\kappa-1)/\kappa} \tag{2-1}$$

$$h_{2p} + W_{2p}^2 \big/ 2 - U_2^2 \big/ 2 = h_T \tag{2-2}$$

$$h_T = h_{00} - U_1 C_{\theta 1t} = c_p T_{1t} + C_{1t}^2 / 2 - U_1 C_{\theta 1t} \tag{2-3}$$

$$U_2 = 2\pi r_2 N \tag{2-4}$$

$$h_{2p} = c_p T_{2p} \tag{2-5}$$

$$C_{m2p} = \sqrt{W_{wp}^2 - \left(U_2 - C_{\theta 2p}\right)^2} \tag{2-6}$$

$$C_{2p} = \sqrt{C_{m2p}^2 + C_{\theta 2p}^2} \tag{2-7}$$

$$T_{02p} = T_{2p} + C_{2p}^2 \big/ 2C_p \tag{2-8}$$

$$p_{02p} = p_{2p}\left(\frac{T_{02p}}{T_{2p}}\right)^{\kappa/(\kappa-1)} \tag{2-9}$$

$$(1-\varepsilon)\rho_{2p} W_{2p} A_{geo} \cos\beta_{2p} = m(1-\chi) \tag{2-10}$$

$$\chi = m_s \big/ m \tag{2-11}$$

$$\varepsilon = A_s / A_{geo} \tag{2-12}$$

$$\rho_{2p} = p_2 \big/ RT_{2p} \tag{2-13}$$

$$A_{geo} = 2\pi r_2 b_2 - Z_b b_2 t_{2b} \big/ \cos\beta_{2b} \tag{2-14}$$

$$\beta_{2p} = \beta_{2b} + \delta_{2p} \tag{2-15}$$

$$C_{\theta 2p} = U_2 + C_{m2p} \tan \beta_{2p} \tag{2-16}$$

Or: $$\beta_{2p} = -\tan^{-1}\left[\left(U_2 - C_{\theta 2p}\right)/C_{m2p}\right] \tag{2-17}$$

The secondary zone or wake flow equations are following:

$$p_{2p} = p_{2s} = p_2 \tag{2-18}$$

$$\rho_{2s} R T_{2s} = p_2 \tag{2-19}$$

$$C_{m2s} = \left[m/2\pi r_2 b_2 - \rho_2 C_{m2p}\left(1-\varepsilon\right)\right]/\rho_{2s}\varepsilon \tag{2-20}$$

$$W_{2s} = C_{m2s}/\cos\beta_{2s} \tag{2-21}$$

$$\beta_{2s} = \beta_{2b} + \delta_{2s} \tag{2-22}$$

$$C_{\theta 2s} = U_2 + C_{m2s} \tan \beta_{2s} \tag{2-23}$$

$$C_{2s} = \sqrt{C^s_{m2s} + C^2_{\theta 2s}} \tag{2-24}$$

$$h_{T2s} = h_T + W_{front\ \text{cover}} \tag{2-25}$$

$$h_{2s} = h_{T2s} - \left(W^2_{2s}/2\right) + \left(U^2_2/2\right) \tag{2-26}$$

$$h_{2s} = c_p T_{2s} \tag{2-27}$$

$$T_{02s} = T_{2s} + C^2_{2s}/2c_p \tag{2-28}$$

$$p_{02s} = p_{2s}\left(\frac{T_{02s}}{T_{2s}}\right)^{\kappa/(\kappa-1)} \tag{2-29}$$

Mixed out conditions are derived by following equations.

From radial momentum equation

$$m_p C_{m2p} + m_s C_{m2s} = m C_{m2m} + (p_{2m} - p_2) 2\pi r_2 b_2 \tag{2-30}$$

From tangential momentum equation

$$m_p C_{\theta 2p} + m_s C_{\theta 2s} = m C_{\theta 2m} \tag{2-31}$$

From energy equation

$$m_p c_p T_{02p} + m_s c_p T_{20s} + (P_{disk\ \text{friction}} + P_{recirc}) = m c_p T_{02m} \tag{2-32}$$

And continuity equation becomes

$$\dot{m} = 2\pi r_2 b_2 C_{m2m} \rho_{2m} \tag{2-33}$$

$$T_{2m} = T_{02m} - C_{2m}^2 \big/ 2c_p \tag{2-34}$$

$$\rho_{2m} = p_{2m} / RT_{2m} \tag{2-35}$$

$$C_{2m}^2 = C_{\theta 2m}^2 + C_{m2m}^2 \tag{2-36}$$

$$M_{2m} = C_{2m} \big/ \sqrt{\kappa R T_{2m}} \tag{2-37}$$

$$p_{02m} = p_{2m} \left(\frac{T_{02m}}{T_{2m}} \right)^{\kappa/(\kappa - 1)} \tag{2-38}$$

$$\lambda_{2m} = C_{\theta 2m} / C_{m2m} \tag{2-39}$$

$$\sigma_{2m} = \mu_{2m} (\lambda_{2m} - \tan \beta_{2b}) / \lambda_{2m} \tag{2-40}$$

$$\mu_{2m} = C_{\theta 2m} / U_2 \tag{2-41}$$

2.1.1. TEIS MODEL

In order to predict the relative velocity at the impeller exit, there is some convenient parameter, such as the relative Mach number ratio for the primary flow. This ratio means the ratio of relative Mach number the inlet to exit of the impeller ($M_{1t,rel}/M_{2p,rel}$). It is a good parameter to get the relative velocity at the impeller exit. With sufficient kinetic energy within the impeller, efficiency drop can always be found. Therefore, it is necessary to focus on diffusing the impeller primary flow (core flow).

The TEIS model starts with considering the impeller passage as a rotating diffuser [1]. And the impeller inlet part, element “a”, can be considered a diffuser or nozzle according to its flow rate as shown in Fig 2-1. The part of the impeller throat to exit, element “b”, is diffuser in character. The second element is a constant geometry element regardless of flow rate since throat and exit area does not change. The variables in TEIS model are defined as the following.

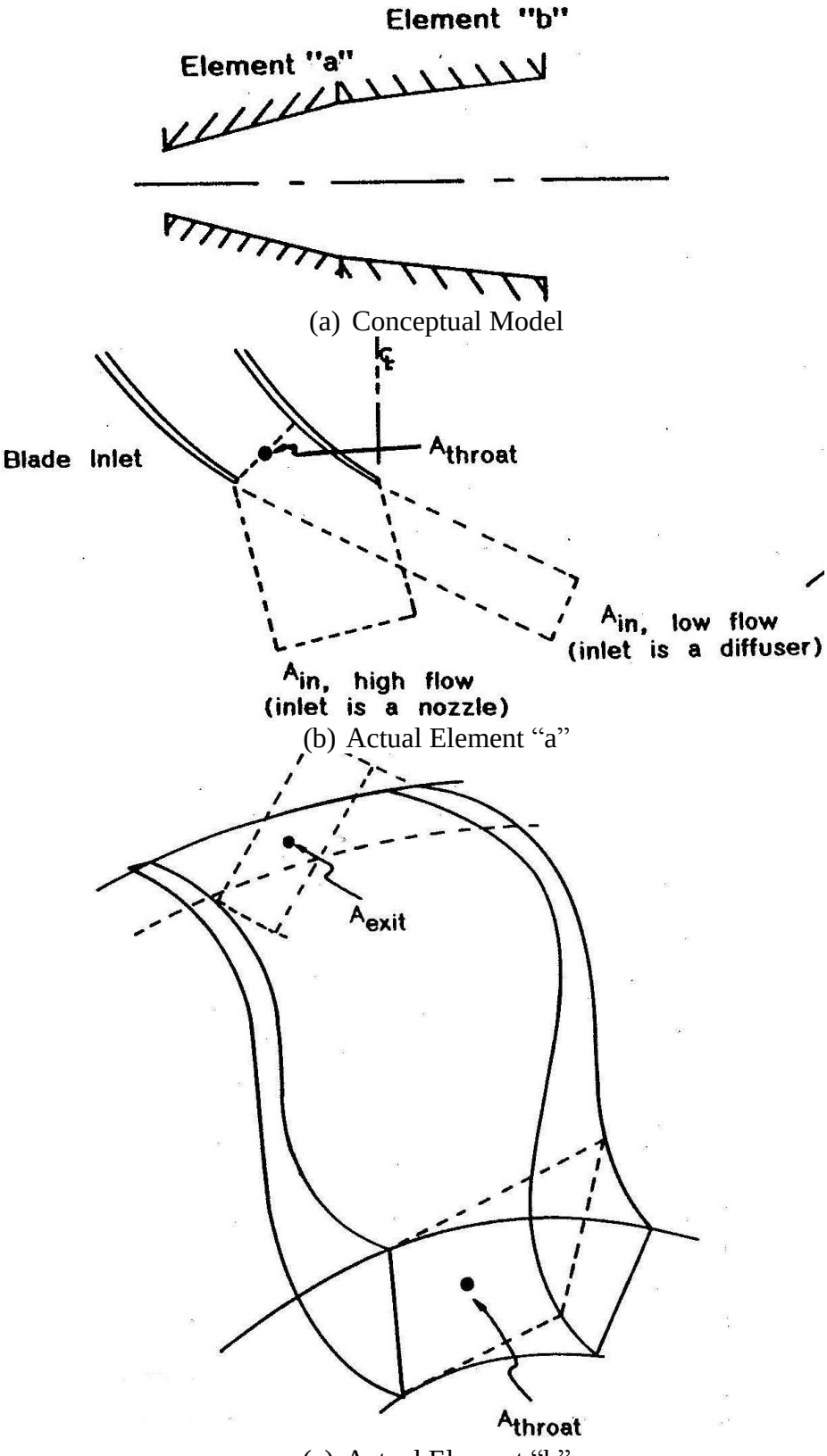

Fig.2- 1 TEIS conceptual model [1]

Pressure recovery coefficient:

$$C_p = \frac{\Delta p}{q} \tag{2-42}$$

Effectiveness: η

Inlet portion:

$$\eta_a = \frac{C_{pa}}{C_{pa,i}} \tag{2-43}$$

$$C_{pa,i} = 1 - \frac{1}{AR_a^2} = 1 - \left(\frac{\cos \beta_1}{\cos \beta_{1b}} \right)^2 \tag{2-44}$$

Passage portion:

$$\eta_b = \frac{C_{pb}}{C_{pb,i}} \tag{2-45}$$

$$C_{pbi,i} = 1 - \frac{1}{AR_b^2} = 1 - \left(\frac{A_{throat}}{A_2} \right)^2 \tag{2-46}$$

Overall:

$$DR_2 = W_{1t} / W_{2p} \tag{2-47}$$

$$DR_2^2 = \frac{1}{1 - \eta_a C_{pa,i}} \frac{1}{1 - \eta_b C_{pb,i}} \tag{2-48}$$

The constants η_a, η_b can determine the diffusion ratio. Table 2-1 shows that suggested values for primitive TEIS model.

Table 2- 1 Suggested values for primitive TEIS model. (Japikse Centrifugal Compressor Design and performance) [1]

Case	η_a	η_b	DR_{stall}	$Re = \frac{U_2 D_2}{\nu_{00}}$	χ
Large ,well-designed rotors	0.9 to 1.1	0.4 to 0.6	1.5 to 1.8	$\geq 1.2\times10^6$	0.1 to 0.2
(>10" to 12"D, or smaller if well-designed)					
Medium size, well designed	0.8 to 0.9	0.3 to 0.5	1.3 to 1.6	$\geq 0.5\times10^6$	0.15 to 0.25
(0.4" to 10"D)					
Medium size, ordinary design	0.6 to 0.8	0.0 to 0.4	1.2 to1.5	$\geq 0.5\times10^6$	0.20 to 0.30
(0.4" to 10"D)					
Small or poorly designed	0.4 to 0.6	-0.3 to +0.3	1.1 to 1.4	$\geq 0.5\times10^6$	0.25 to 0.35
(<4"D)					

This study uses either a relative Mach number ratio or the TEIS model to determine the diffusion ratio of the impeller.

2.2. EMPIRICAL BASED METHOD

The empirical-based method for the 1D analysis method used in this study is Ron Aungier's method. The model consists of work-input parameters and relative pressure loss models. The work input parameters are used for calculating head increase within the impeller and between the impeller exit and diffuser inlet. The relative pressure loss models are used to estimate pressure drop within the impeller using the thermodynamic law for entropy.

2.2.1. IMPELLER WORK INPUT

BLADE WORK INPUT

Ron Aungier defines various work input parameters for impeller, blade parameter, disk friction parameter, leakage parameter, and recirculation parameter [2].

$$I = \Delta h_t \Big/ U_2^2 = I_B + I_{DF} + I_L + I_R \tag{2-49}$$

The blade work input coefficient can be determined from the Euler equation.

$$I_B = C_{\theta 2} \Big/ U_2 - U_1 C_{\theta 1} \Big/ U_2^2 \tag{2-50}$$

For the ideal case no slip at the impeller exit

$$C_{\theta 2,i} \Big/ U_2 = 1 - \lambda \dot{m} \cot \beta_2 \Big/ \left(\rho_2 A_2 U_2 \right) = 1 - \lambda \phi_2 \cot \beta_2 \tag{2-51}$$

where, the tip distortion factor $\lambda = 1 \Big/ \left(1 - B_2\right)$ (2-52)

Therefore, the blade work input coefficient can be derived in terms of slip factor

$$I_B = \sigma - \lambda \phi_2 \cot \beta_{2b} - U_1 C_{\theta 1} \Big/ U_2^2 \tag{2-53}$$

Where, slip factor (U.S) $\sigma = 1 - \dfrac{C_{slip}}{U_2}$ (2-54)

Ron Aungier derives the empirical top blockage equation, impeller distortion factor [2]

$$B_2 = \bar{\omega}_{sf} \frac{p'_{v1}}{p'_{v2}} \sqrt{\frac{W_1}{W_2}\frac{d_H}{b_2}} + \left[0.3\frac{b_2^2}{L_B^2}\right]\frac{A_R^2 \rho_2 b_2}{\rho_1 L_B} + \frac{\delta_{CL}}{2b_2} \tag{2-55}$$

where p_υ = velocity pressure (p_t-p) and area ratio defined by

$$A_R = A_2 \sin\beta_{2b} / \left(A_1 \sin\beta_{th}\right) \tag{2-56}$$

DISK FRICTION PARAMETER

To get the disk friction work parameter, the clearance gap leakage flow has to be determined. Ron Aungier derives empirical relations from the empirical relations [6] using the forced vortex flow model.

$$\frac{\partial p}{\partial r} = K^2 \omega^2 \rho r \tag{2-57}$$

$$\text{Where } K = C_\theta / \omega r \tag{2-58}$$

$$K_0 = 0.46 \Big/ \left(1 + \frac{2s}{d}\right) \tag{2-59}$$

$$K = K_0 + C_q (1.75 K_F - 0.316) r_2 / s \tag{2-60}$$

$$C_q = \frac{m_L \left(\rho r_2 U_2 / \mu\right)^{1/5}}{2\pi\rho r_2^2 U_2} \tag{2-61}$$

For seal leakage from the impeller tip $K_F = C_{\theta 2}/U_2$, but toward the tip, $K_F = 0$.

For an open impeller, the clearance gap leakage flow velocity is given by

$$U_{CL} = 0.816\sqrt{2\Delta p_{CL}/\rho_2} \tag{2-62}$$

The average pressure difference across the gap can be expressed by

$$\Delta p_{CL} = \frac{\dot{m}\left(r_2 C_{\theta 2} - r_1 C_{\theta 1}\right)}{z\bar{r}\bar{b}L} \tag{2-63}$$

$$\bar{r} = (r_1 + r_2)/2 \tag{2-64}$$

$$\bar{b} = (b_1 + b_2)/2 \tag{2-65}$$

Consequently, the blade gap leakage flow is given by

$$\dot{m}_{CL} = \rho_2 z s L U_{CL} \tag{2-66}$$

Ron Aungier brings in windage and disk friction losses from Daily and Nece's correlation [7, 8]. The disk torque coefficient is defined by

$$C_M = \frac{2\tau}{\rho\omega^2 r^5} \tag{2-67}$$

And in order to determine the disk torque coefficient, it is necessary to consider four different flow conditions.

1. Laminar, merged boundary layers

$$C_{M1} = \frac{2\pi}{(s/r)\,\mathrm{Re}} \tag{2-68}$$

2. Laminar, separate boundary layers

$$C_{M2} = \frac{3.7(s/r)^{0.1}}{\sqrt{\mathrm{Re}}} \tag{2-69}$$

3. Turbulent, merged boundary layers

$$C_{M3} = \frac{0.08}{(s/r)^{1/6}\,\mathrm{Re}^{1/4}} \tag{2-70}$$

4. Turbulent, separate boundary layers

$$C_{M4} = \frac{0.102(s/r)^{0.1}}{\mathrm{Re}^{0.2}} \tag{2-71}$$

where Reynolds number is

$$\mathrm{Re} = \frac{\rho \omega r^2}{\mu} \tag{2-72}$$

The torque coefficient can be taken to be the largest one among the four different values from the above equations.

And the fully rough disk torque is given by

$$\frac{1}{\sqrt{C_{Mr}}} = 3.8 \log_{10}\left(r/e\right) - 2.4\left(s/r\right)^{0.25} \tag{2-73}$$

And for the smooth wall

$$\mathrm{Re}_s \sqrt{C_{Ms}} = 1100\left(e/r\right)^{-0.4} \tag{2-74}$$

Ron Aungier suggests the Reynolds number for the fully rough disk instead of the correlations of Daily and Nece [7].

$$\mathrm{Re}_r = 1100\, r/e - 6 \cdot 10^6 \tag{2-75}$$

$$C_{M0} = C_{Ms} + \left(C_{Mr} - C_{Ms}\right)\left[\log\left(\mathrm{Re}/\mathrm{Re}_s\right)/\log\left(\mathrm{Re}_r/\mathrm{Re}_s\right)\right] \tag{2-76}$$

Aungier develops the following torque coefficient using the above equation from Daily and Nece.

$$C_M = C_{M0}\left(1-K\right)^2 \Big/ \left(1-K_0\right)^2 \tag{2-76}$$

For the disk

$$C_{MD} = 0.75 C_M \tag{2-77}$$

For the cover

$$C_{MC} = 0.75 L C_M \left[1-\left(d_{1s}/d_2\right)^5\right] \Big/ \left(r_2 - r_1\right) \tag{2-78}$$

Therefore, the disk friction work parameter is given by

$$I_{DF} = \left(C_{MD} + C_{MC}\right)\rho_2 U_2 r_2^2 \Big/ 2\dot{m} \tag{2-79}$$

LEAKAGE FLOW PARAMTER

Ron Aungier provides seal leakage mass flow from Egli's formulation[9].

$$\dot{m}_L = \pi d \delta C_t C_c C_r \rho \sqrt{RT} \tag{2-80}$$

$$C_r = 1 - \frac{1}{3 + \left[\dfrac{54.3}{1 + 100\delta / t}\right]^{3.45}} \tag{2-81}$$

$$C_t = \frac{2.143\left[\ln N - 1.464\right]}{N - 4.322}\left(1 - p_R\right)^{0.375} p_R \tag{2-82}$$

$$C_c = 1 + X_1\left[\delta / p - X_2 \ln(1 + \delta / p)\right] \Big/ \left(1 - X_2\right) \tag{2-83}$$

$$\delta / p \le X_2 - 1$$

$$X_1 = 15.1 - 0.05255 e^{\left[0.507\left(12 - N\right)\right]}\ ; \qquad \text{N}\le 12 \tag{2-84}$$

$$X_1 = 13.15 + 0.1625N\ ; \qquad \text{N}>12 \tag{2-85}$$

$$X_2 = 1.058 + 0.0218N\ ; \qquad \text{N}\le 12 \tag{2-86}$$

$$X_2 = 1.32\ ; \qquad \text{N}>12 \tag{2-87}$$

Therefore, the leakage flow work parameter is given by

$$I_L = \dot{m}_L I_B / \dot{m} \tag{2-88}$$

RECIRCULATION WORK

Lieblein suggests a diffusion factor, D_{eq}, for radial and mixed flow blades [10].

$$W_{\max} = \left(W_1 + W_2 + \Delta W\right)/2 \tag{2-89}$$

$$D_{eq} = W_{\max} / W_2 \tag{2-90}$$

The average blade velocity difference, ΔW, can be calculated using irrotational flow relations.

$$\Delta W = 2\pi d_2 U_2 I_B / z L_B \tag{2-91}$$

$$I_R = \left(D_{eq}/2 - 1\right)\left[W_{\theta 2}/C_{m2} - 2\cot\beta_{2b}\right] \tag{2-92}$$

$$I_R \geq 0$$

2.2.2. RELATIVE PRESSURE LOSSES WITHIN IMPELLER

Ron Aungier suggests various loss mechanisms that result in a relative pressure drop within the impeller [2]. From the fundamental thermodynamic relation, entropy rise equation, he shows a total relative pressure equation at the impeller exit.

$$p'_{t2} = p'_{t2,i} - f_c(p'_{t1} - p_1)\sum_i \bar{\omega}_i \tag{2-93}$$

And Ron Aungier uses a correction factor.

$$f_c = \left(\rho'_{t2} T'_{t2}\right)/\left(\rho'_{t1} T'_{t1}\right) \tag{2-94}$$

Total relative pressure loss models suggested by Aungier are the following:

1. Incidence loss due to the difference between the inlet blade angle and flow angle.

$$C_{mh1} = C_{m1}\left[1 + \kappa_{m1} b_1/2\right] \tag{2-95}$$

$$C_{ms1} = C_{m1}\left[1 - \kappa_{m1} b_1/2\right] \tag{2-96}$$

$$\bar{\omega}_{inc} = 0.8\left[1 - C_{m1}/\left(W_1 \sin\beta_1\right)\right]^2 + \left[z_{FB} t_{b1}/\left(2\pi r_1 \sin\beta_1\right)\right]^2 \tag{2-97}$$

Total incidence loss can be calculated by weighted average 10 times as heavy as the hub and shroud values.

2. Entrance diffusion loss due to the diffusion inlet to throat.

$$\bar{\omega}_{DIF} = 0.8\left[1 - W_{th}/W_1\right]^2 - \bar{\omega}_{inc} \tag{2-98}$$

$$\bar{\omega}_{DIF} \geq 0$$

Inducer stall criterion is

$$W_{1s}/W_{th} \geq 1.75 \tag{2-99}$$

When occurring inducer stall

$$\bar{\omega}_{DIF} \geq \left[\left(W_{1s} - 1.75W_{th}\right)/W_1\right] - \bar{\omega}_{inc} \tag{2-100}$$

3. Chocking loss due to the relative Mach number at the throat.

Contraction ratio is used to evaluate aerodynamic blockage.

$$C_r = \sqrt{A_1 \sin\beta_1 / A_{th}} \tag{2-101}$$

$$C_r \leq 1 - \left(A_1 \sin\beta_1 / A_{th} - 1\right)^2 \tag{2-102}$$

$$X = 11 - 10C_r A_{th} \Big/ A^* \tag{2-103}$$

$$\bar{\omega}_{CH} = 0; \qquad X \leq 0 \tag{2-104}$$

$$\bar{\omega}_{CH} = \frac{1}{2}\left(0.05X + X^7\right); \qquad X > 0 \tag{2-105}$$

4. Skin friction loss due to wall skin friction

Reynolds number based on pipe diameter;

$$\mathrm{Re}_d = \rho V d / \mu \tag{2-106}$$

For Re_d<2,000 and laminar flow, Skin friction coefficient is

$$C_{fl} = 16/\mathrm{Re}_d \tag{2-107}$$

For Re_d>2,000, turbulent flow and smooth wall

$$\frac{1}{\sqrt{4C_{fts}}} = -2\log_{10}\left[\frac{2.51}{\mathrm{Re}_d\sqrt{4C_{fts}}}\right] \tag{2-108}$$

and for turbulent flow but fully rough surface

$$\frac{1}{\sqrt{4C_{ftr}}} = -2\log_{10}\left[\frac{e}{3.71d}\right] \tag{2-109}$$

The surface roughness has to be considered when

$$\mathrm{Re}_e = \left(\mathrm{Re}_e - 2000\right)e/d > 60 \tag{2-110}$$

When $\mathrm{Re}_d > 4000$ turbulent skin friction coefficient becomes

$$C_{ft} = C_{fts}\ ; \qquad \mathrm{Re_e}<60 \tag{2-111}$$

$$C_{ft} = C_{fts} + \left(C_{ftr} - C_{fts}\right)\left(1 - 60/\mathrm{Re}_e\right)\ ; \quad \mathrm{Re_e}\geq 60 \tag{2-112}$$

When $2000 \leq \mathrm{Re}_d \leq 4000$, the skin friction coefficient is given by

$$C_f = C_{fl} + \left(C_{ft} - C_{fl}\right)\left(\mathrm{Re}_d/2000 - 1\right) \tag{2-113}$$

5. Blade loading loss due to the pressure difference between blade to blade.

$$\bar{\omega}_{BL} = \left(\Delta W/W_1\right)^2/24 \tag{2-114}$$

6. Hub to shroud loading loss is given by

$$\bar{\omega}_{HS} = \left(\bar{\kappa}_m\bar{b}\bar{W}/W_1\right)^2/6 \tag{2-115}$$

$$\bar{\kappa}_m = \left(\alpha_{c2} - \alpha_{c1}\right)/L \tag{2-116}$$

$$\bar{b} = \left(b_1 + b_2\right)/2 \tag{2-117}$$

$$\bar{W} = \left(W_1 + W_2\right)/2 \tag{2-118}$$

7. Abrupt expansion loss due to the distorted flow mixing with the free stream flow

$$\bar{\omega}_{\lambda} = \left[(\lambda - 1) C_{m2} / W_1 \right]^2 \tag{2-119}$$

8. Wake mixing loss due to mixing with jet flow right after impeller exit.

   Separation velocity is given by

$$W_{SEP} = W_2 \; ; \qquad D_{eq} \leq 2 \tag{2-120}$$

$$W_{SEP} = W_2 \, D_{eq} / 2 \; ; \; D_{eq} > 2 \tag{2-121}$$

$$C_{m,wake} = \sqrt{W_{SEP}^2 - W_{\theta}^2} \tag{2-122}$$

$$C_{m,mix} = C_{m2} \, A_2 / (\pi d_2 b_2) \tag{2-123}$$

$$\bar{\omega}_{mix} = \left[\left(C_{m,wake} - C_{m,mix} \right) / W_1 \right]^2 \tag{2-124}$$

9. Blade clearance loss due to clearance gap flow.

$$\bar{\omega}_{CL} = 2 \dot{m}_{CL} \Delta p_{CL} \Big/ \left(\dot{m} \rho_1 W_1^2 \right) \tag{2-125}$$

10. Super critical Mach number loss due to shock wave loss.

$$M'_{cr} = M_1 W^* / W_{\max} \tag{2-126}$$

$$\bar{\omega}_{cr} = 0.4 \left[(M'_1 - M'_{cr}) W_{\max} / W_1 \right]^2 \tag{2-127}$$

   After a summation of all losses, relative pressure loss can be calculated. Since all ideal conditions are known, all thermodynamic conditions at the impeller exit can be computed using isentropic equations, the equation of state, and conservation of rothalpy.

2.2.3. VANELESS DIFFUSER ANALYSIS

This study uses only Ron Aungier's method to calculate the vaneless diffuser flow because this method is well known for good prediction of the vaneless diffuser flow.

Aungier developed governing equations for 1-dimensional flow analysis from Johnston and Dean's equation[11] in vaneless diffuser.

$$2\pi r \rho b C_m (1-B) = \dot{m} \tag{2-128}$$

$$bC_m \frac{d(rC_\theta)}{dm} = -rCC_\theta c_f \tag{2-129}$$

$$\frac{1}{\rho}\frac{dp}{dm} = \frac{C_\theta^2 \sin\alpha_c}{r} - C_m \frac{dC_m}{dm} - \frac{CC_m c_f}{b} - \frac{dI_D}{dm} - I_c \tag{2-130}$$

$$h_t = h + \frac{1}{2}C^2 \tag{2-131}$$

The divergence parameter is given by

$$D = -\frac{b}{c}\frac{dC}{dm} \tag{2-132}$$

$$D_m = 0.4(b_1/L)^{0.35} \sin\alpha_c \tag{2-133}$$

Empirical diffusion efficiency is the following:

$$E = 1\ ; \qquad D \le 0 \tag{2-134}$$

$$E = 1 - 0.2(D/D_m)^2\ ; \qquad 0 < D < D_m \tag{2-135}$$

$$E = 0.8\sqrt{D_m/D}\ ; \qquad D \ge D_m \tag{2-136}$$

The diffusion term is given by

$$\frac{dI_D}{dm} = -2(p_t - p)(1-E)\frac{1}{\rho C}\frac{dC}{dm} \tag{2-137}$$

Local maximum area is

$$(rb)_m = (rb)_1 [1 + 0.16m/b_1] \tag{2-138}$$

If $(rb) > (rb)_m$,

$$I_D = 0.65(p_t - p)\left[1 - (rb)_m/(rb)\right]/\rho \tag{2-139}$$

And curvature loss term is obtained by

$$I_C = \kappa_m (p_t - p) C_m/(13\rho c) \tag{2-140}$$

Blockage in the vaneless diffuser is given by

$$B = 2\delta/(8b) \tag{2-141}$$

If the boundary layer at the diffuser inlet is known, $C_{\theta e}$ can be calculated from following equation.

$$rC_\theta = rC_{\theta e}\left[1 - 2\delta/(4.5b)\right] \tag{2-142}$$

And $C_{\theta e}$ must be conserved until the boundary layer fills the passage, i.e. $2\delta = b$.

If the boundary layer at the diffuser inlet is not given, the inlet boundary layer can be calculated from

$$2\delta/b = 1 - (b/r)_{in}^{0.15} \tag{2-143}$$

3. 1D ANALYSIS CODE VALIDATION WITH TESTED IMPELLER DATA

Two tested impellers are used to validate two 1D analysis codes, table 3-1 shows information of the two tested impellers. Impeller #1 and impeller #2 are tested in Solar Turbines, Inc. The design rotational speed is 19240 rpm and design flow coefficients of the impeller #1 and #2 are 0.026 and 0.045 respectively. And their exit angles are 60 and 40 degree respectively. Fig.3-1 shows meridional shape of the impellers.

Impeller #	Design speed, N	Φ	b_2/d_2	β_2
1	19240	0.026	0.036	60
2	19240	0.54	0.044	40

Table 3- 1 Tested Impeller information

The tests are performed along the three different rotational speeds of 13k, 19k, 21k rpm. Impeller #1 and #2 are tested at 544R and 90 psi, 544R and 44psi respectively. And both impellers have vaneless diffuser with pinch. All tested results, work factor, head coefficient and absolute flow angles are taken at the exit of vaneless diffuser.

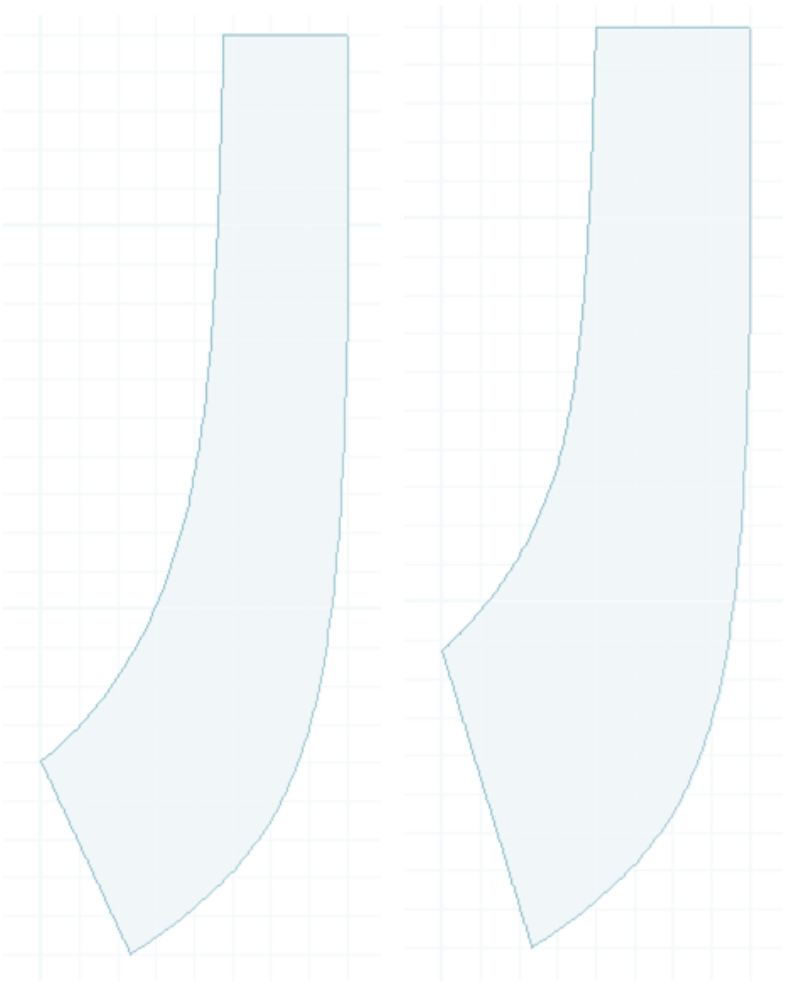

(a) impeller #1 (b) impeller #2

Fig.3- 1 Meridional shape of two tested impellers (Impeller #1, Impeller #2)

3.1. COMPARISON RESULTS

Fig 3.2 and Fig 3.3 show the head coefficient and work factor of the tested impellers according to flow coefficient,t comparing 1D analysis results and tested data with different rotational speeds. As shown in the figures, Ron Aungier's method predicts better than the Two Zone model in the head coefficient map. While the Two-Zone model predicts well around the design point, the Two-Zone model does not capture the head coefficient at the surge and choking

region. However, the results of Ron Aungier's method predicts more accurately around the surge and choking region.

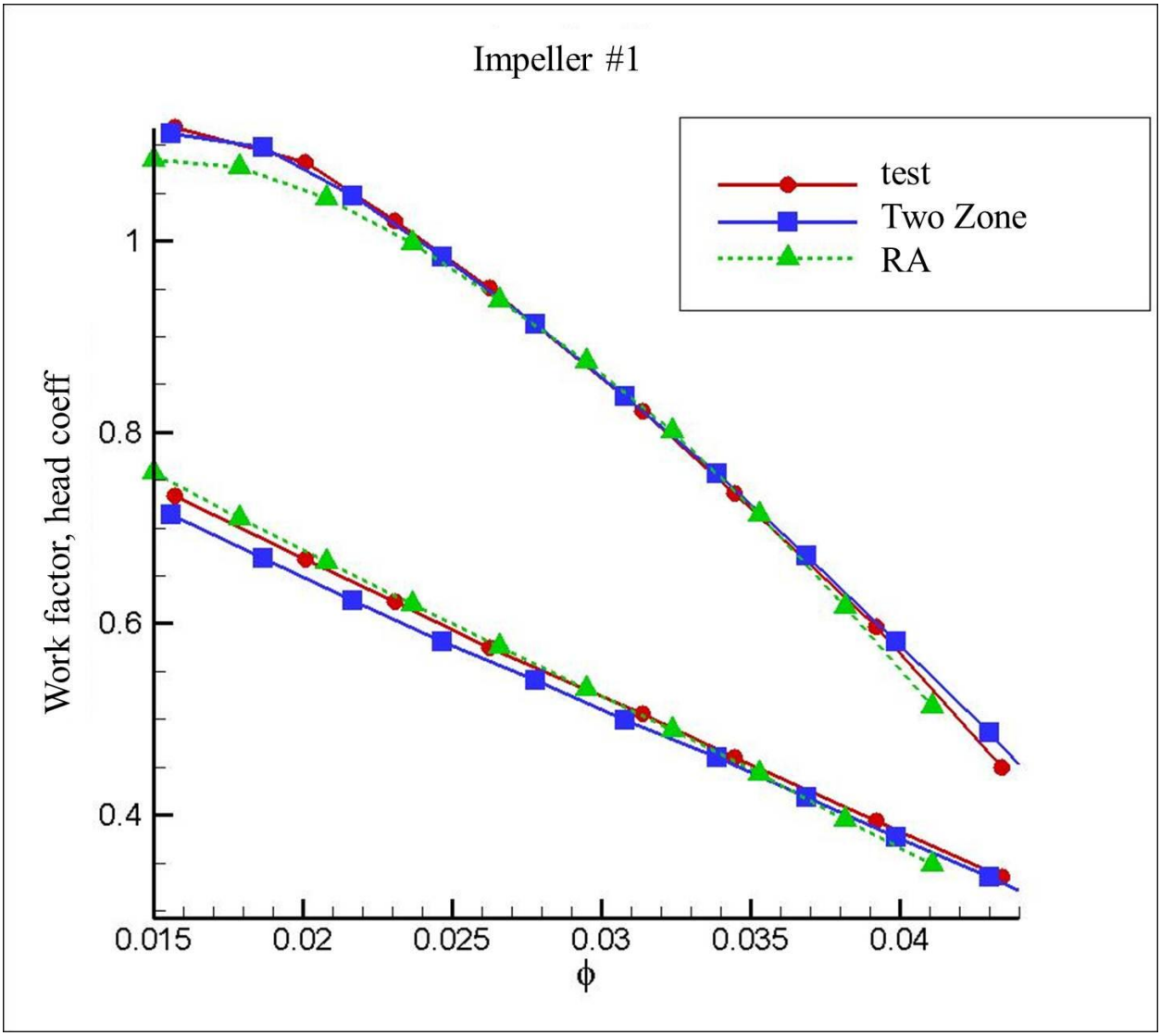

Fig.3- 2 Work factor and Head Coefficient result according to flow coefficient using Two Zone model with TEIS and Ron Aungier's model. (Impeller #1,13k, 19k, 21k rpm)

For interpretation of the references to color in this and all other figures, the reader is referred to the electronic version of this dissertation.

Fig.3-2 (cont'd)

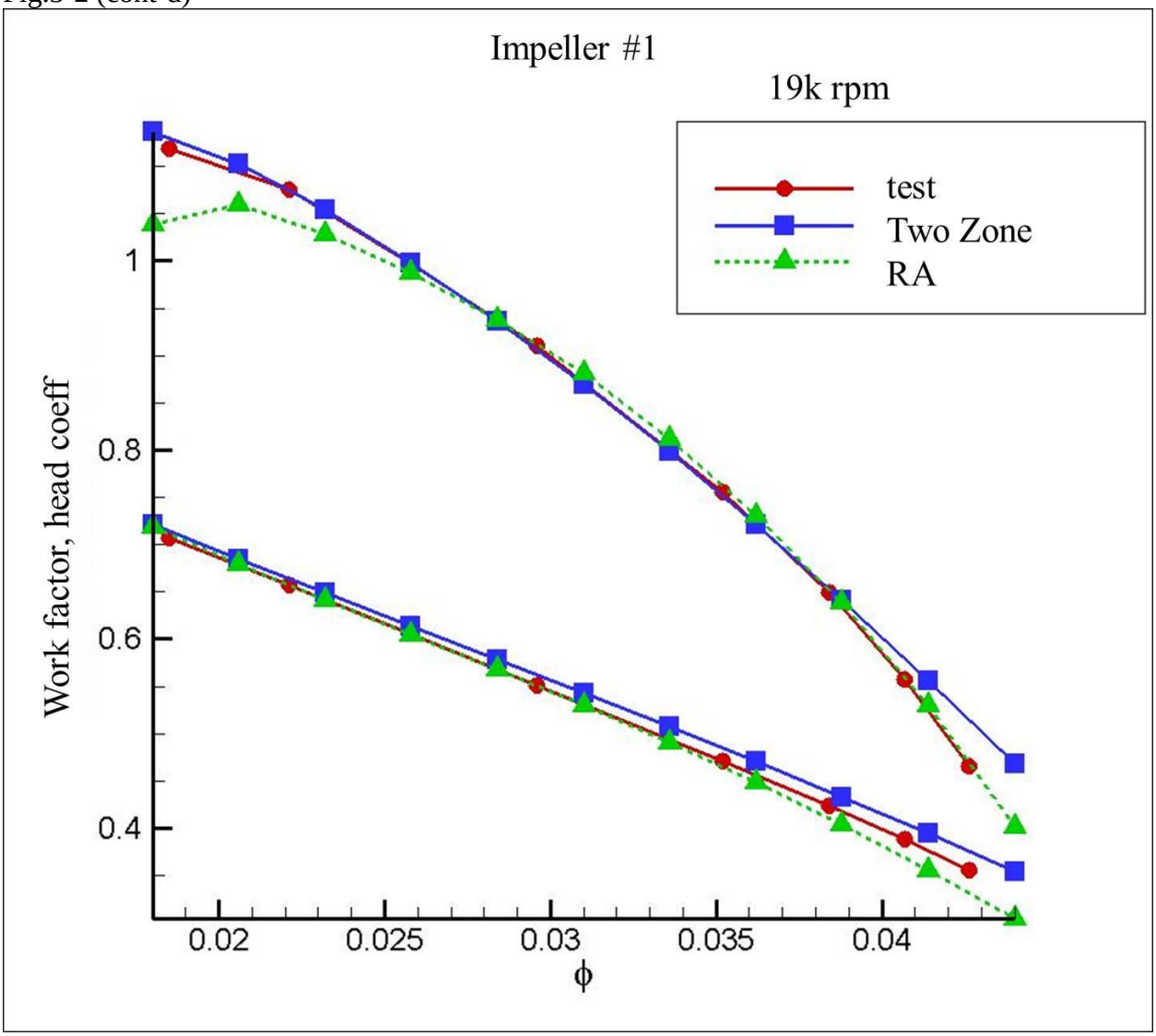
Impeller #1
19k rpm
test
Two Zone
RA
Work factor, head coeff
1
0.8
0.6
0.4
0.02
0.025
0.03
0.035
0.04
ϕ

Fig.3-2(cont'd)

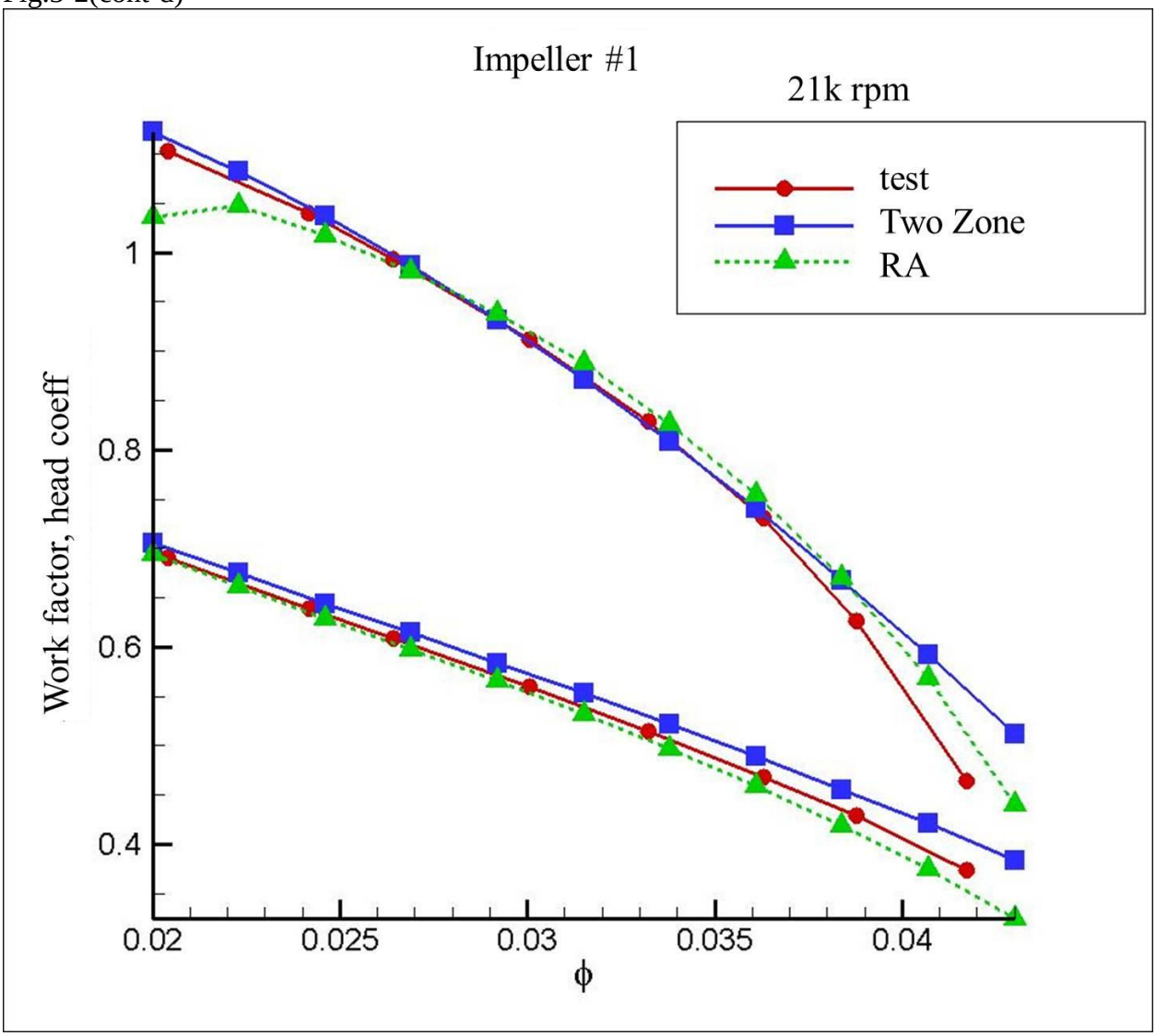

As shown in fig. 3-2, Ron Aungier's 1D analysis method, which is the empirical method, is more accurate at 19k and 21k rpm around surge region.

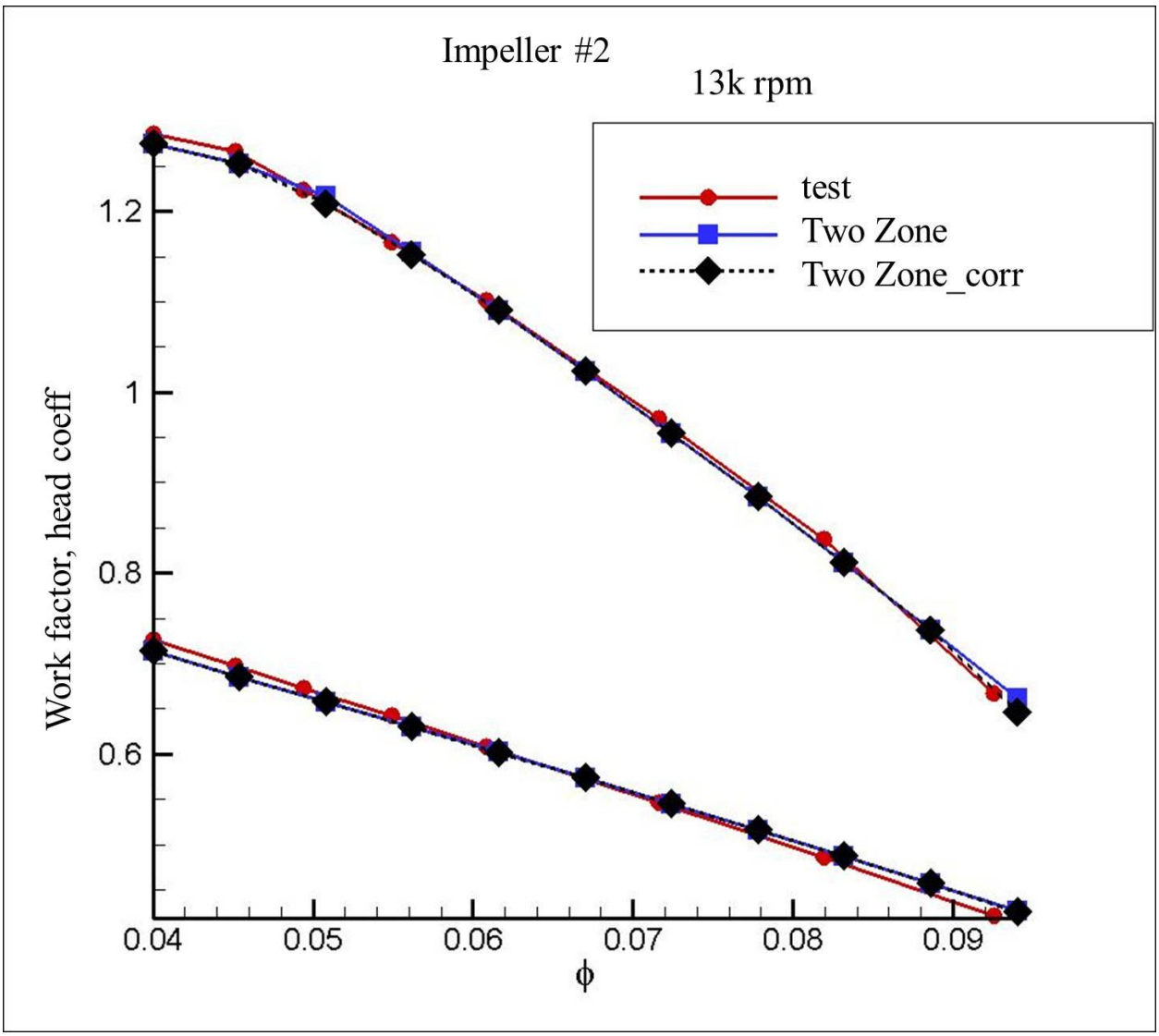

Fig.3- 3 Work factor and Head Coefficient result according to flow coefficient using Two Zone model with TEIS and Ron Aungier's model. (Impeller #2, 13k, 19k, 21k rpm)

Fig.3-3 (cont'd)

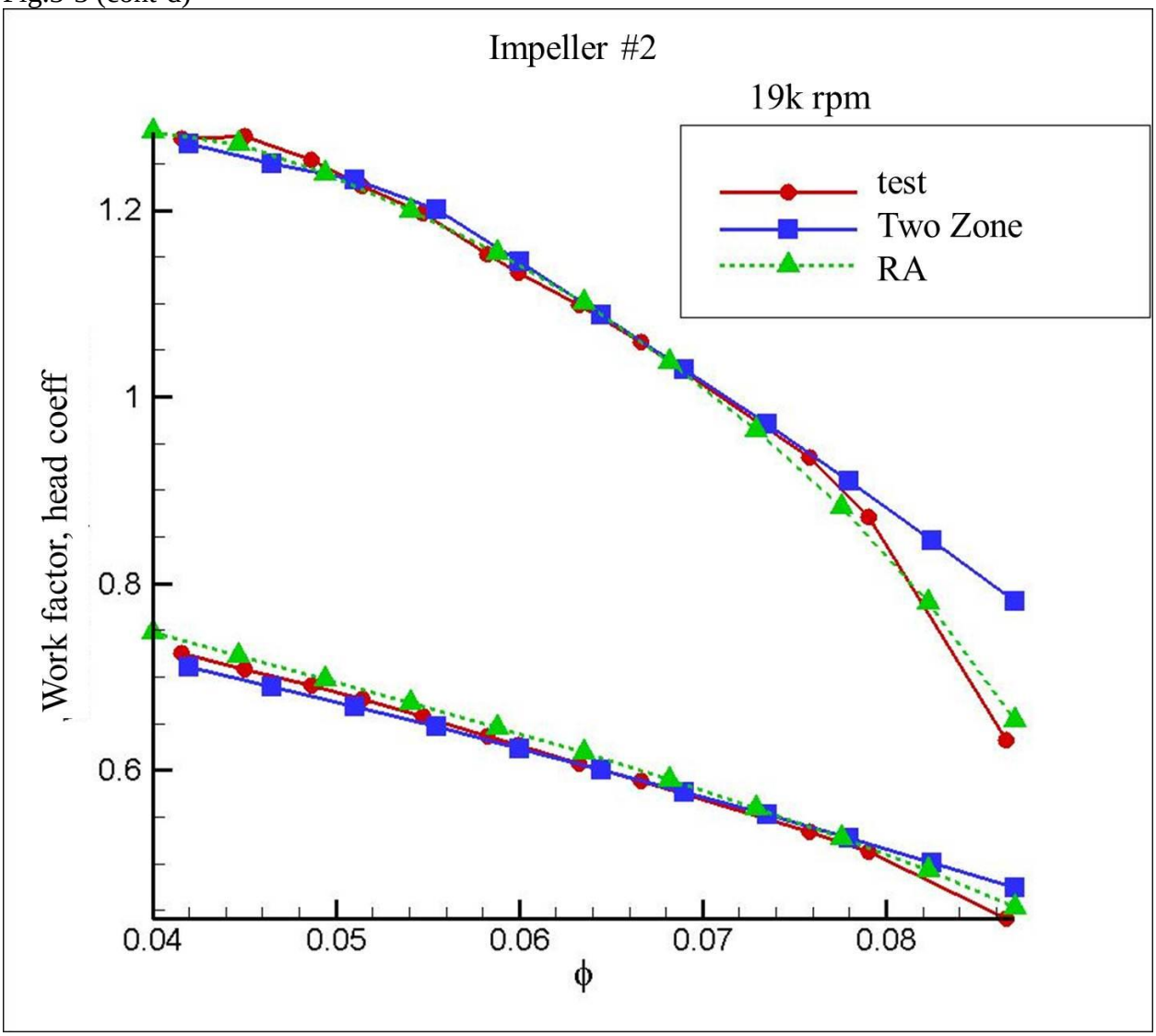
Impeller #2
19k rpm
test
Two Zone
RA
Work factor, head coeff
1.2
1
0.8
0.6
0.04
0.05
0.06
0.07
0.08
ϕ

Fig.3-3 (cont'd)

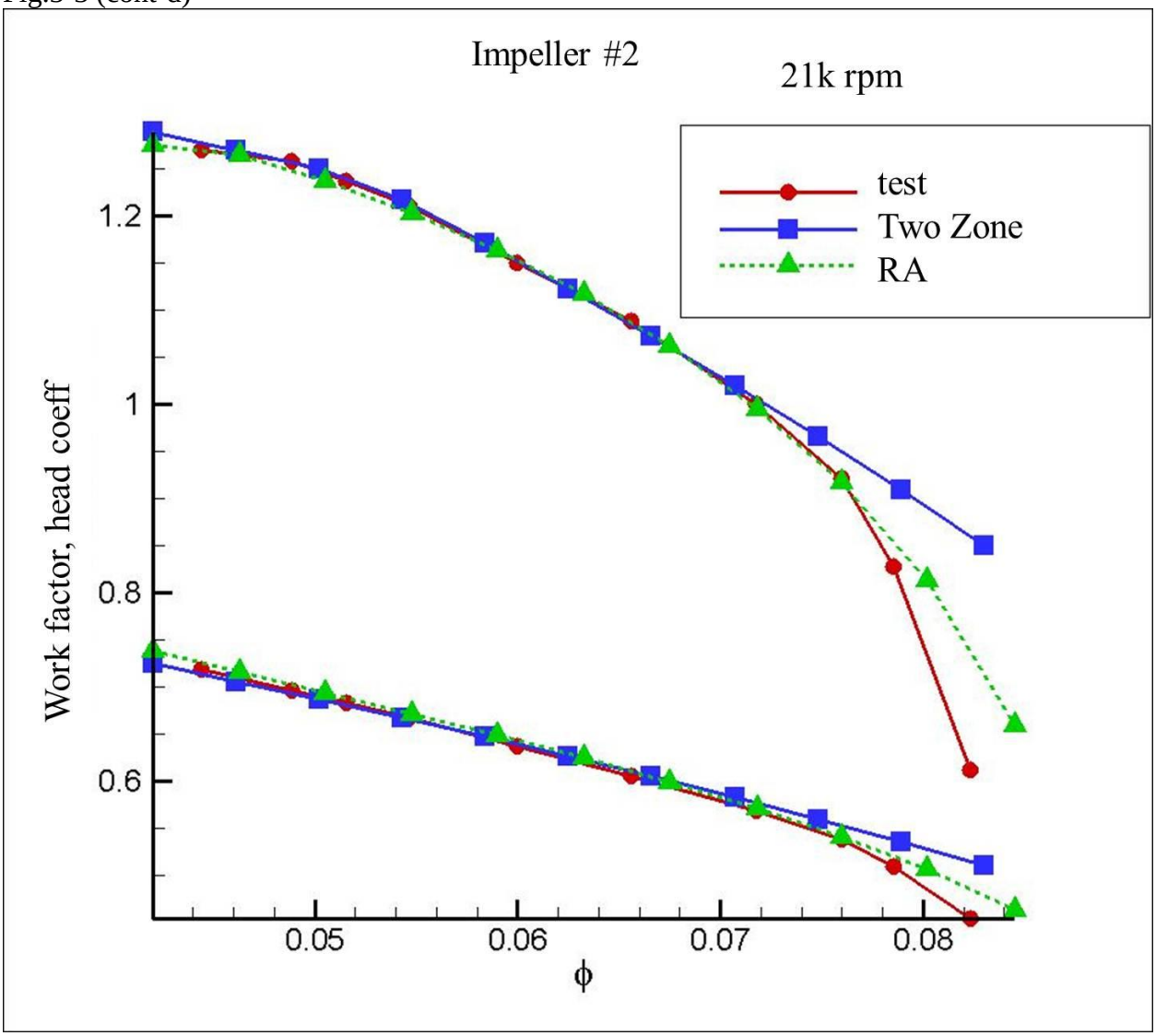

Fig. 3-3 clearly shows that the head coefficient result of Ron Aungier's method is more accurate than the results of the Two-Zone model around the choking region. At an increased rotational speed, Ron Aungier's model predicts the head coefficient and work factor better than the results of Two-Zone model.

Fig. 3.4 and Fig 3.5 present the absolute flow angle at the exit of vaneless diffuser of the impeller #1 and impeller #2 respectively. As shown in the figures, around the choking area Ron

Aungier's method predicts flow angles better, especially in impeller #2 as the rotational speed increases as well as the head coefficient prediction.

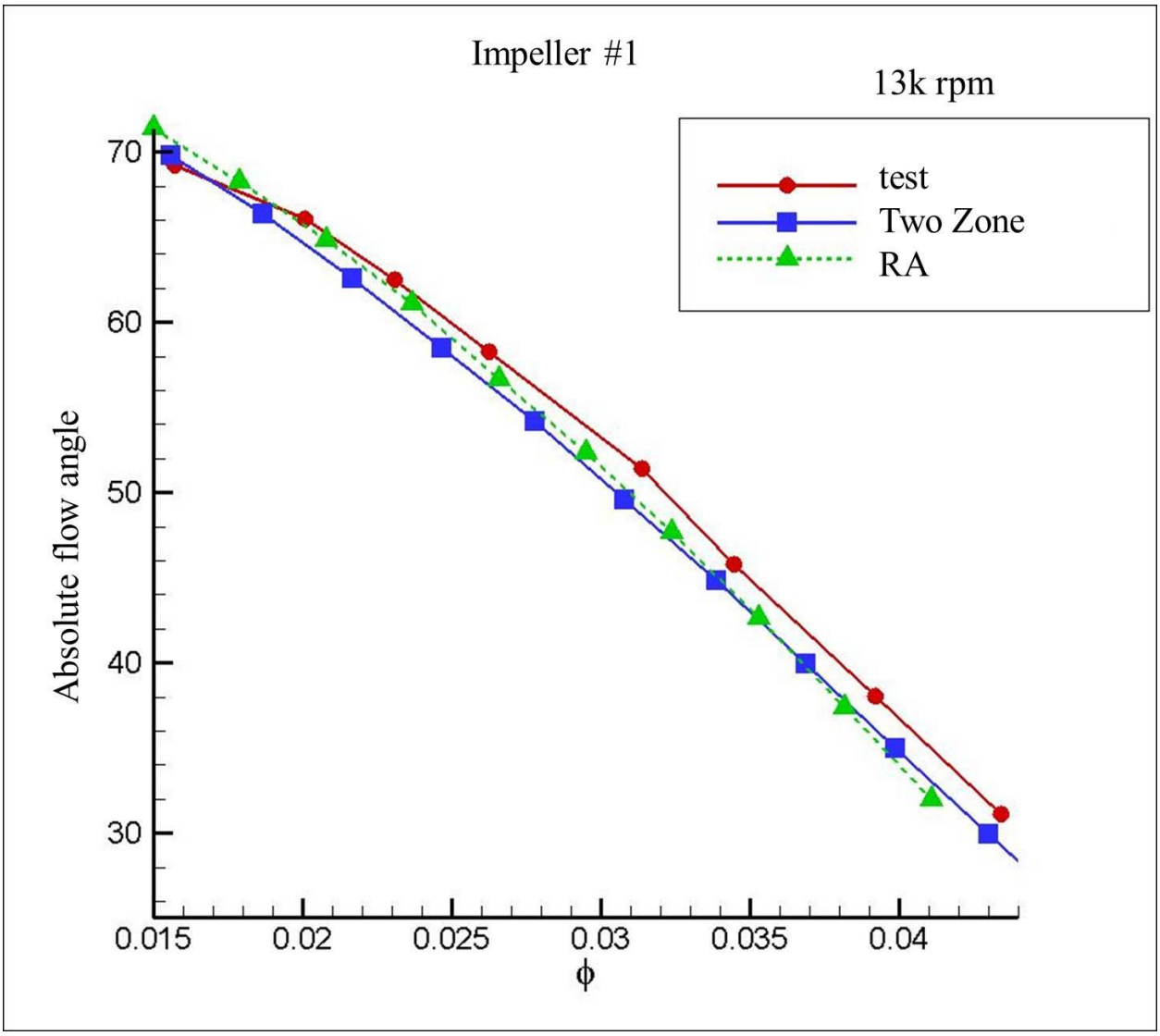

Fig.3- 4 Absolute flow angle according to flow coefficient along the various rotational speeds (impeller #1, 13k, 19k, 21k rpm)

Fig.3-4 (cont'd)

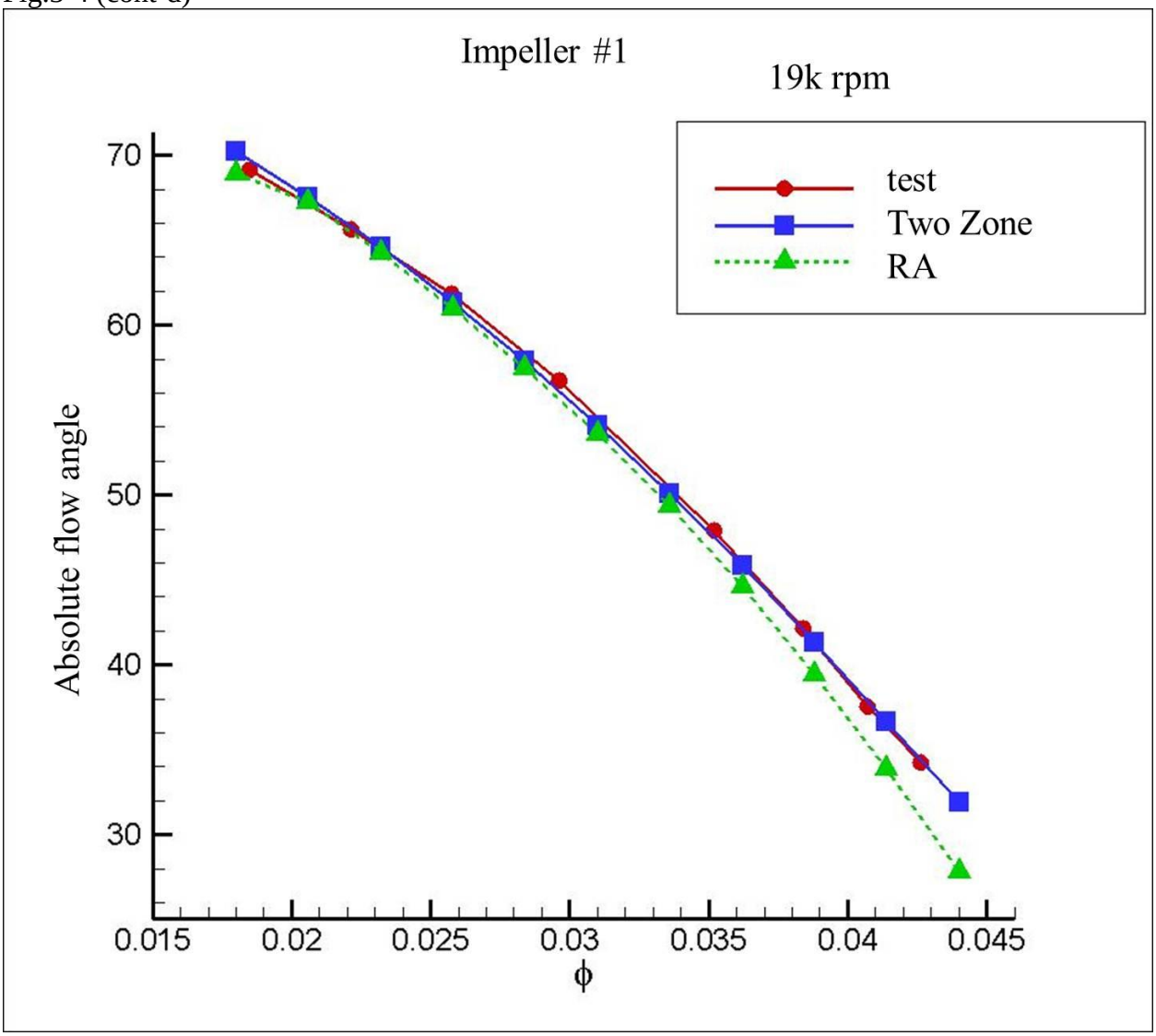
Impeller #1
19k rpm
test
Two Zone
RA
Absolute flow angle
70
60
50
40
30
0.015
0.02
0.025
0.03
0.035
0.04
0.045
ϕ

Fig.3-4 (cont'd)

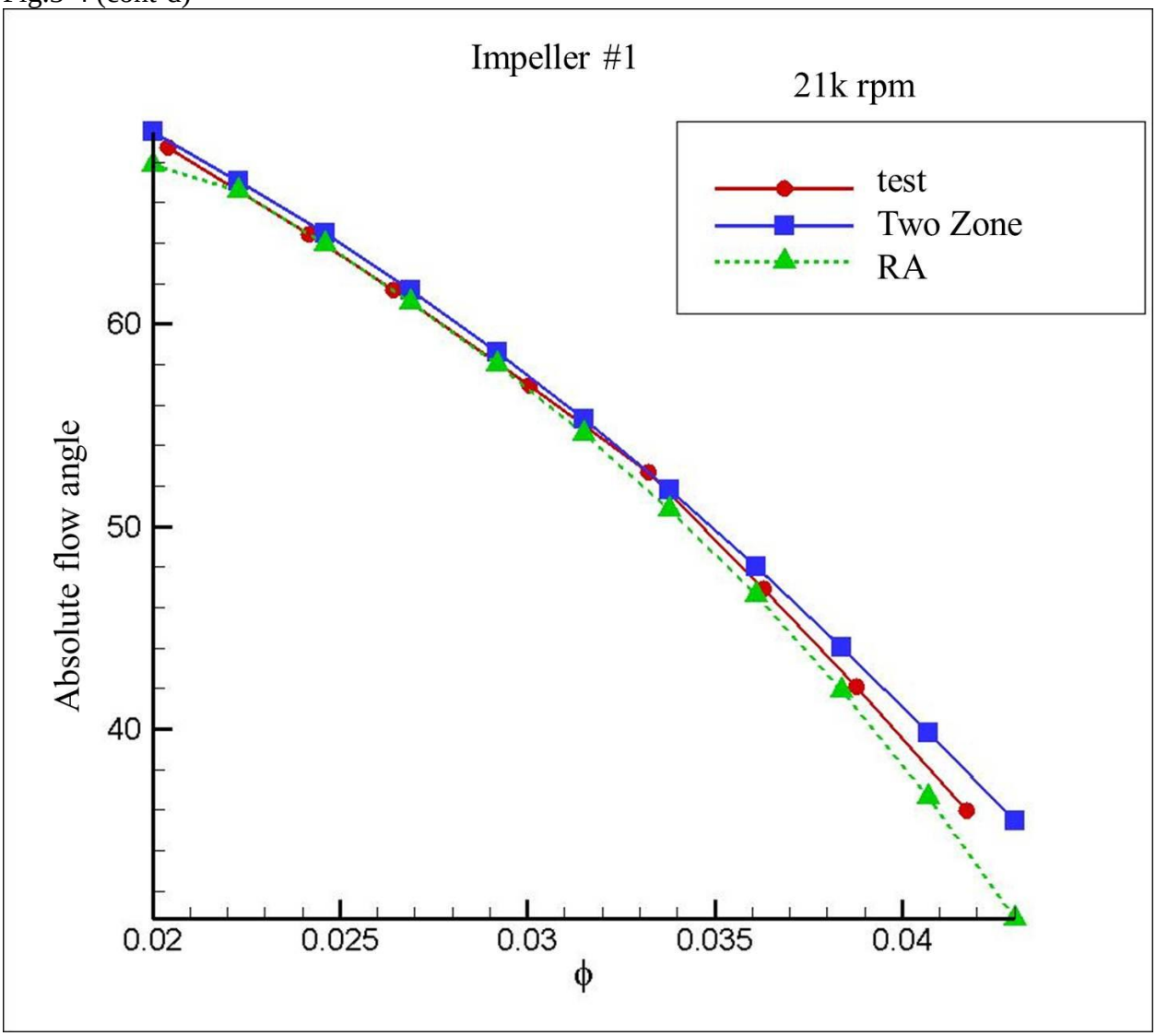
Impeller #1
21k rpm
test
Two Zone
RA
Absolute flow angle
60
50
40
0.02
0.025
0.03
0.035
0.04
ϕ

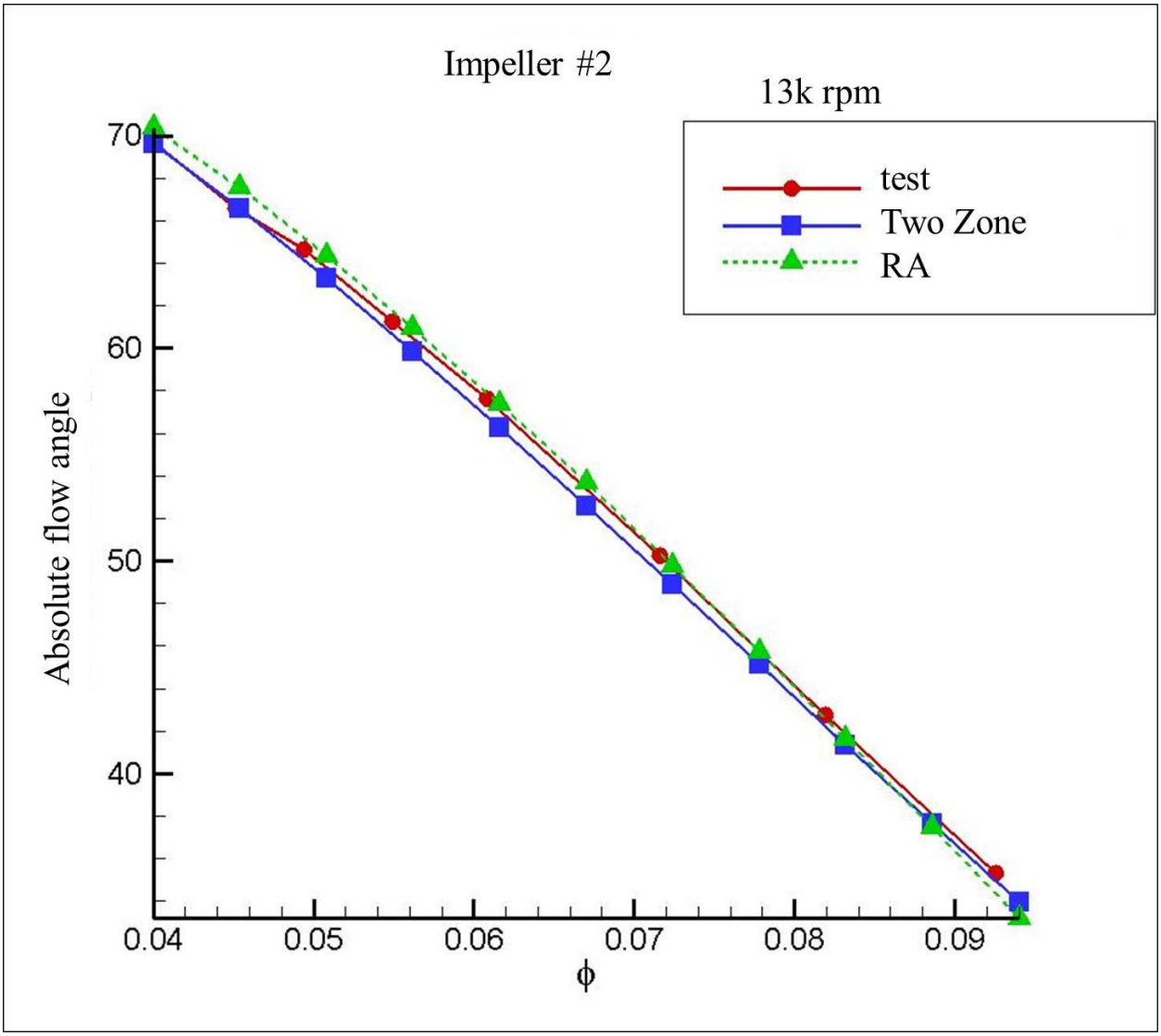

Fig.3- 5 Absolute flow angle according to the flow coefficient along the various rotational speeds (impeller #1, 13k, 19k, 21k rpm)

Fig.3-5 (cont'd)

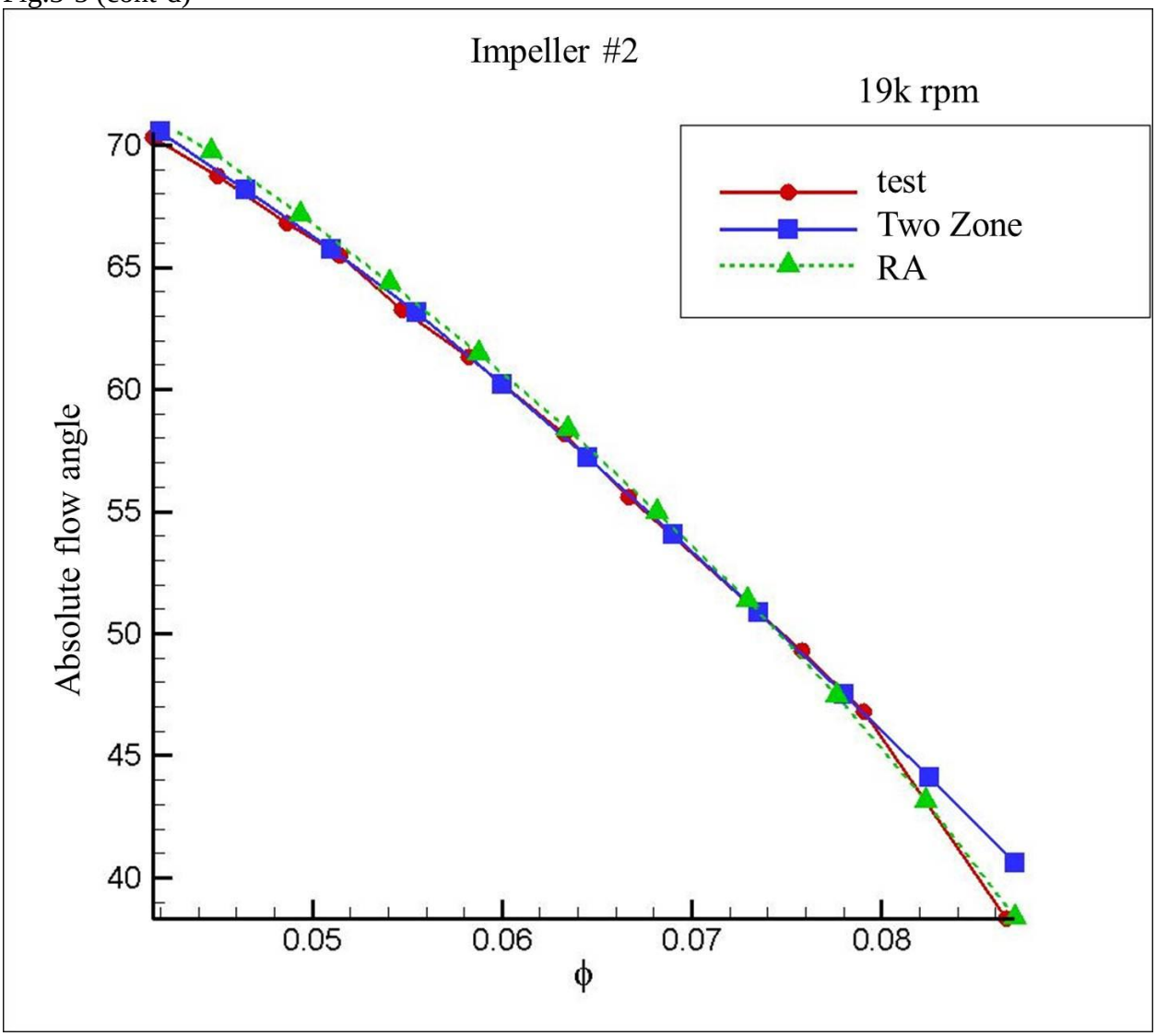
Impeller #2
19k rpm
test
Two Zone
RA
Absolute flow angle
70
65
60
55
50
45
40
0.05
0.06
0.07
0.08
ϕ

Fig.3-5 (cont'd)

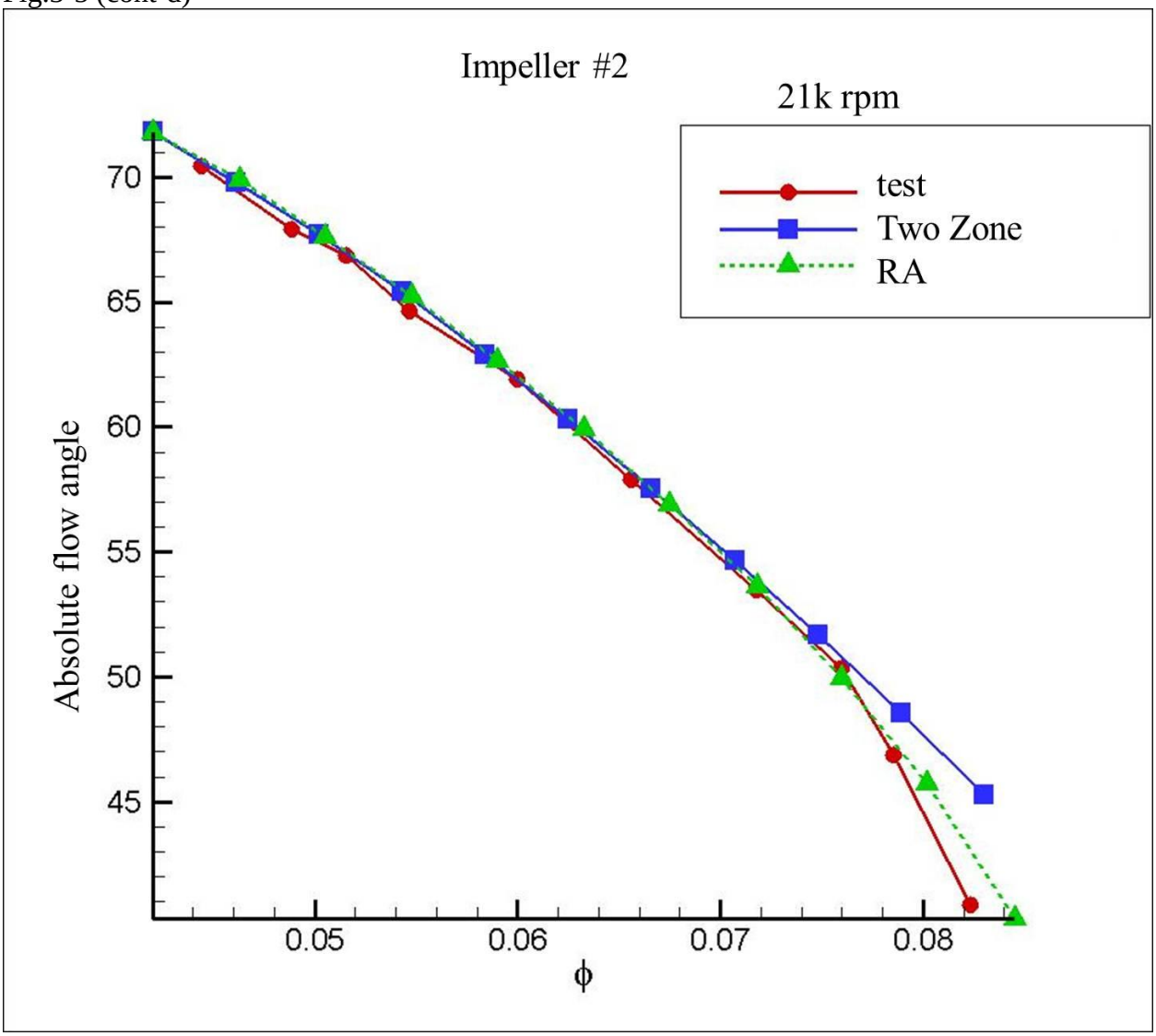
Impeller #2
21k rpm
test
Two Zone
RA
Absolute flow angle
70
65
60
55
50
45
0.05
0.06
0.07
0.08
ϕ

4. CORRECTED TWO ZONE WITH TEIS MODEL

4.1. PROBLEM DEFINITION IN DIFFUSION RATIO IN TEIS MODEL

To predict the head coefficient of a centrifugal compressor, estimating diffusion ratio, which determine pressure through the impeller, is important. As discussed in chapter 2, the TEIS model is one of the popular methods for calculating the diffusion ratio in Two Zone model. Fig. 4-1 presents the diffusion ratio corresponding to pressure recovery effectiveness [1]. There are two effectivenesses for the inlet portion and passage portion. These effectivenesses are used for calculating the diffusion ratio and invariant for whole flow range. As shown in Fig. 4-1, the results of the diffusion ratio calculated by TEIS model are predicted well around the design point. The results, however, depart from the test data in the surge and choking region.

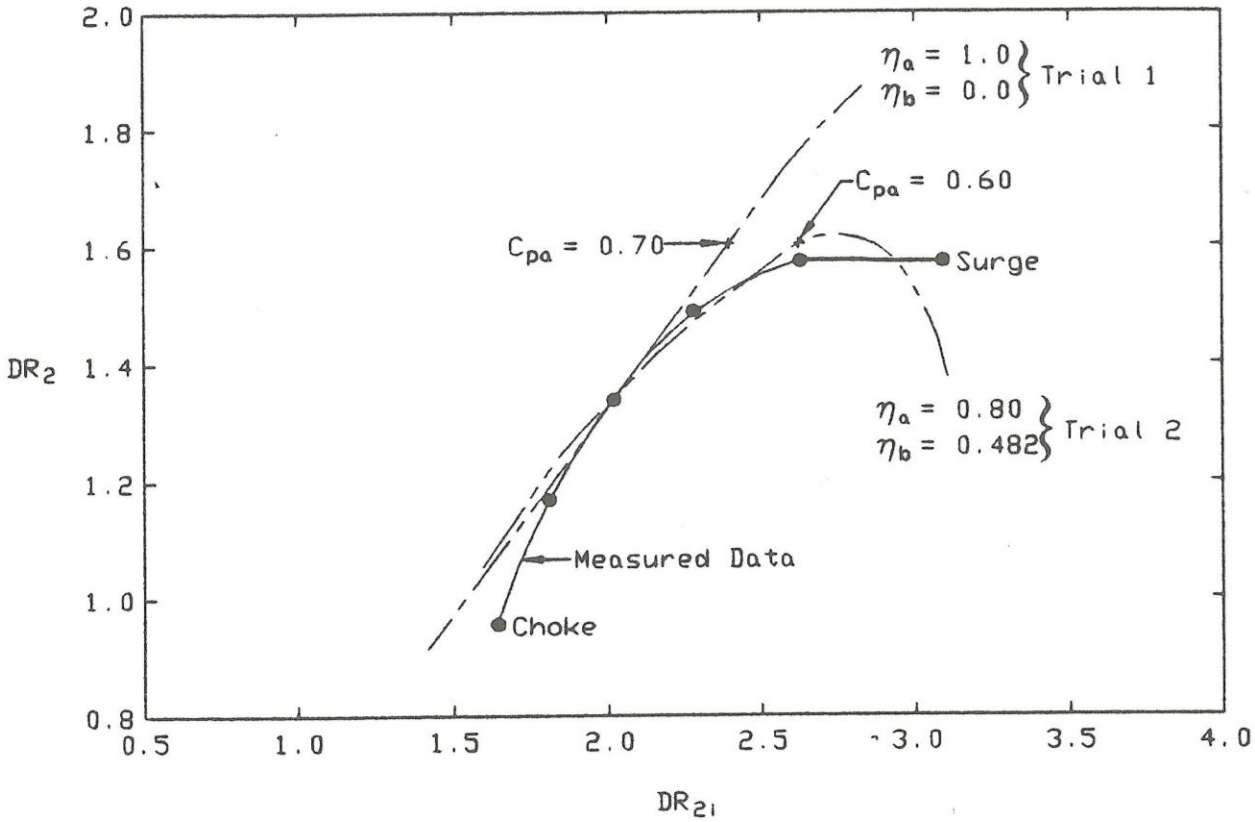

Fig.4- 1 TEIS model characteristic for estimating the diffusion ratio [1]

Fig. 4-2 and Fig. 4-3 show performance prediction results of the Two Zone model with TEIS for the impeller #1 and impeller #2 along the three different rotational speeds. The inlet and passage pressure recovery effectivenesses are fixed during calculating the head coefficients for the whole range of flow. As shown in Fig 4-2 and Fig 4-3, the Two Zone model can predict head coefficients around the design point. The Two-Zone model, on the other hand, cannot capture the head coefficient in the surge and choking region. The errors in head coefficient become larger as the impeller rotational speed increases for both impellers. The differences in the choking region show that they become significant as rotational speeds increase.

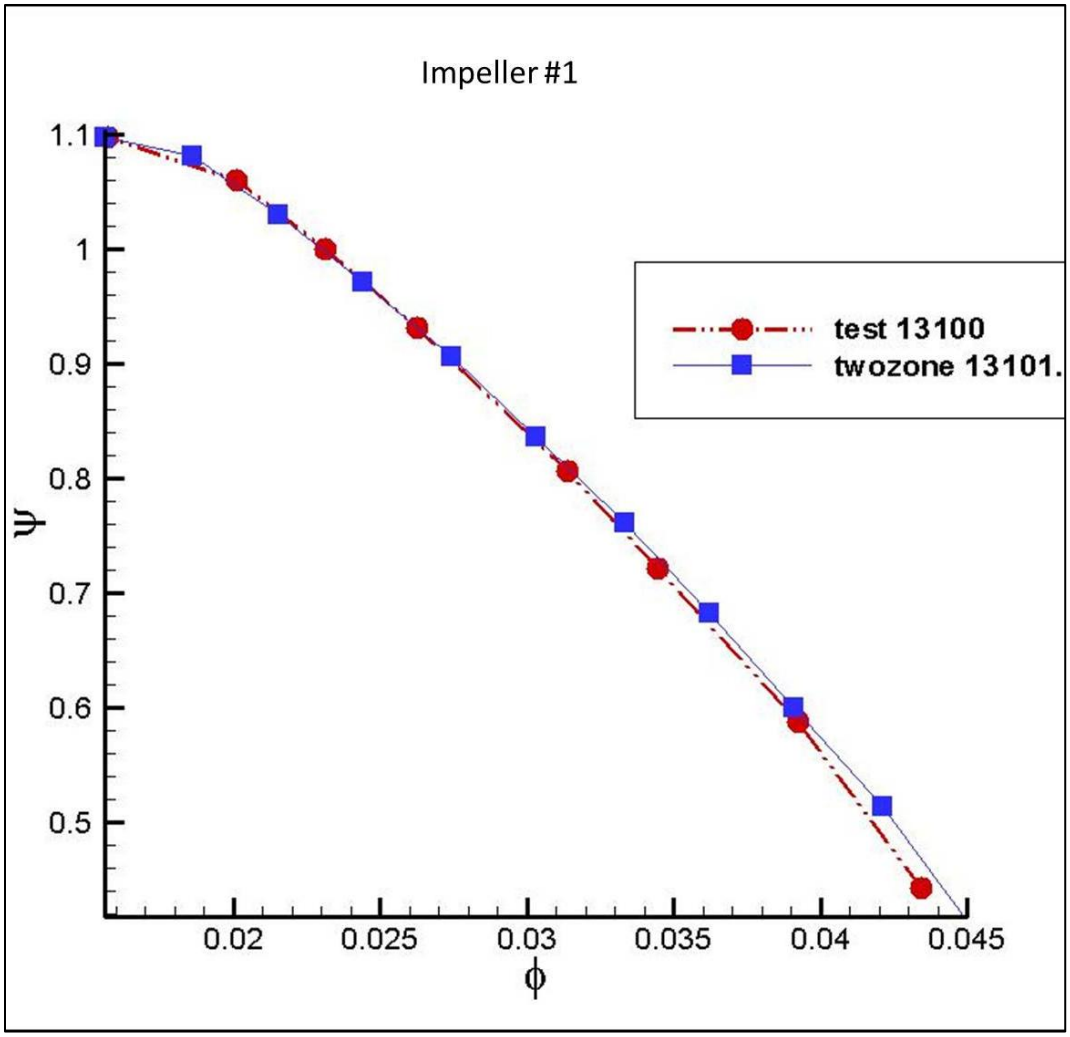

Fig.4- 2 Comparing head coefficient results using the Two Zone model and test results. (Impeller #1, 13k, 19k, 21k rpm)

Fig. 4-2 (cont'd)

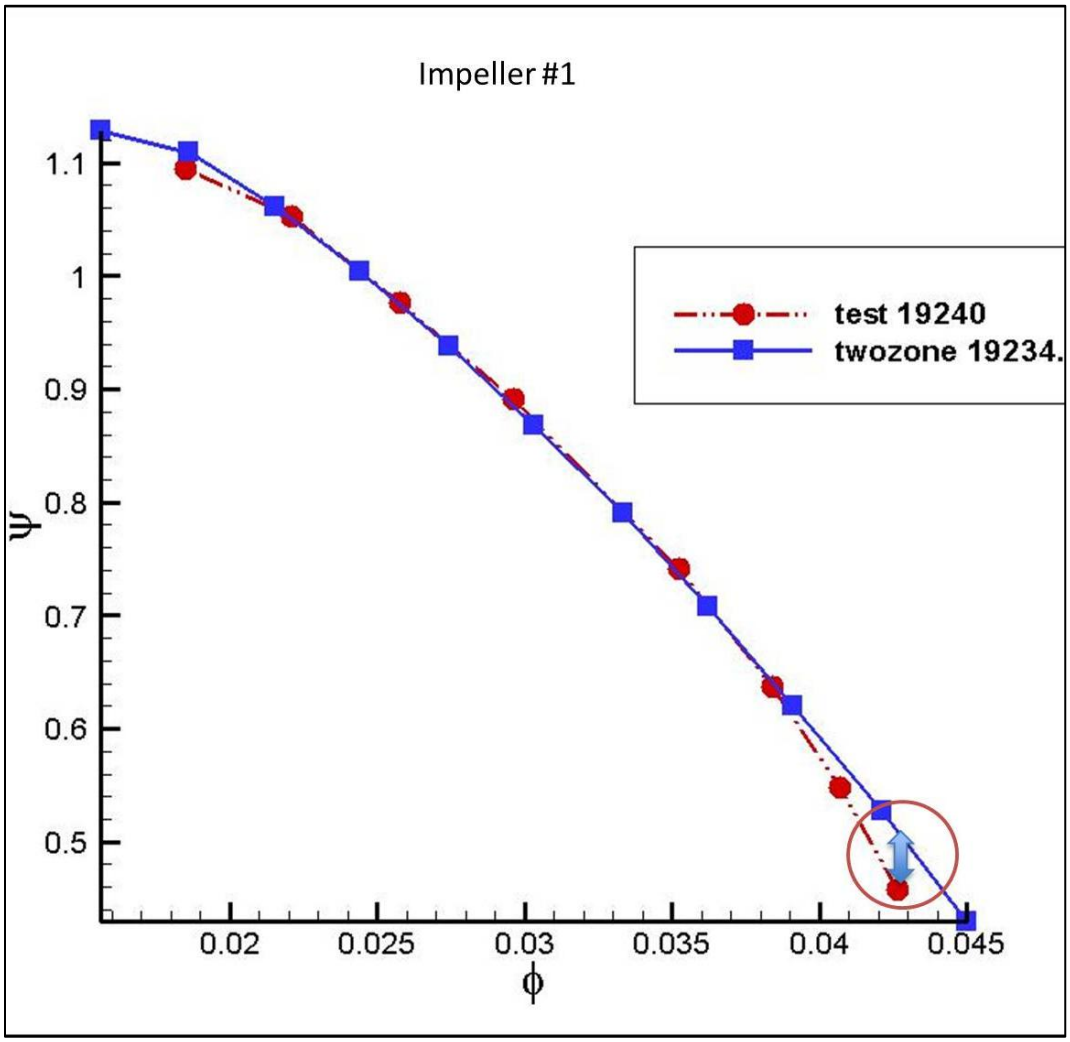
Impeller #1
test 19240
twozone 19234.
1.1
1
0.9
0.8
0.7
0.6
0.5
ψ
0.02
0.025
0.03
0.035
0.04
0.045
ϕ

Fig. 4-2 (cont'd)

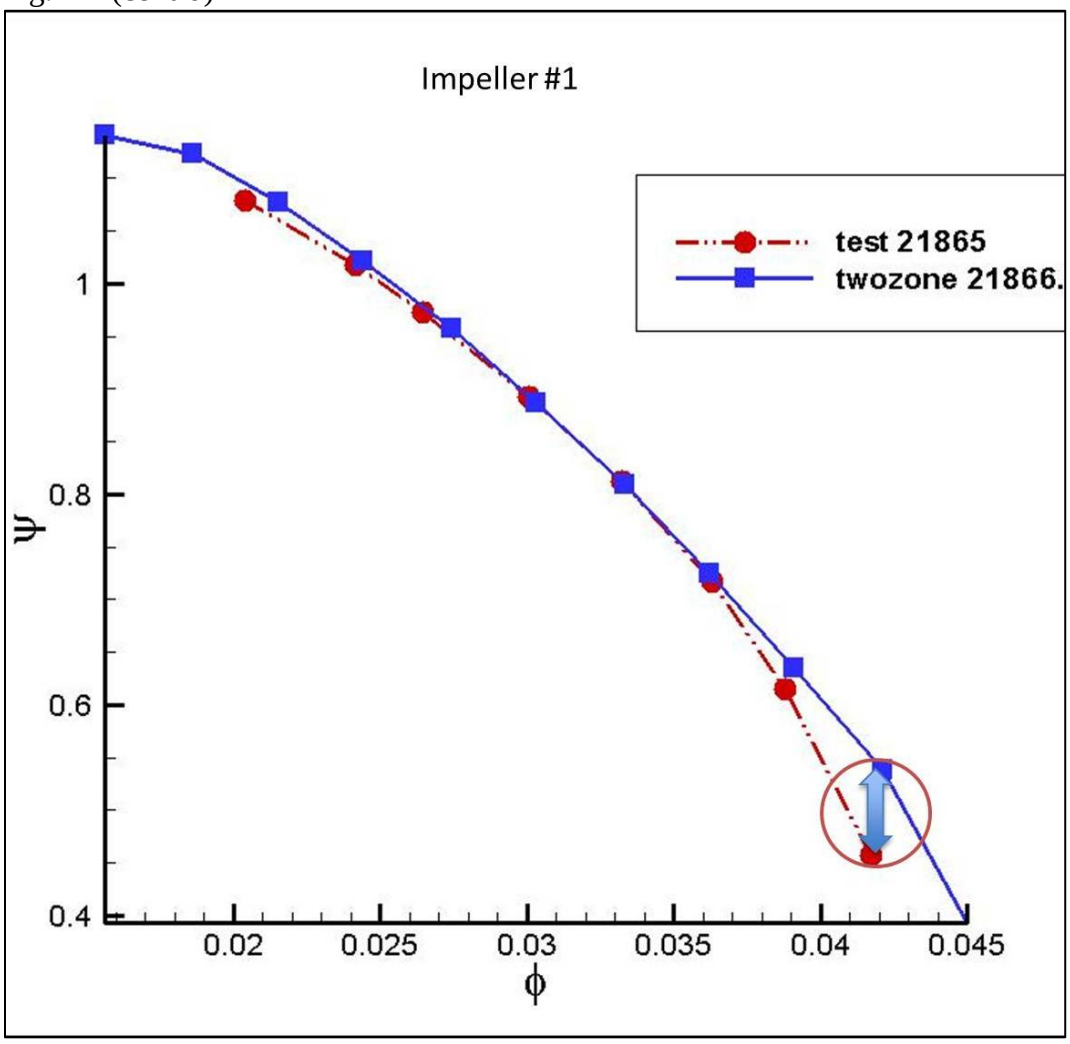
Impeller #1
test 21865
twozone 21866.
1
0.8
0.6
0.4
ψ
0.02
0.025
0.03
0.035
0.04
0.045
ϕ

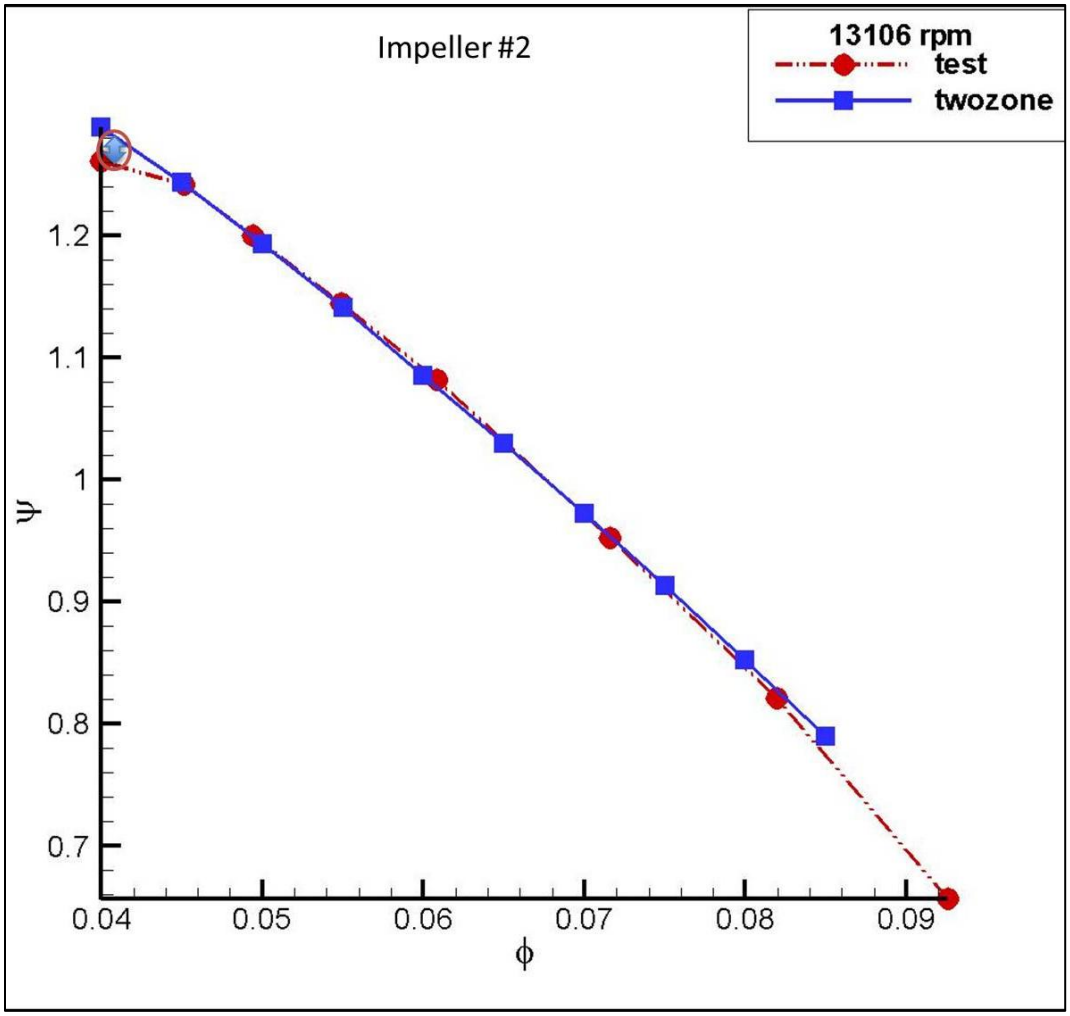

Fig.4- 3 Comparing head coefficient results using the Two Zone model and test results. (Impeller #2, 13k, 19k, 21k rpm)

Fig. 4-3 (cont'd)

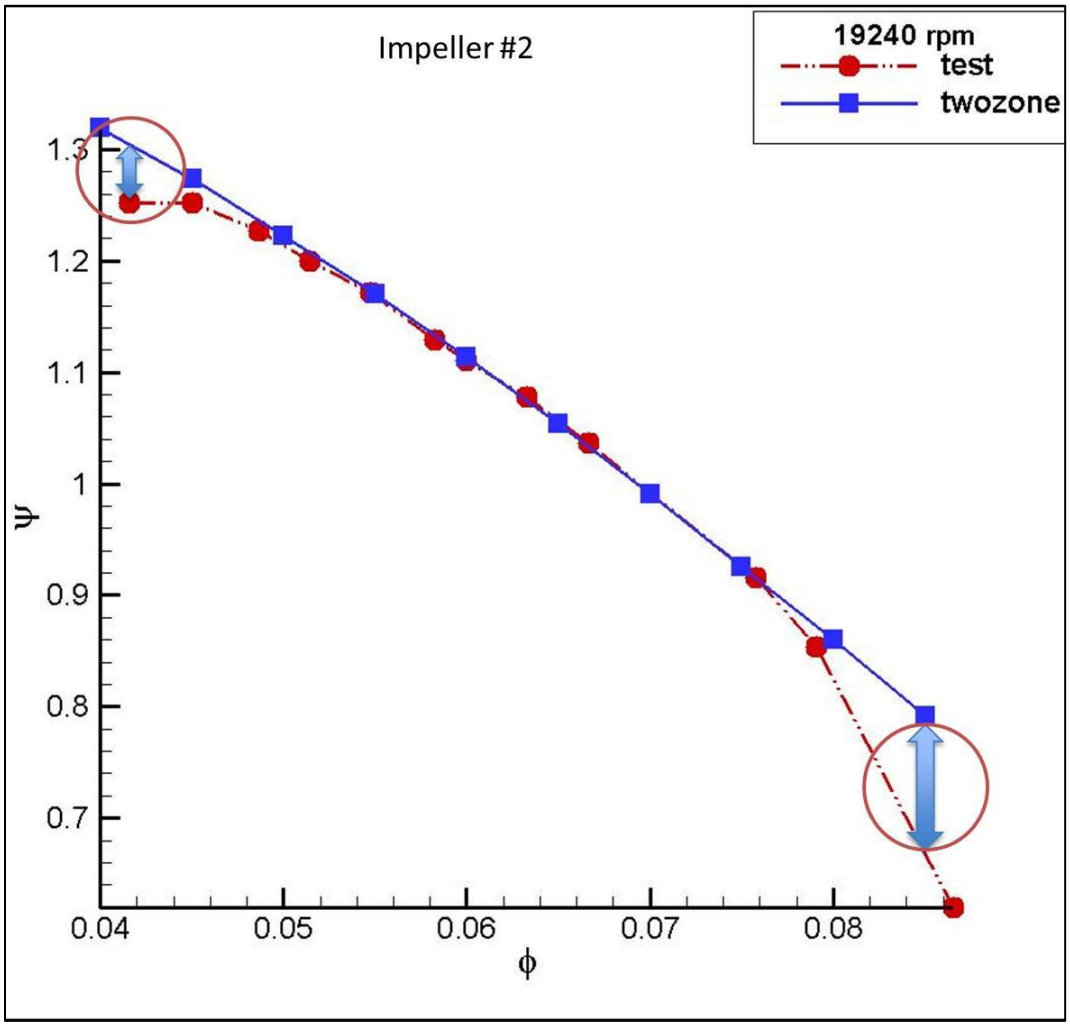
Impeller #2
19240 rpm
test
twozone
1.3
1.2
1.1
1
0.9
0.8
0.7
ψ
0.04
0.05
0.06
0.07
0.08
ϕ

Fig. 4-3 (cont'd)

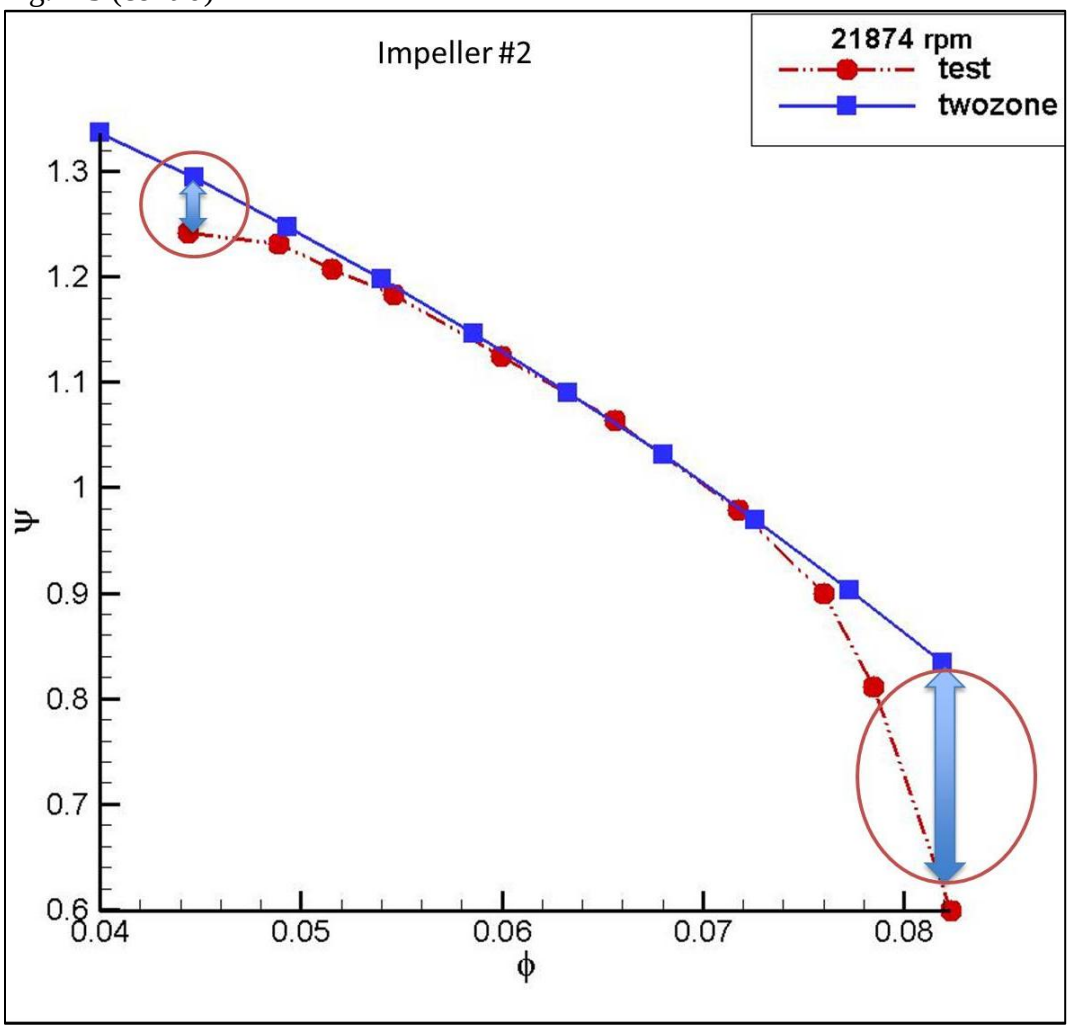

4.2. LOSS MODEL IN EMPIRICAL MODEL

Head coefficient is mainly a function of the total pressure ratio. The 1D performance analysis errors in head coefficient in the surge and choking region result from underestimating the total pressure loss. The Two Zone model with TEIS uses fixed pressure recovery effectiveness to calculate the diffusion ratio, which determines the total pressure ratio. For this reason, the Two Zone model with TEIS can predict the performance of the impeller only in a narrow range of flow.

In order to find the influence of loss model to total pressure ratio, the loss models, which are defined in chapter 2, are applied to impeller #1 and impeller #2. The loss models applied to impeller #1 and impeller #2 are presented in Fig.4-4 for three different speeds, 13k, 19k, 21k rpm. As shown in the Fig. 4-4, the loss coefficients are independent on the impeller speeds except the diffusion loss. The diffusion loss coefficient shows that there are differences in the surge and choking region by the three speeds. Particularly in the choking region, there are substantial differences compared to the surge region as well as the total loss coefficient. In terms of the total pressure loss coefficient, there are differences in the choking region as much as the diffusion loss coefficient. As the figure shows, the diffusion loss coefficient shows similar tendency as total pressure loss coefficient and differences between the speeds are almost same. In this sense, the differences in the total pressure loss coefficient resulted from the inlet diffusion loss coefficients. In other words, influence of the inlet condition to the total pressure ratio is very significant in the total pressure ratio or total head rise.

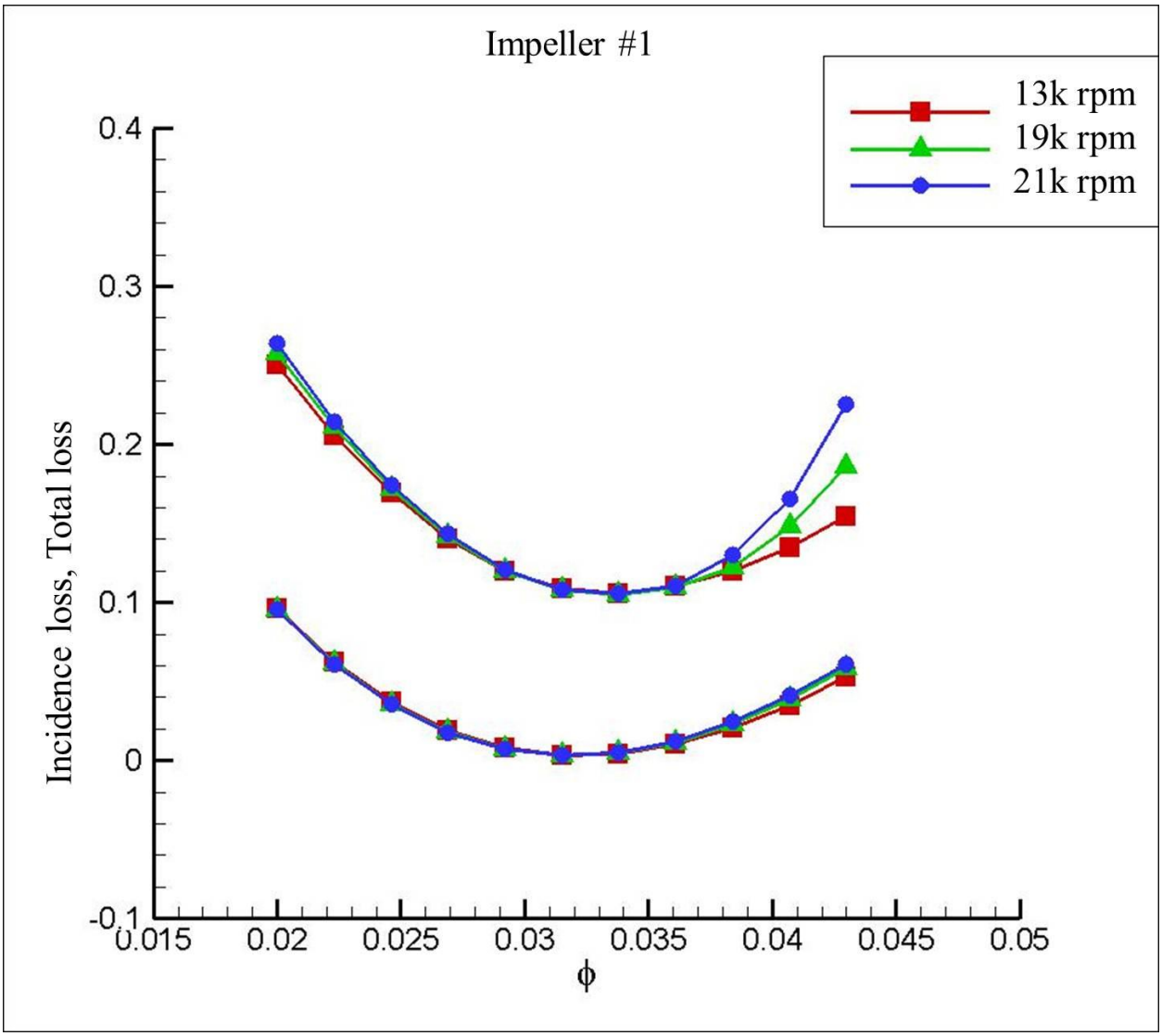

(a) Incidence loss coefficient according to flow rate along with 3 different speeds.(13k, 19k, 21k rpm)

Fig.4- 4 Loss models in impeller #1 and impeller #2 with various speeds.

Fig. 4-4 (cont'd)

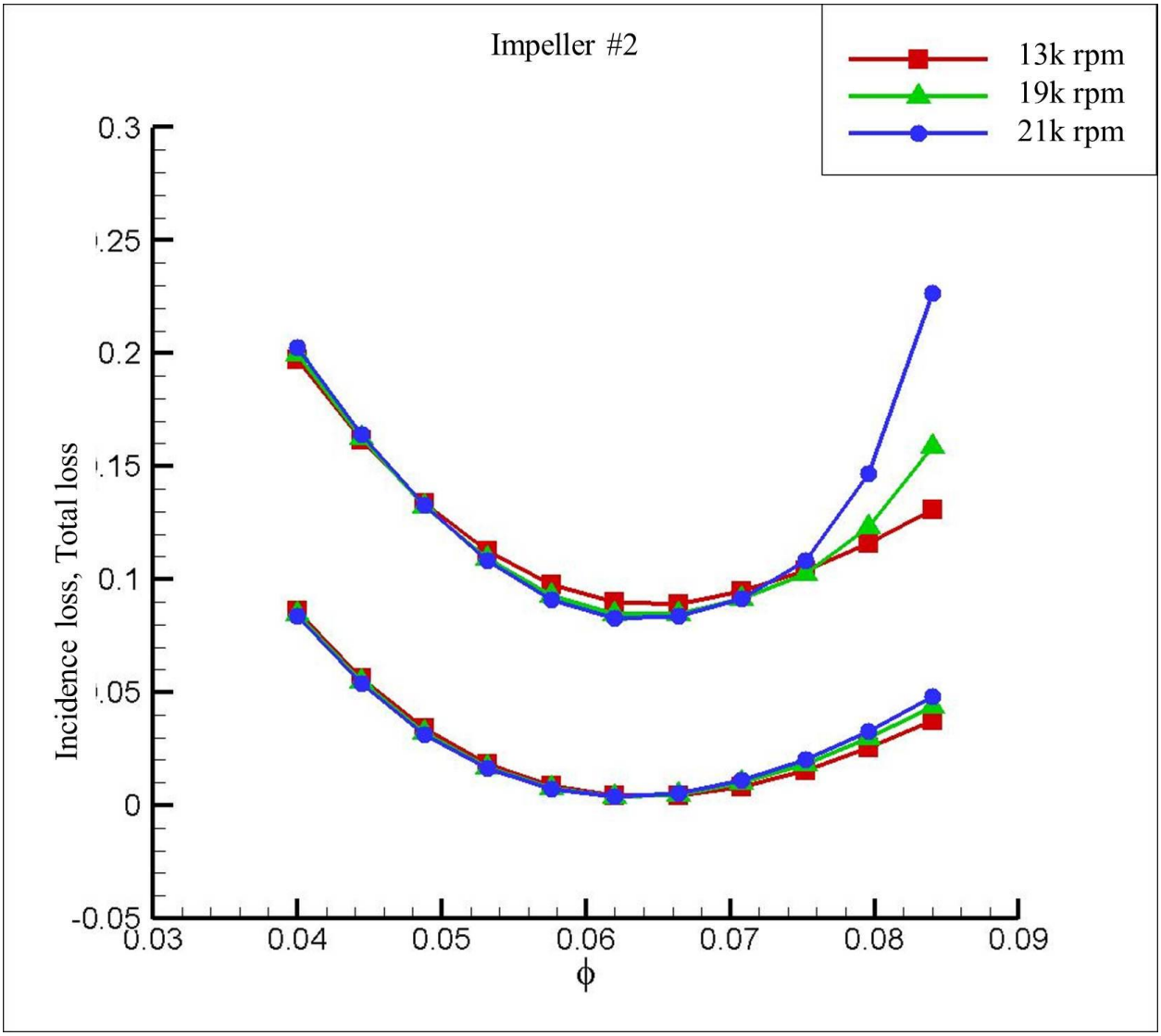
Impeller #2
13k rpm
19k rpm
21k rpm
Incidence loss, Total loss
0.3
.25
0.2
.15
0.1
.05
0
-0.05
0.03
0.04
0.05
0.06
0.07
0.08
0.09
ϕ

Fig. 4-4 (cont'd)

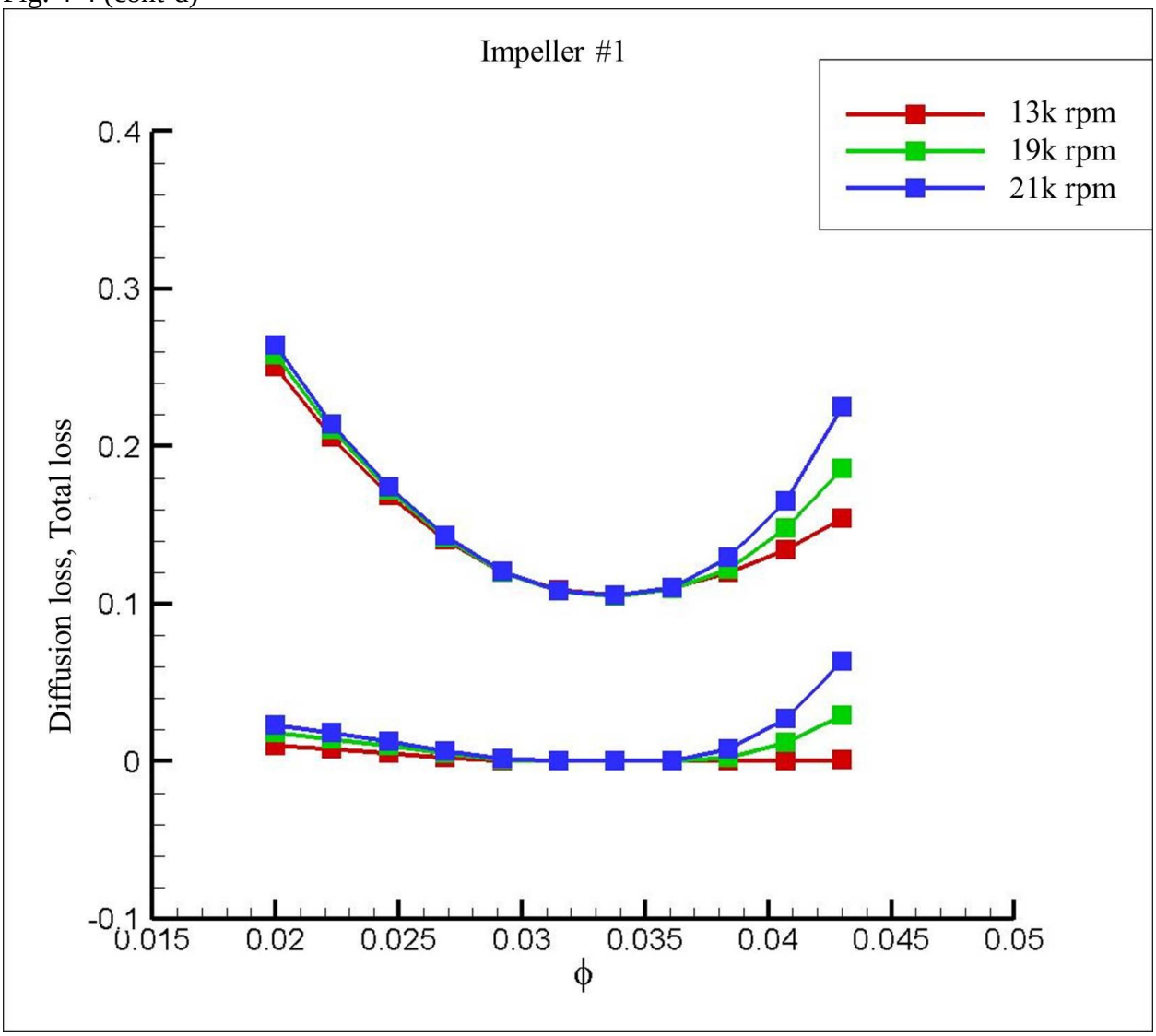
Impeller #1
13k rpm
19k rpm
21k rpm
Diffusion loss, Total loss
0.4
0.3
0.2
0.1
0
-0.1
0.015
0.02
0.025
0.03
0.035
0.04
0.045
0.05
ϕ

Fig. 4-4 (cont'd)

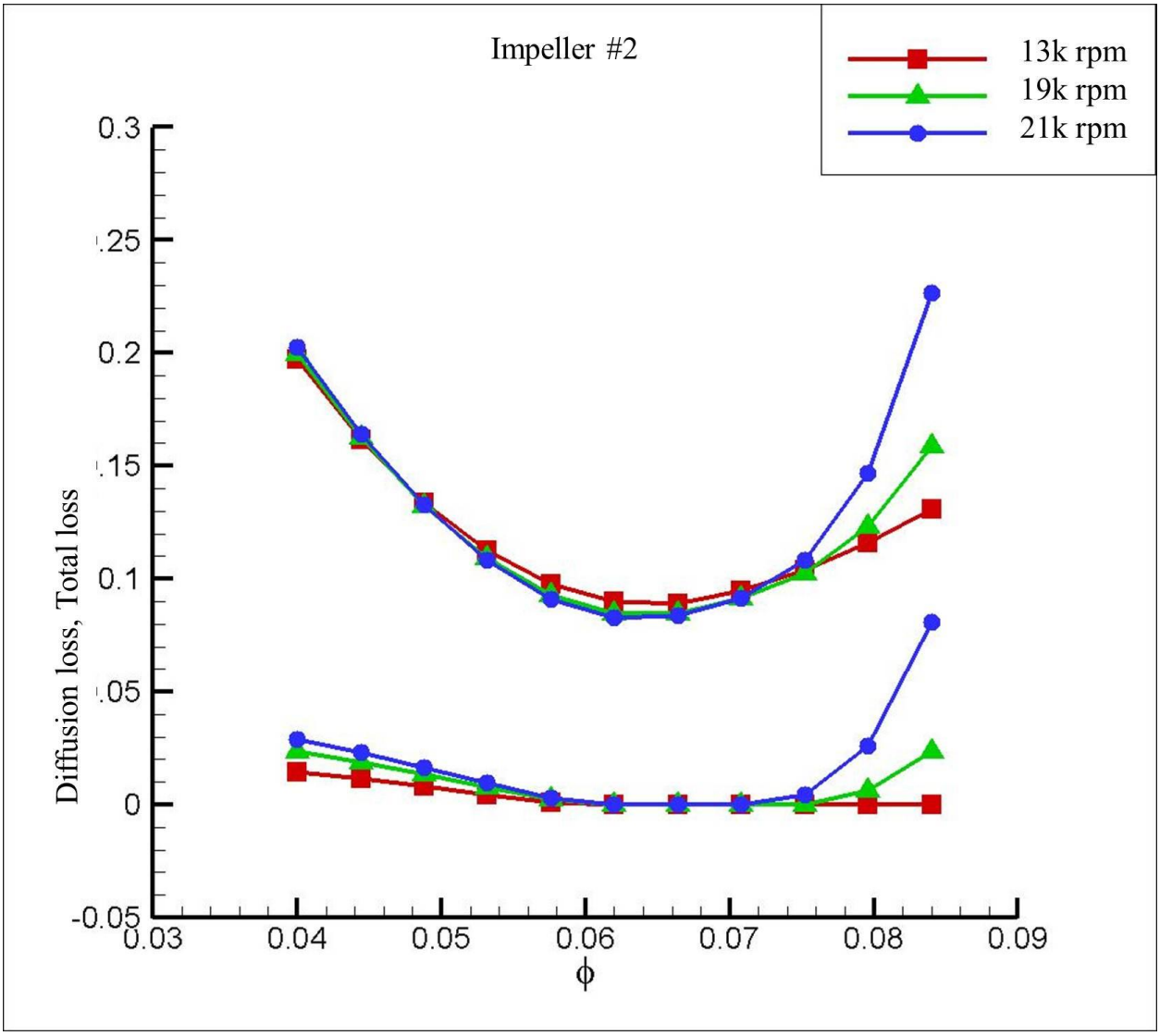

(b) Diffusion loss coefficient according to flow rate along with 3 different speeds.(13k, 19k, 21k rpm)

Fig. 4-4 (cont'd)

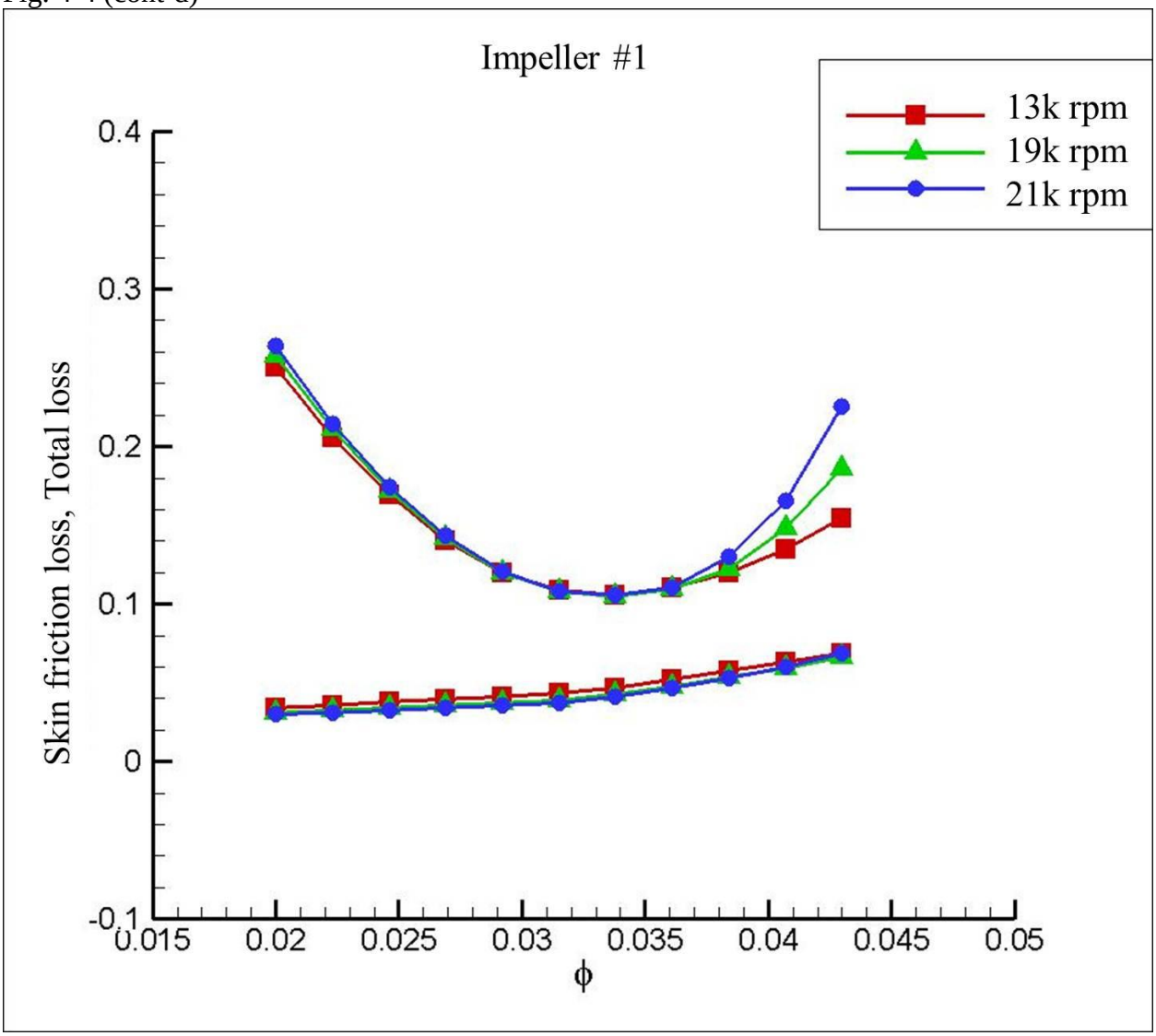
Impeller #1
13k rpm
19k rpm
21k rpm
Skin friction loss, Total loss
0.4
0.3
0.2
0.1
0
-0.1
0.015
0.02
0.025
0.03
0.035
0.04
0.045
0.05
ϕ

Fig. 4-4 (cont'd)

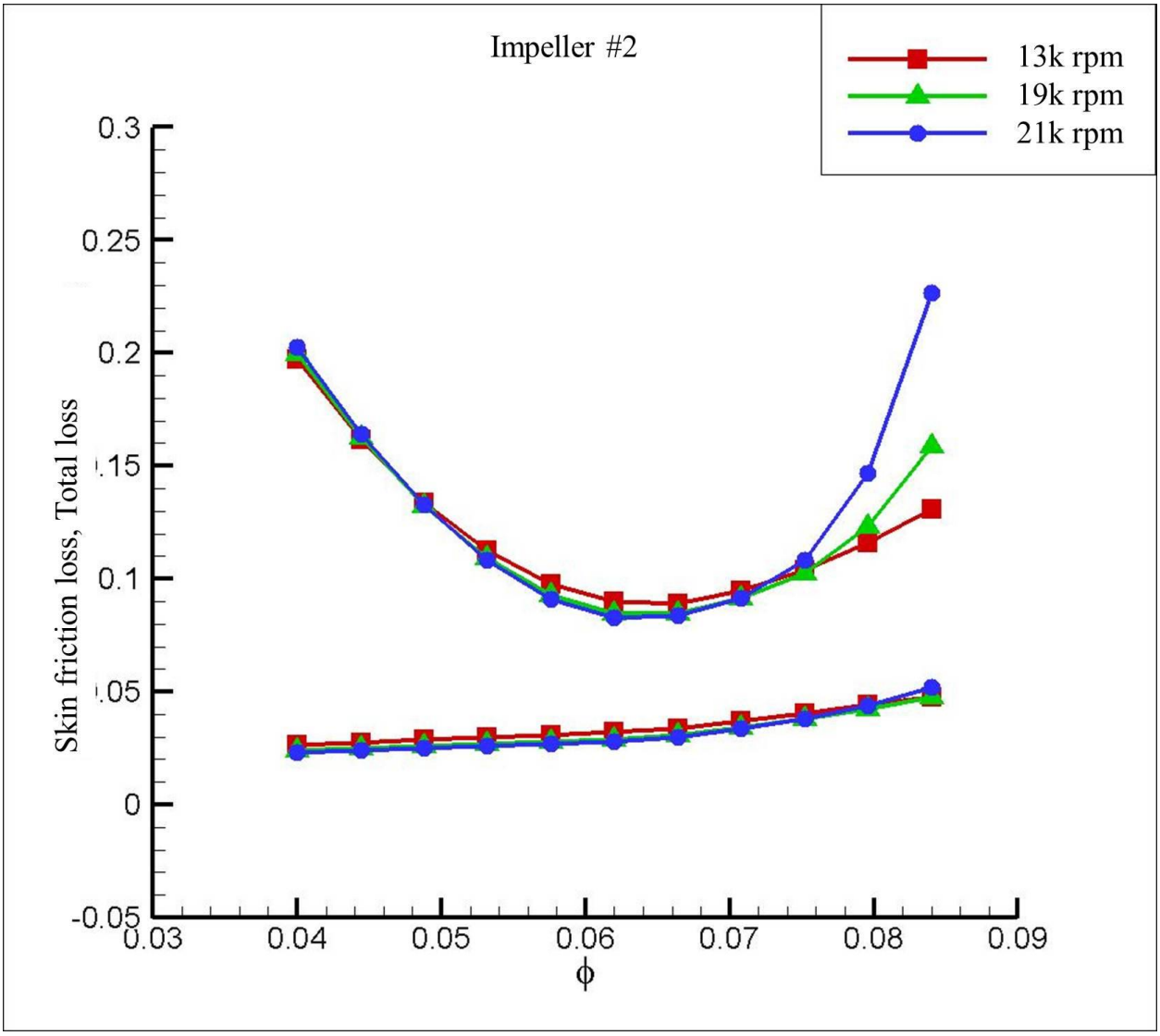

(c) Skin friction loss coefficient according to flow rate along with 3 different speeds.(13k, 19k, 21k rpm)

Fig. 4-4 (cont'd)

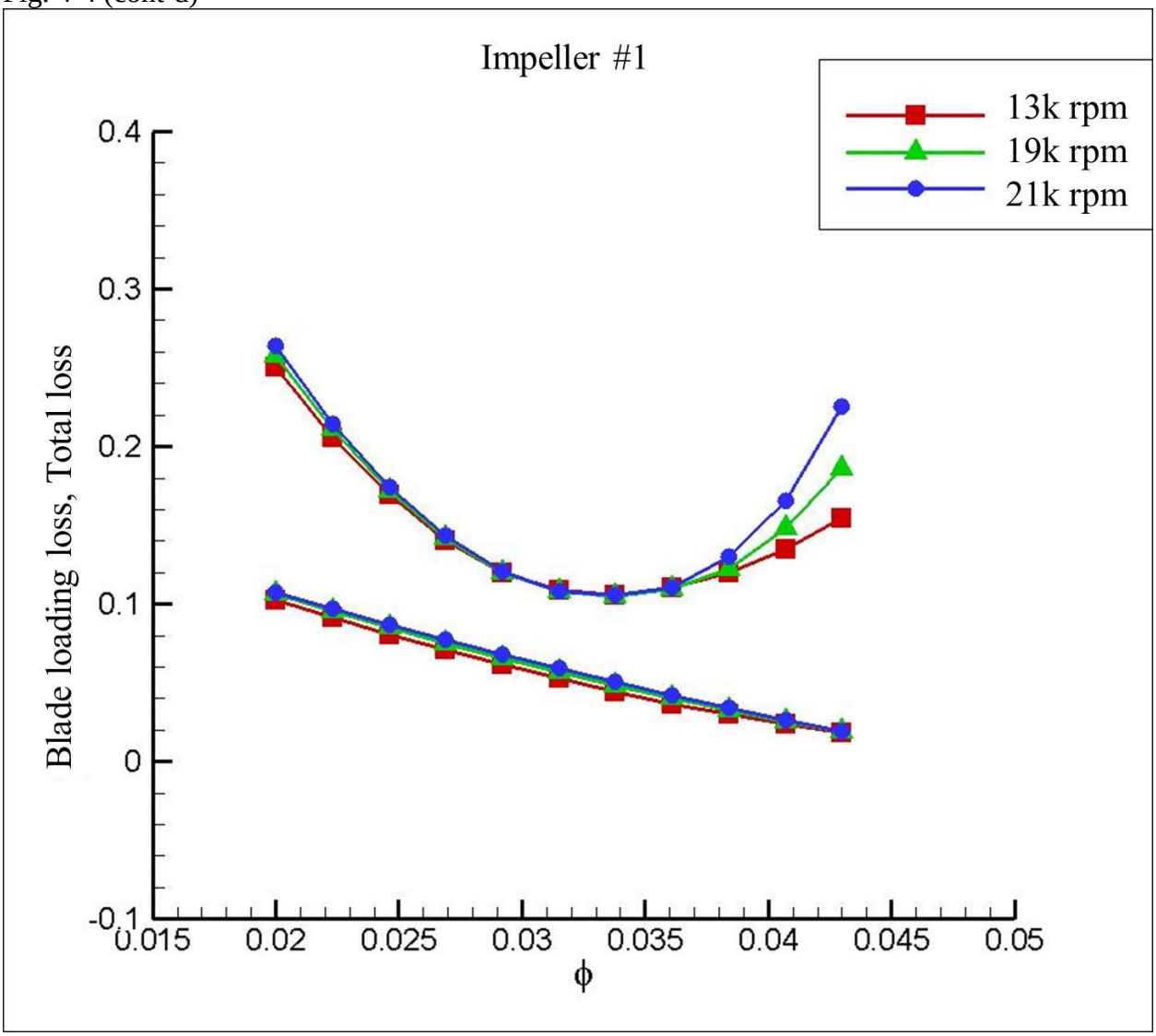
Impeller #1
13k rpm
19k rpm
21k rpm
Blade loading loss, Total loss
0.4
0.3
0.2
0.1
0
-0.1
0.015
0.02
0.025
0.03
0.035
0.04
0.045
0.05
ϕ

Fig. 4-4 (cont'd)

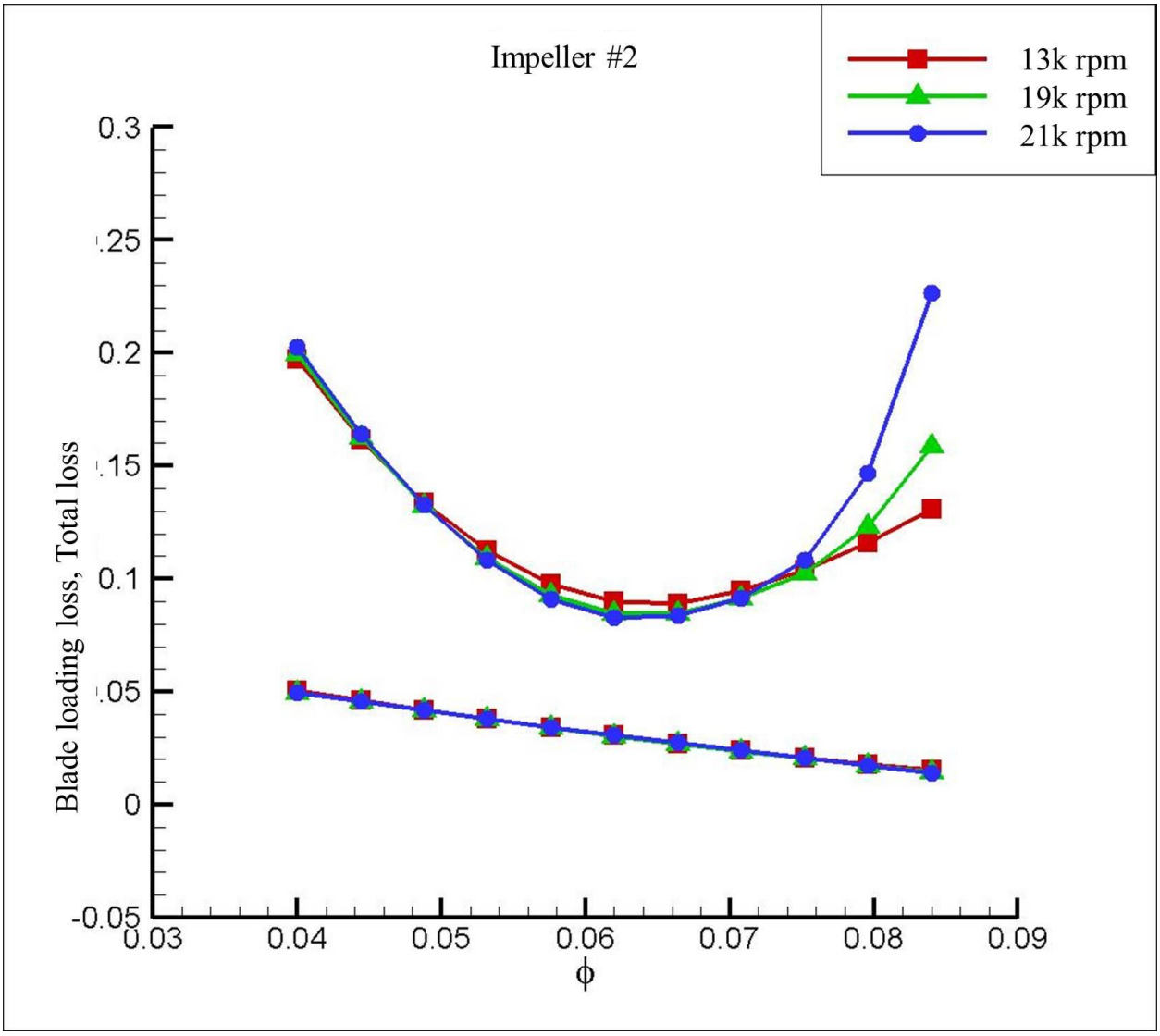

(d) Blade loading loss coefficient according to flow rate along with 3 different speeds.(13k, 19k, 21k rpm)

Fig. 4-4 (cont'd)

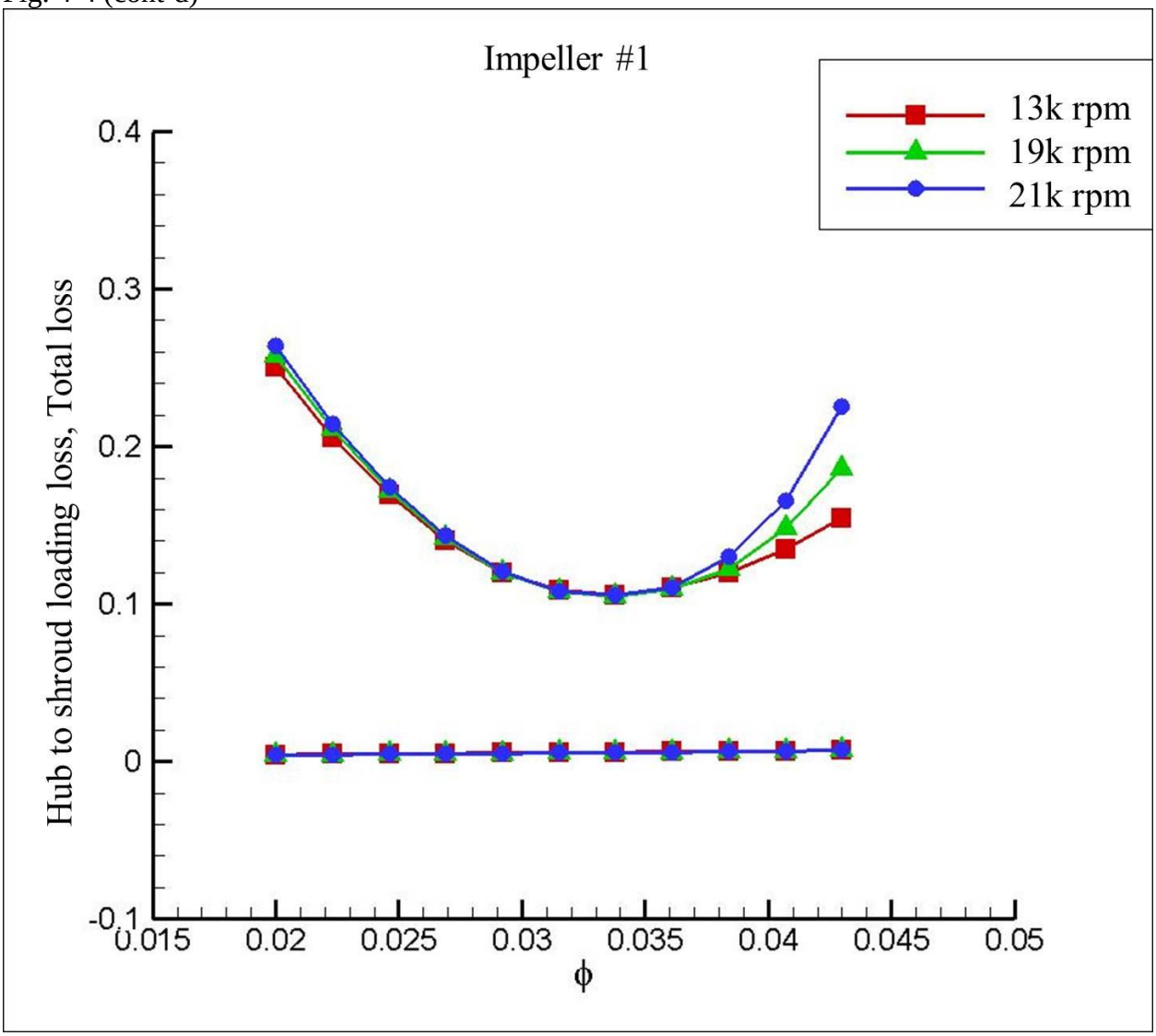
Impeller #1
13k rpm
19k rpm
21k rpm
Hub to shroud loading loss, Total loss
0.4
0.3
0.2
0.1
0
-0.1
0.015
0.02
0.025
0.03
0.035
0.04
0.045
0.05
ϕ

Fig. 4-4 (cont'd)

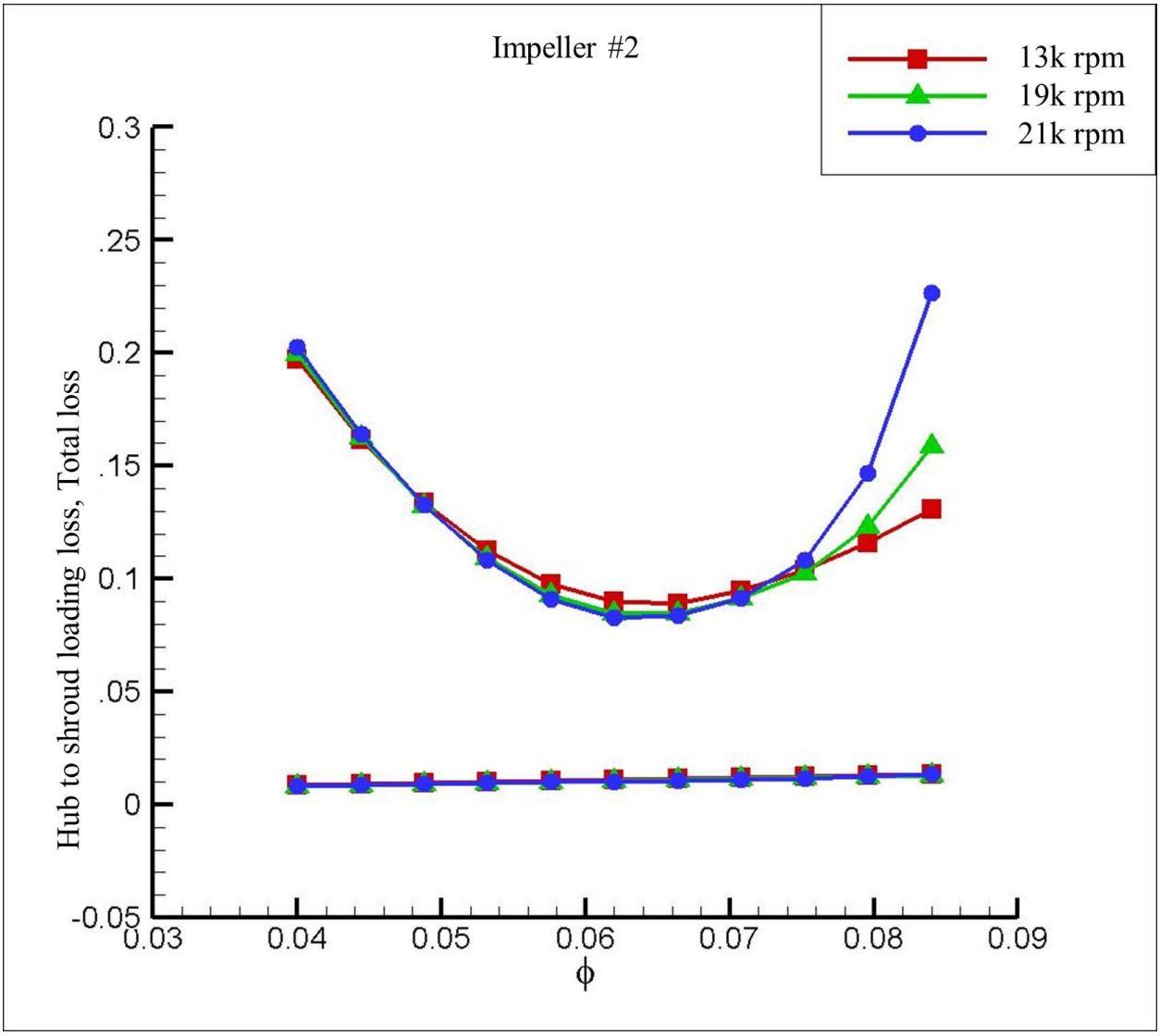

(e) Hub to shroud loading loss coefficient according to flow rate along with 3 different speeds(13k, 19k, 21k rpm)

Fig. 4-4 (cont'd)

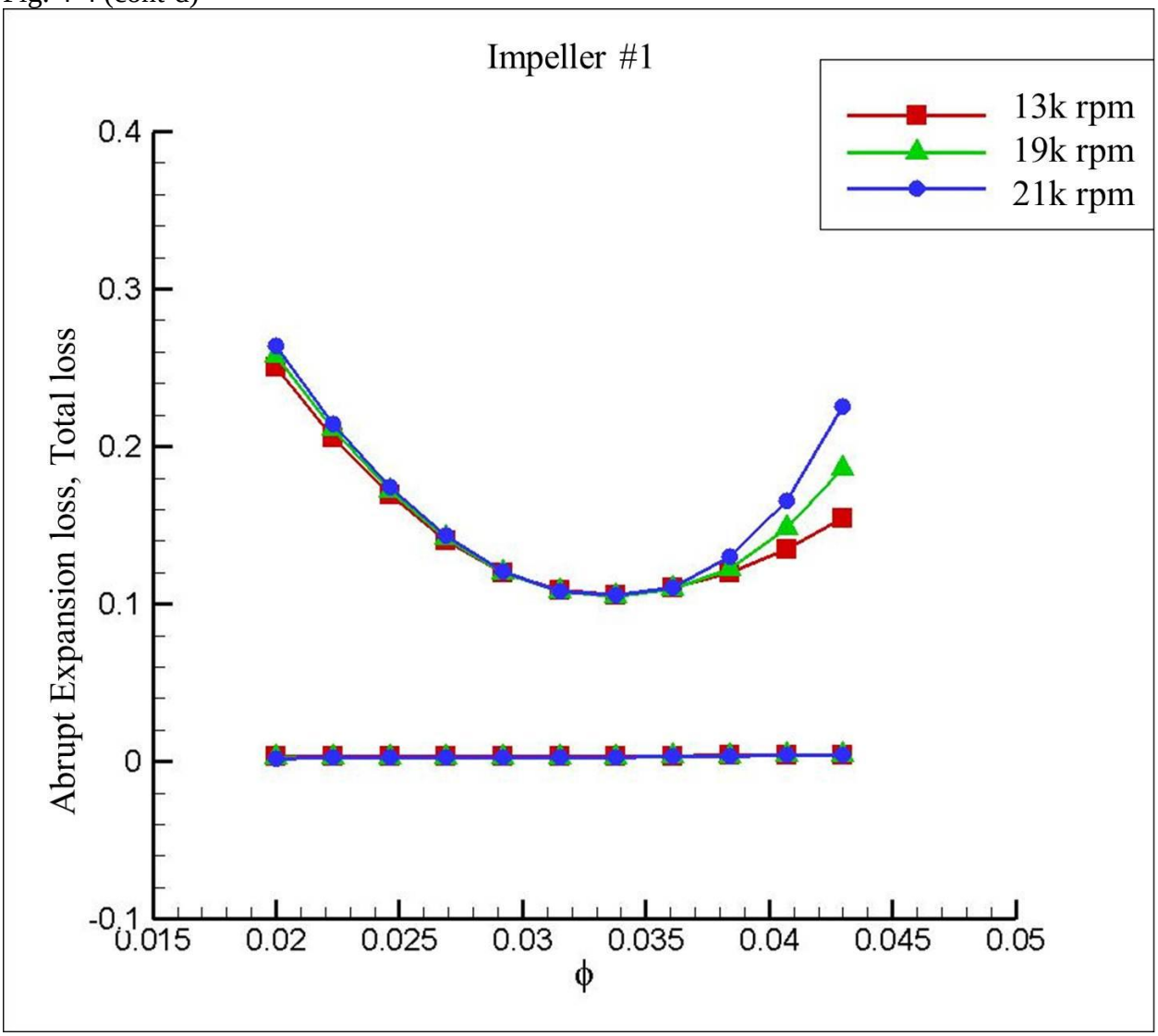
Impeller #1
13k rpm
19k rpm
21k rpm
Abrupt Expansion loss, Total loss
0.4
0.3
0.2
0.1
0
-0.1
0.015
0.02
0.025
0.03
0.035
0.04
0.045
0.05
ϕ

Fig. 4-4 (cont'd)

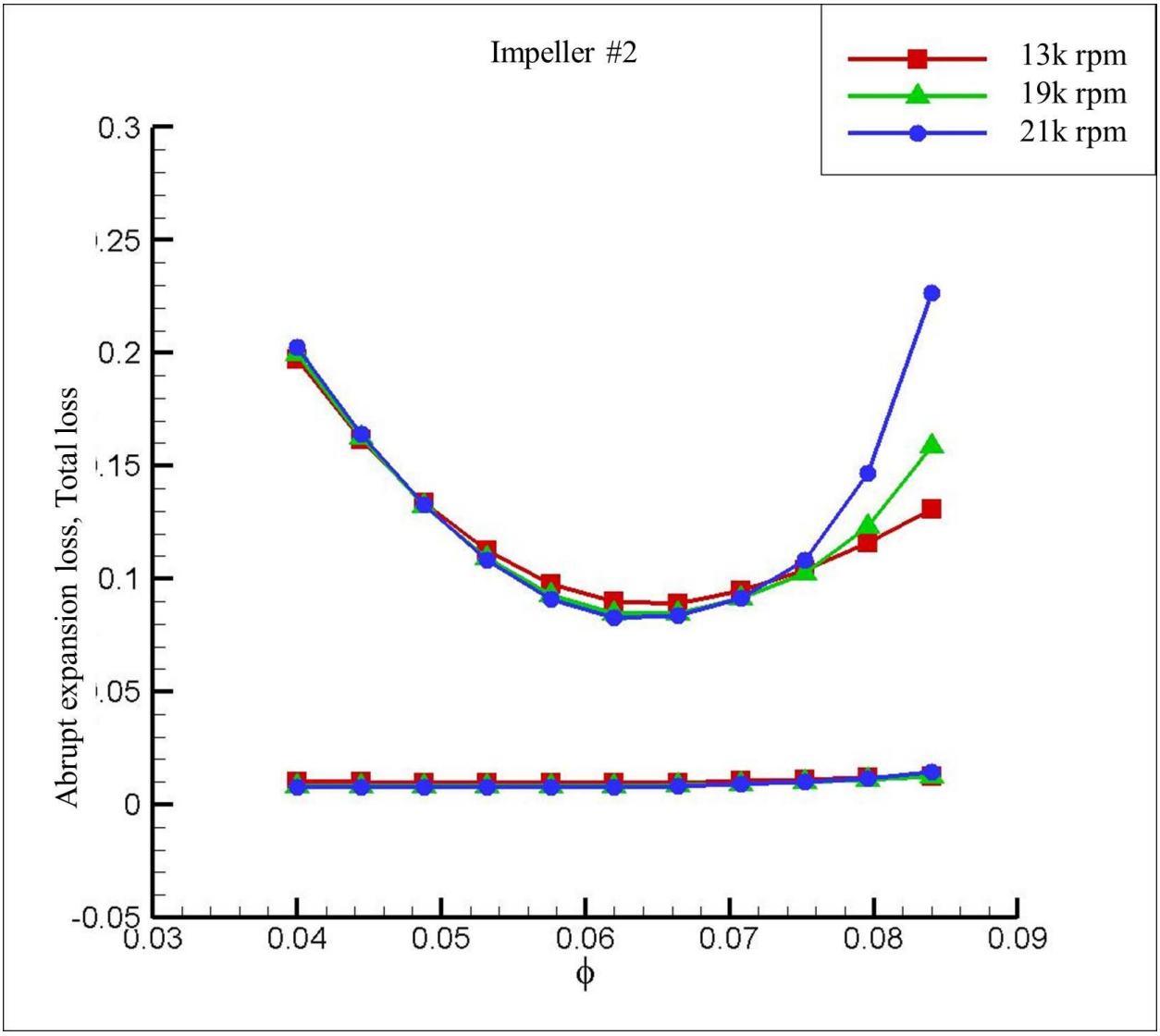

(f) Abrupt expansion loss coefficient according to flow rate along with 3 different speeds.(13k, 19k, 21k rpm)

Fig. 4-4 (cont'd)

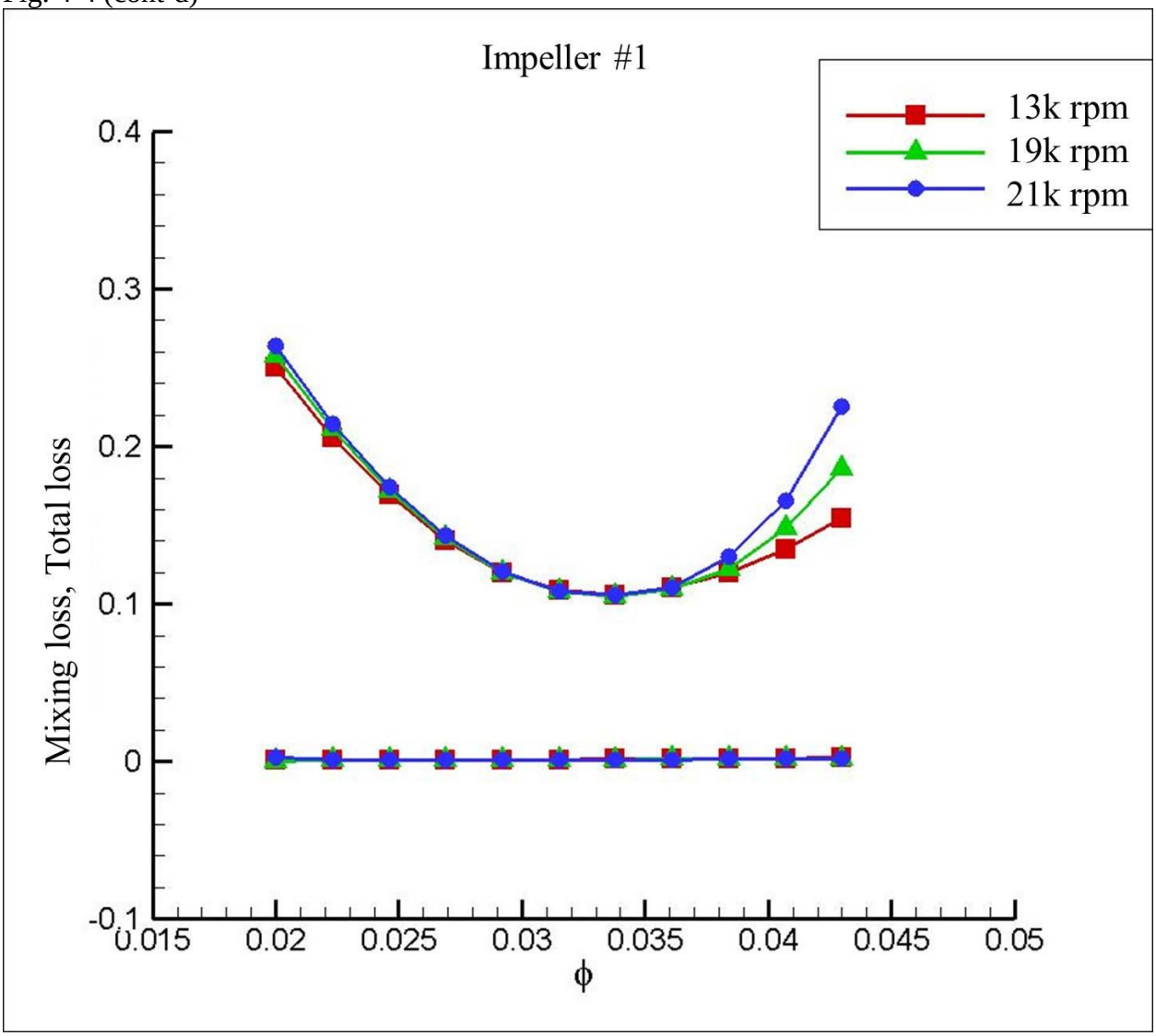
Impeller #1
13k rpm
19k rpm
21k rpm
Mixing loss, Total loss
0.4
0.3
0.2
0.1
0
-0.1
0.015
0.02
0.025
0.03
0.035
0.04
0.045
0.05
ϕ

Fig. 4-4 (cont'd)

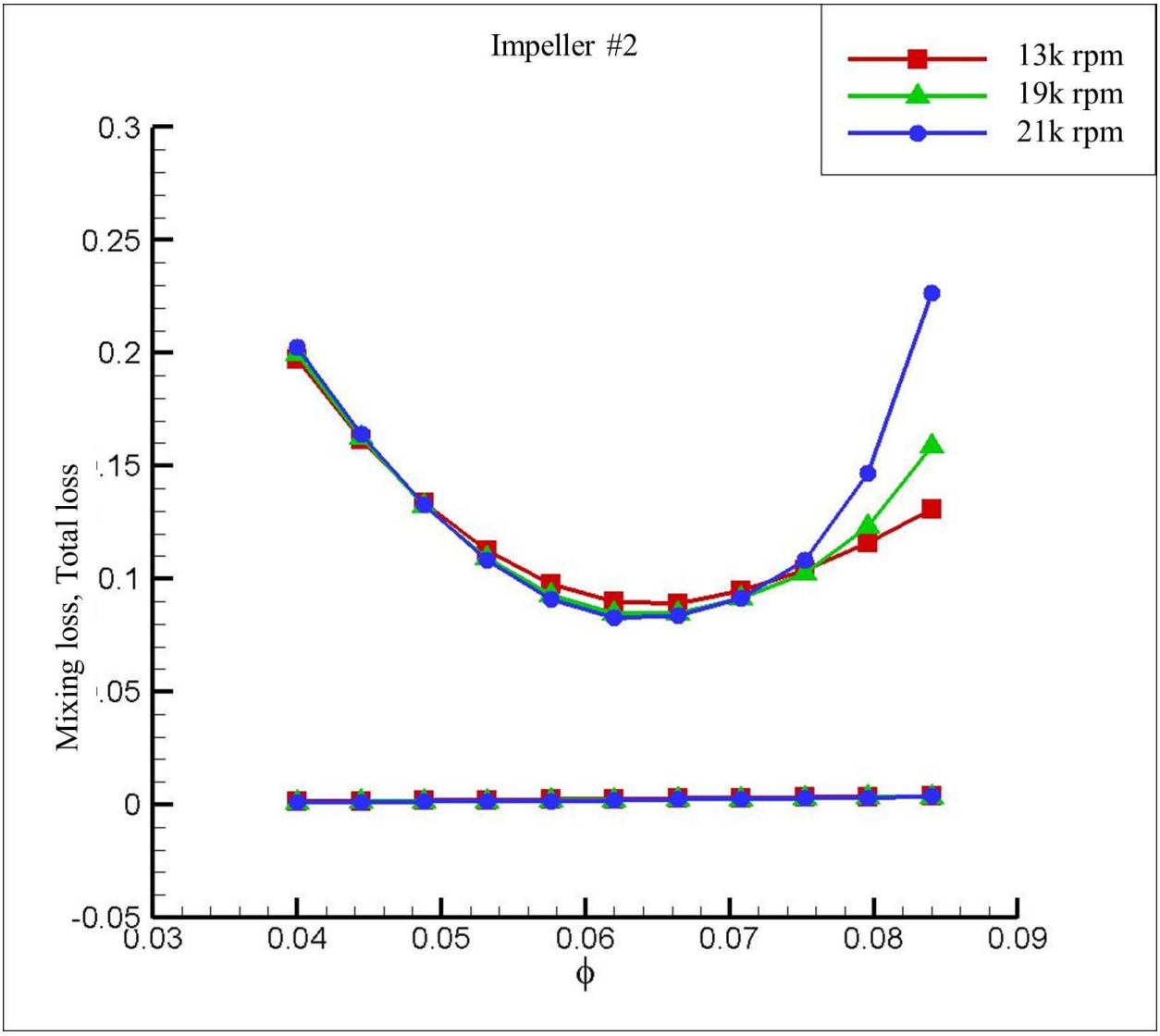

(g) Mixing loss coefficient according to flow rate along with 3 different speeds(13k, 19k, 21k rpm)

4.3. CORRECTED DIFFUSION MODEL IN TWO ZONE MODEL

As discussed in previous section, to improve accuracy of total pressure ratio through the impeller, it is important to predict the diffusion ratio through the impeller. The TEIS model, which is used for predicting the diffusion ratio in the Two-Zone model, divides the impeller passage into two elements as shown in Fig.2-1. Element "a" and element "b" mean impeller inlet to throat and impeller throat to exit respectively. Each element estimates their diffusion ratio and

calculates the diffusion ratio through the impeller whole passage by multiplying. The TEIS model uses pressure recovery effectiveness to estimate relative velocity losses. Using fixed pressure recovery effectiveness through the whole range of flow rates, the TEIS model does not estimate impeller performance in the surge and choking region where the losses are too large to neglect compared to around the design point. To compensate these problems, the TEIS model needs to consider internal losses through the passage.

The internal loss models can be divided into the inlet portion and passage portion. Incidence loss and inlet diffusion loss are included in the inlet category and others are placed in the passage portion. The inlet losses, incidence and inlet diffusion loss, can be applied to element "a". The passage losses can be applied to element "b". To apply all loss models to the TEIS model, all loss models should be calculated.

One of the important things in the Two Zone model and Ron Aungier's method when calculating impeller exit condition is that a different slip factor is applied. The reason for using a different slip factor is that the Two-Zone model does not consider impeller exit aerodynamic blockage, but Ron Aungier's model calculates aerodynamic blockage using an iterative method and applies to the impeller exit area. The blockage makes a different exit velocity diagram so that two different 1D analysis models share the same slip factor. The inlet loss models, incidence loss and inlet diffusion loss, are functions of the inlet condition and not affected by the slip factor. In order to apply all loss models to TEIS, a different slip factor for Two-Zone and loss models should be used. As shown in Fig. 4-4 (b), however, inlet diffusion loss is very useful to predict total loss model and a new slip factor is not necessary to calculate it.

For these reasons, this study focuses on improving the accuracy of the Two-Zone model with TEIS using the inlet loss models. Corrected diffusion models applying to Tow-Zone are the following.

$$\eta_{a,new} = \eta_a \left(1 - 10\bar{\omega}_{dif}\right) \quad \text{(Inlet is diffuser)} \quad (4\text{-}1)$$

$$\eta_{a,new} = \eta_a \Big/ \left(1 - 10\bar{\omega}_{dif}\right) \quad \text{(Inlet is nozzle)} \quad (4\text{-}2)$$

$$0 < \eta_{a,new} < 2$$

4.4. CORRECTED DIFFUSION MODEL RESULTS

The corrected diffusion model is applied to impeller #1 and impeller #2. Table 4-1 shows the effectiveness used in this analysis. New effectiveness is calculated for every flow rate by equations (4-1) and (4-2). The corrected effectivenesses are shown in Fig. 4-5.

	η_a	η_b
Impeller #1	0.79	0.0
Impeller #2	1.0	0.4

Table 4- 1 pressure recovery effectiveness used in this study

Fig. 4-6 and Fig. 4-7 present the head coefficient and work factor calculated by corrected diffusion loss. As shown in the figure, the corrected Two-Zone model can capture the head coefficient and work factor better in the choking region in both impeller #1 and impeller #2. In the surge region, the corrected model overestimates total pressure loss in impeller #1.

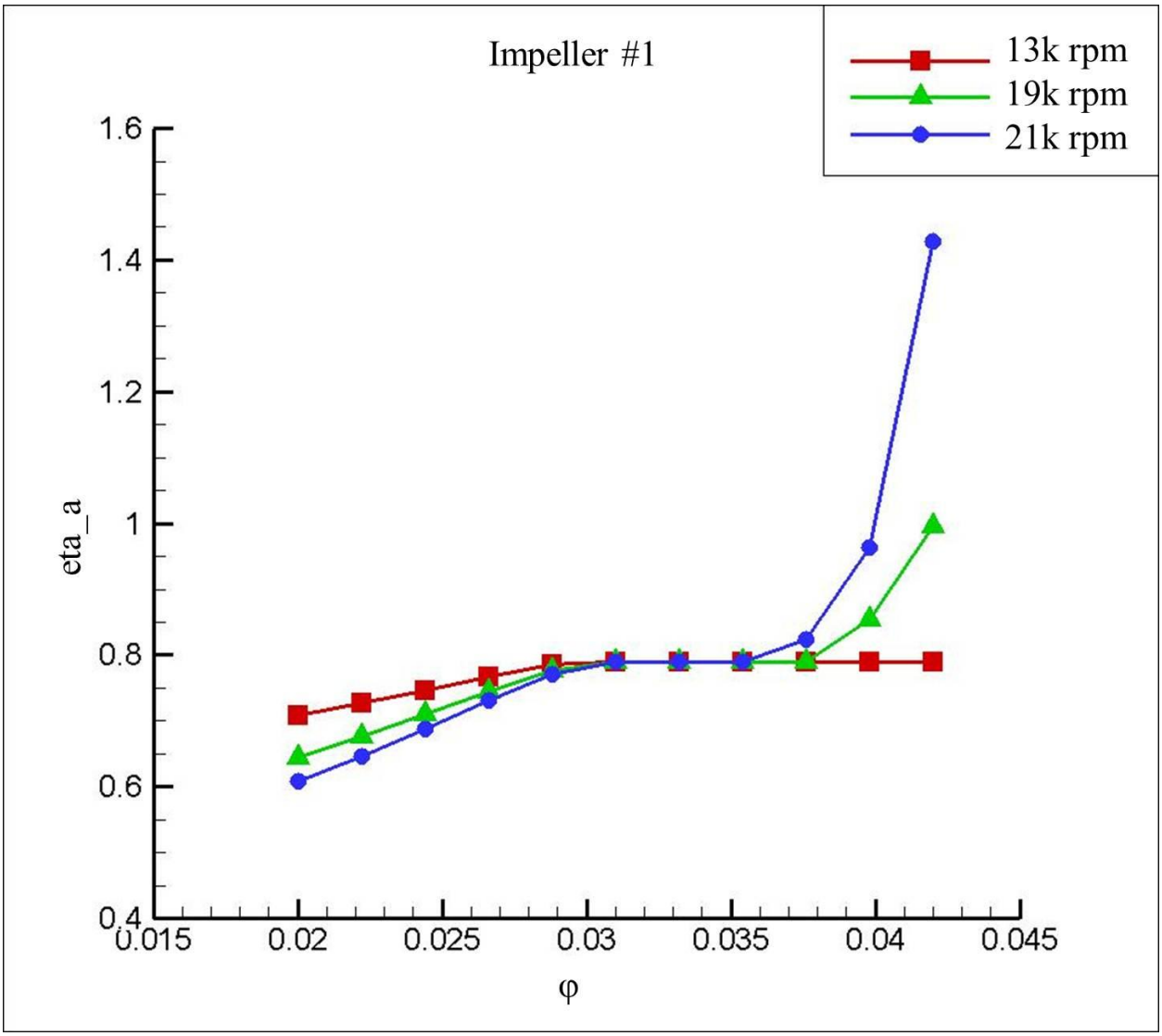

Fig.4- 5 effectiveness calculated by the corrected diffusion model (impeller #1, impeller #2)

Fig.4-5 (cont'd)

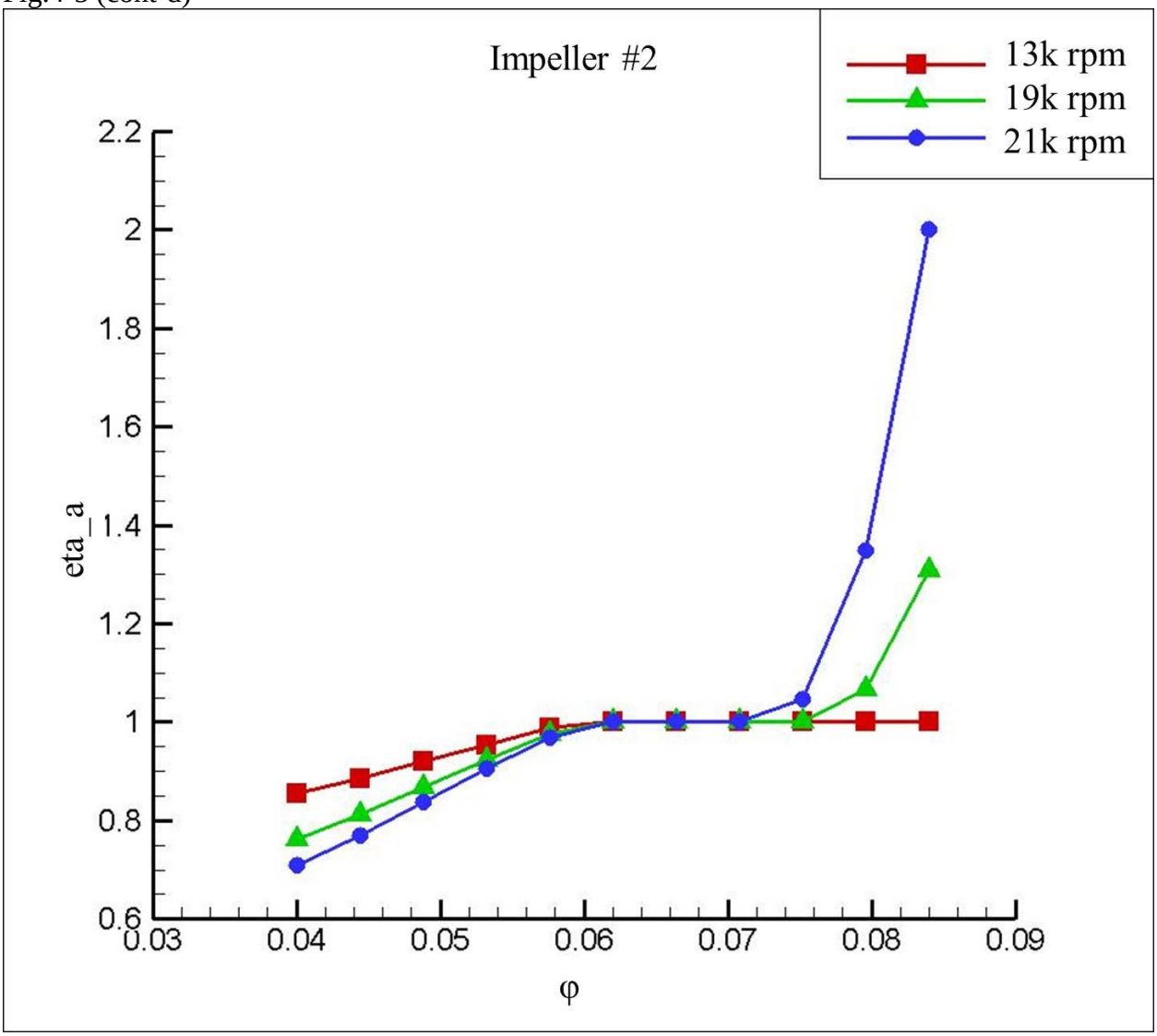
Impeller #2
13k rpm
19k rpm
21k rpm
eta_a
2.2
2
1.8
1.6
1.4
1.2
1
0.8
0.6
0.03
0.04
0.05
0.06
0.07
0.08
0.09
φ

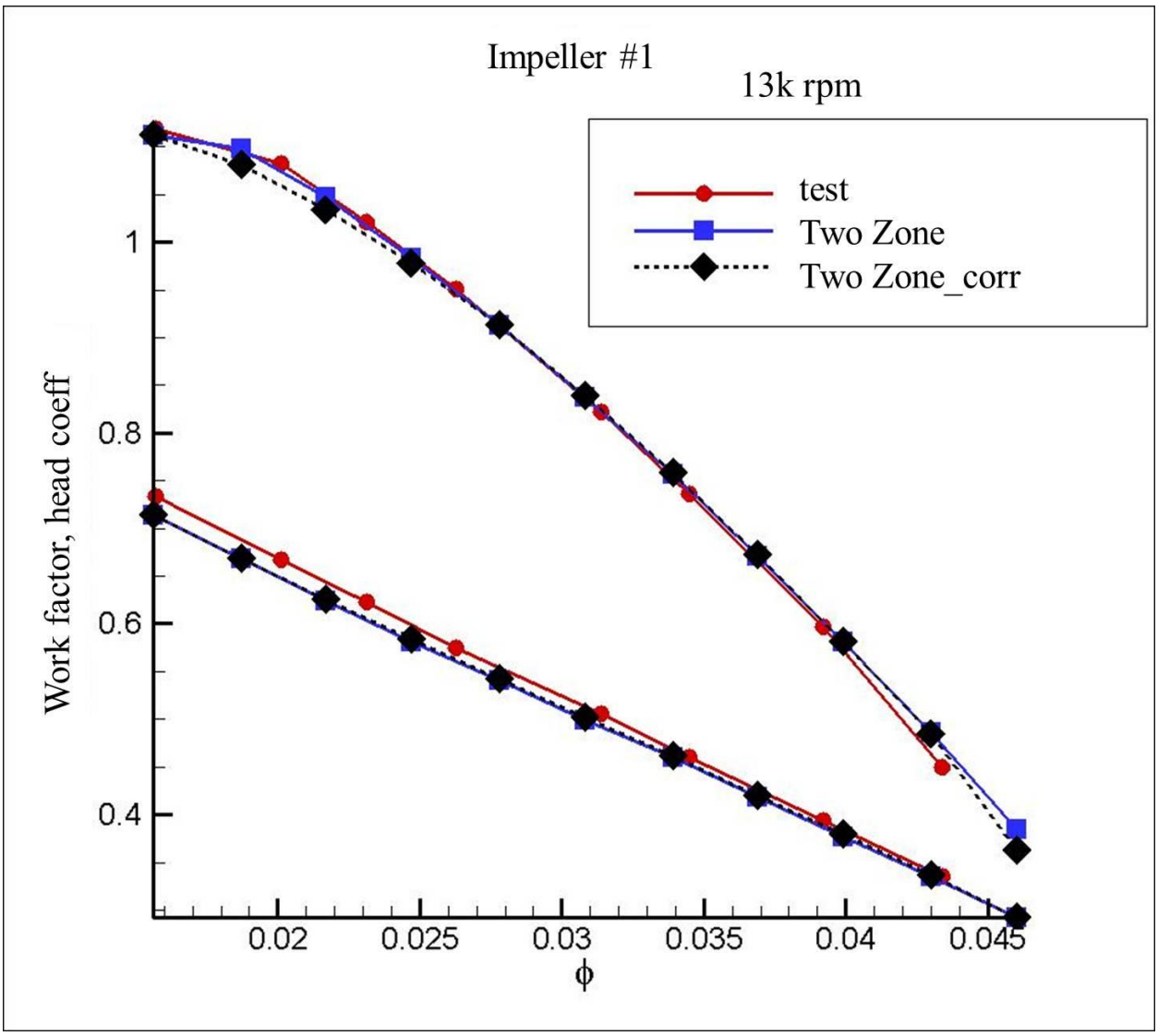

Fig.4- 6 head coefficient and work factor calculated by the corrected diffusion model (impeller #1, 13k, 19k, 21k rpm)

Fig. 4-6 (cont'd)

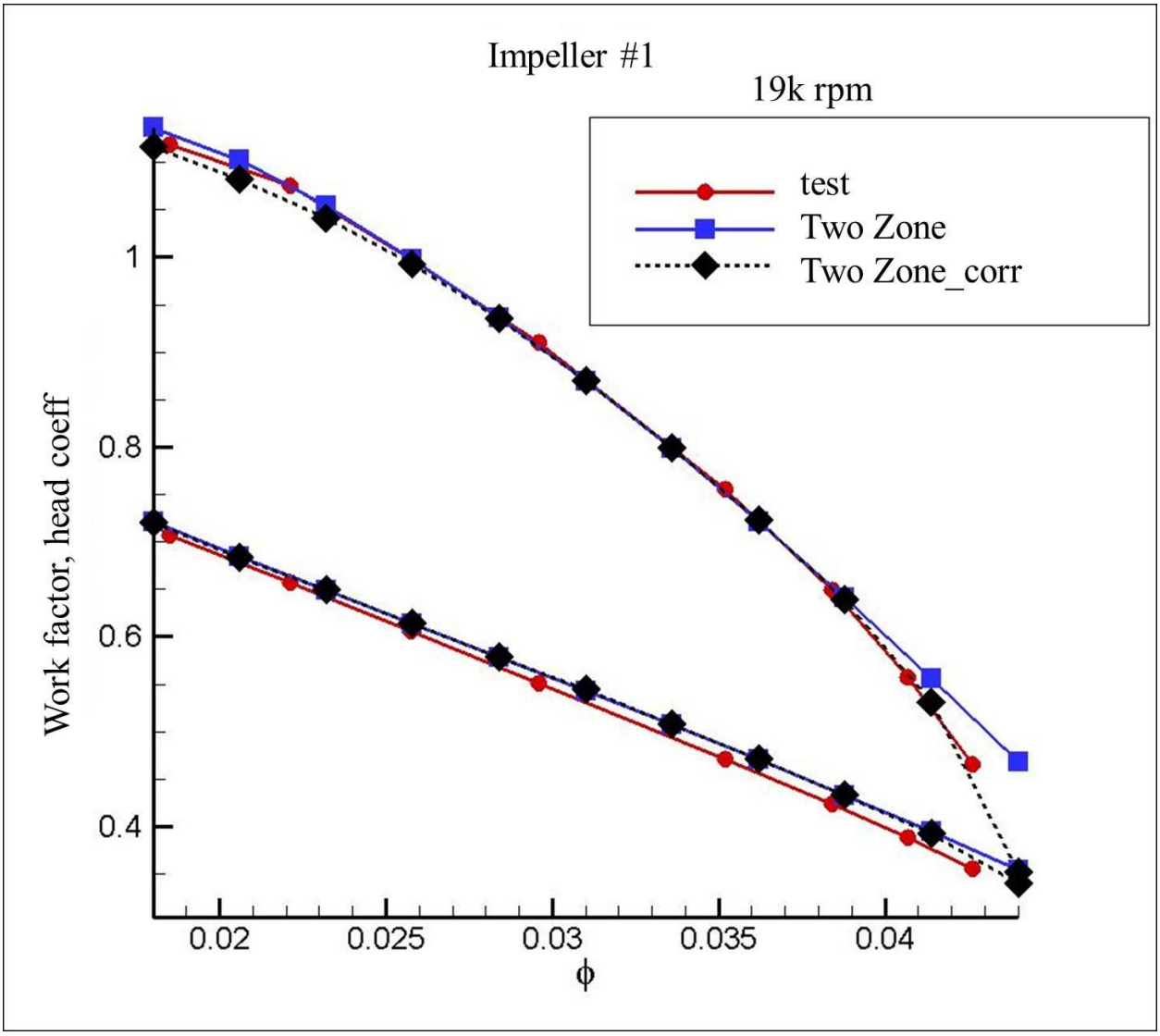
Impeller #1
19k rpm
test
Two Zone
Two Zone_corr
Work factor, head coeff
1
0.8
0.6
0.4
0.02
0.025
0.03
0.035
0.04
ϕ

Fig. 4-6 (cont'd)

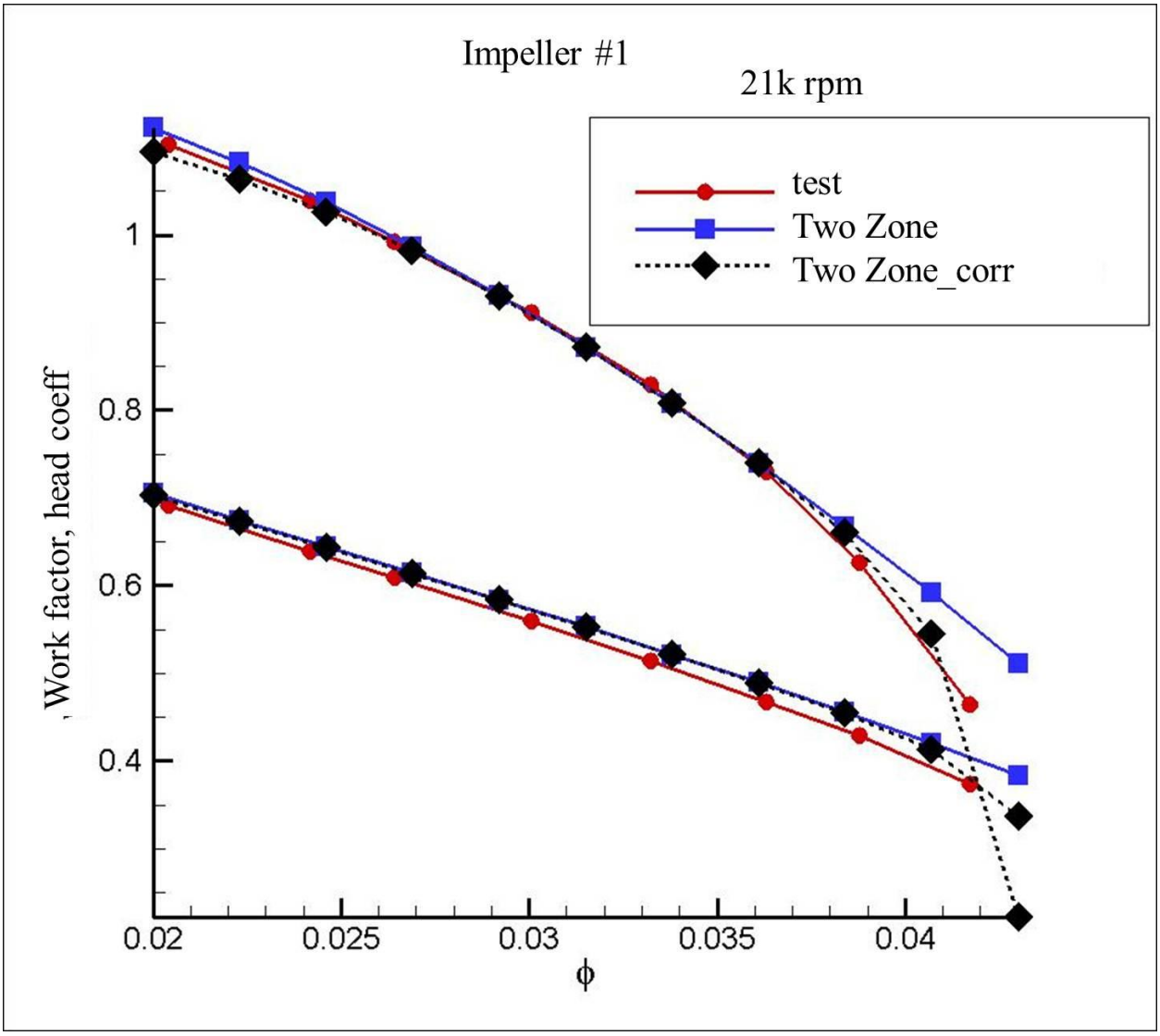
Impeller #1
21k rpm
test
Two Zone
Two Zone_corr
Work factor, head coeff
1
0.8
0.6
0.4
0.02
0.025
0.03
0.035
0.04
ϕ

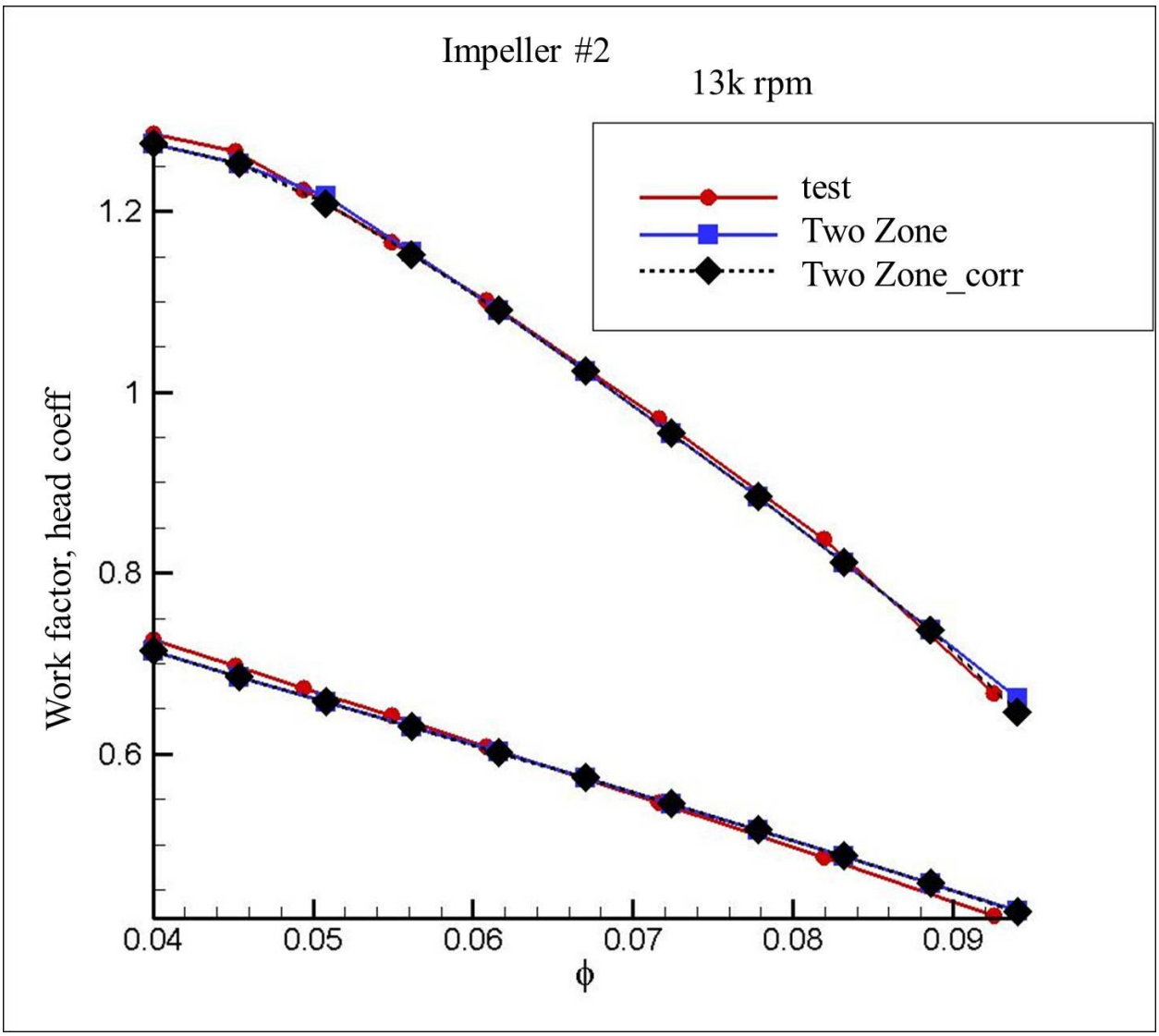

Fig.4- 7 head coefficient and work factor calculated by the corrected diffusion model (impeller #2, 13k, 19k, 21k rpm)

Fig. 4-7 (cont'd)

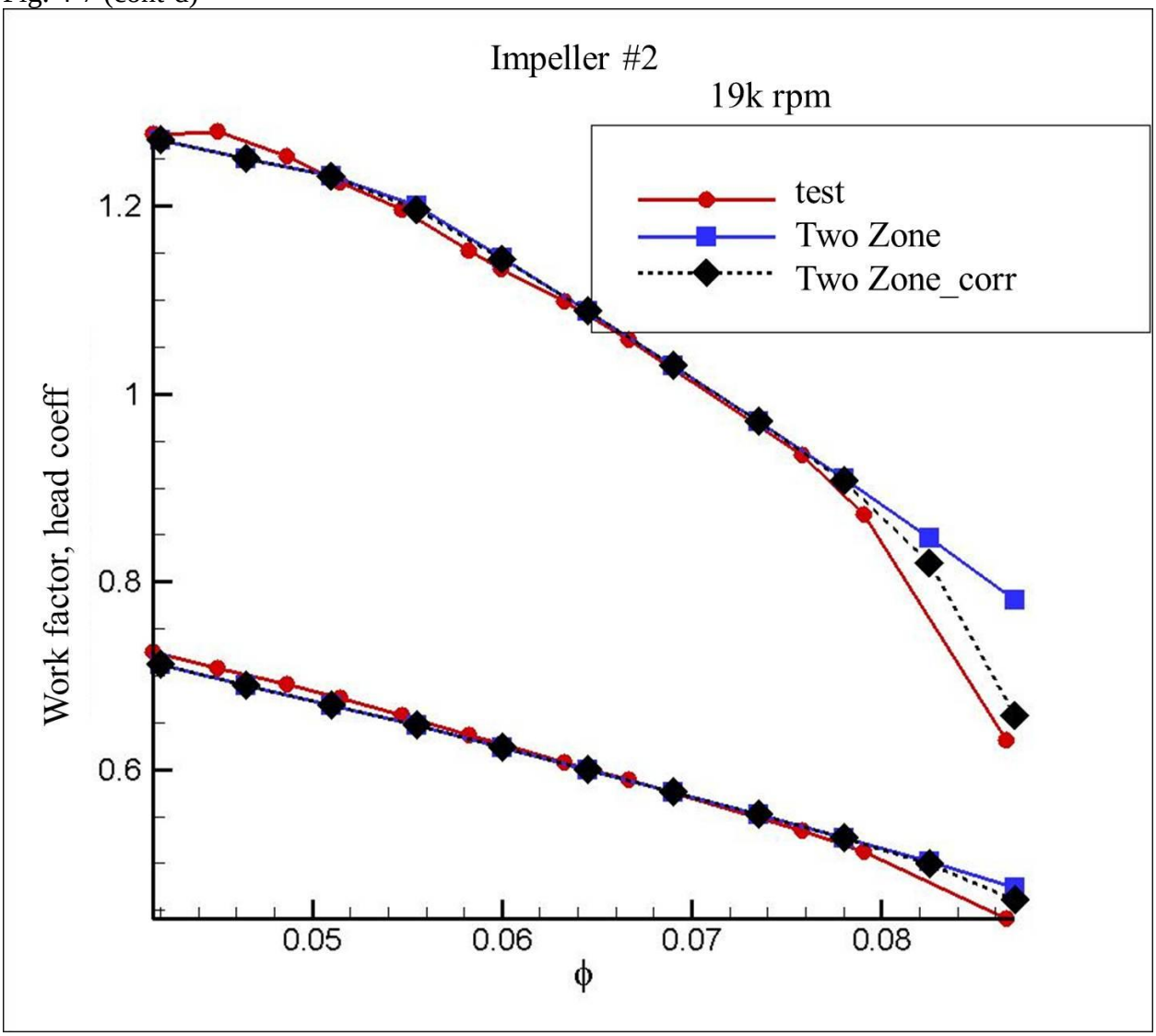
Impeller #2
19k rpm
test
Two Zone
Two Zone_corr
Work factor, head coeff
1.2
1
0.8
0.6
0.05
0.06
0.07
0.08
ϕ

Fig.4-7 (cont'd)

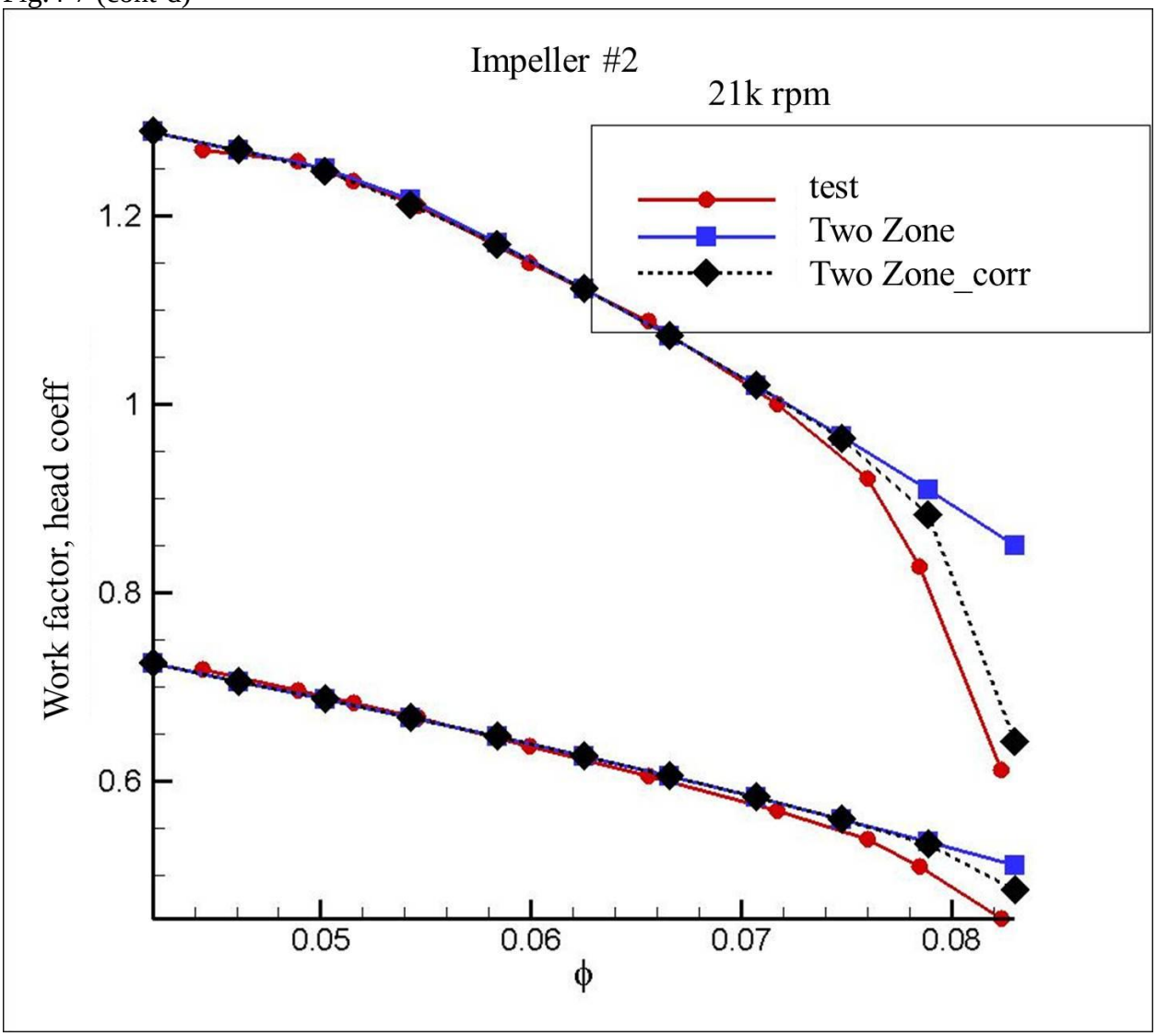
Impeller #2
21k rpm
test
Two Zone
Two Zone_corr
Work factor, head coeff
1.2
1
0.8
0.6
0.05
0.06
0.07
0.08
ϕ

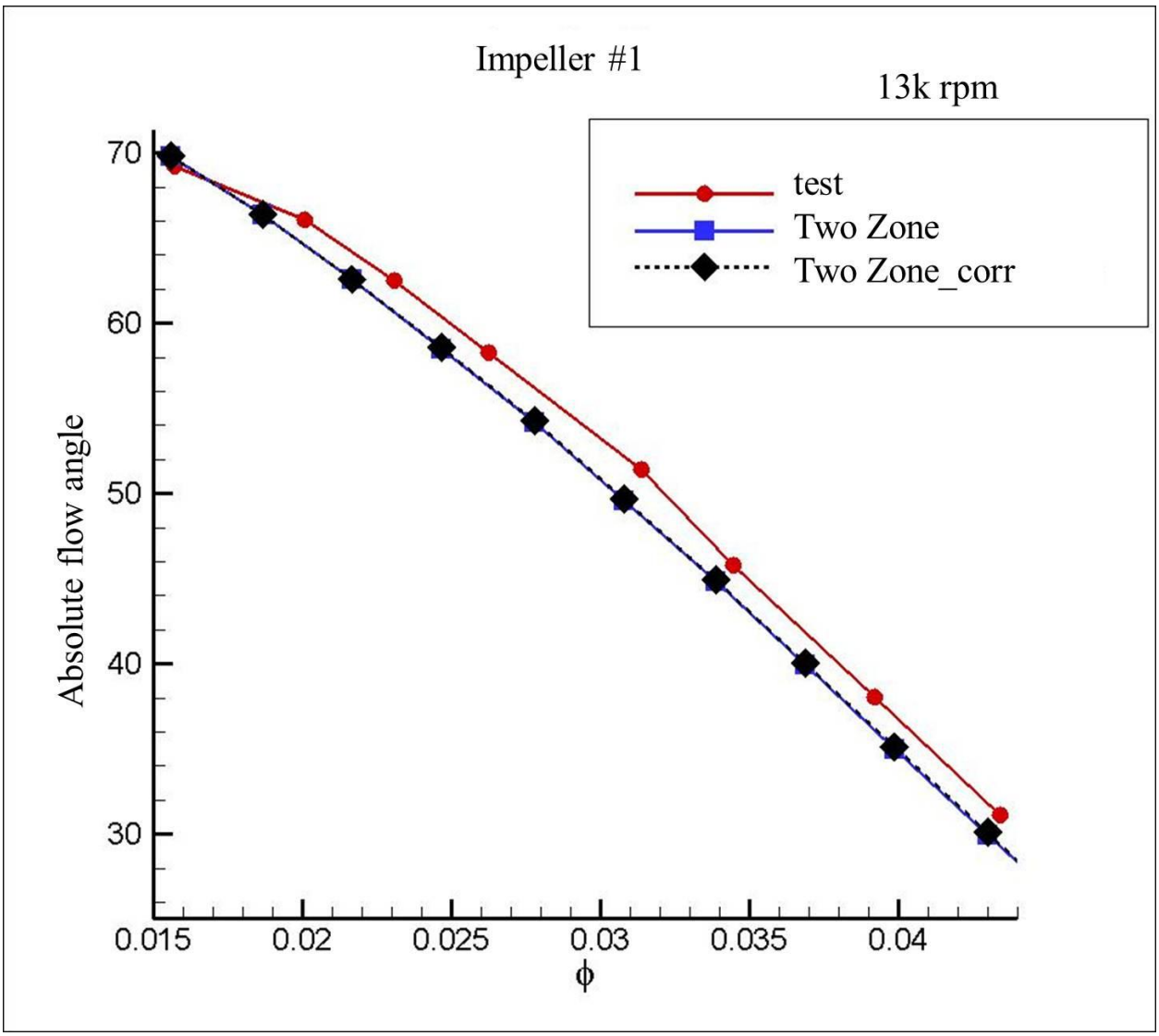

Fig.4- 8 Absolute flow angle calculated by the corrected diffusion model (impeller #1, 13k, 19k, 21k rpm)

Fig.4-8 (cont'd)

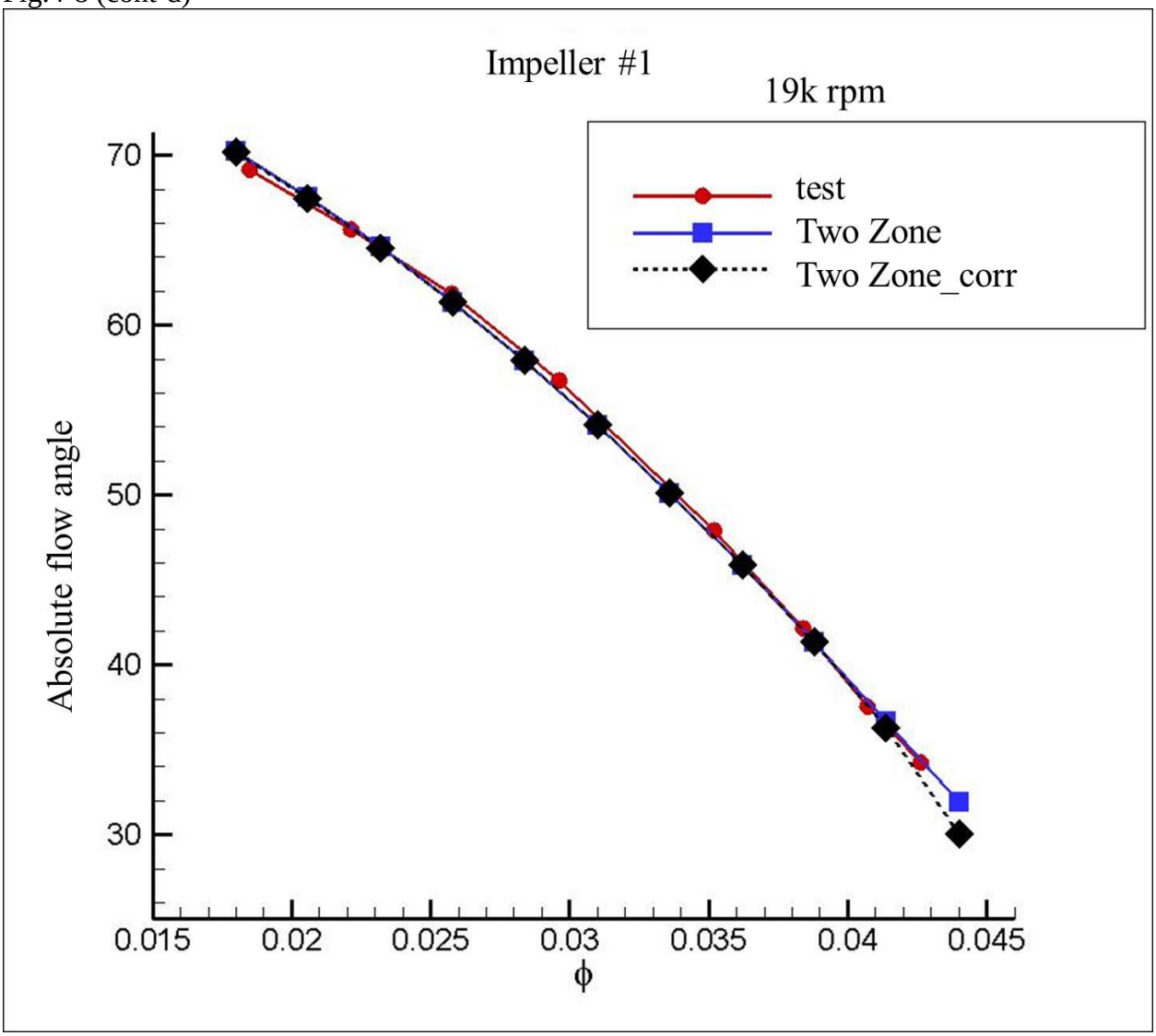
Impeller #1
19k rpm
test
Two Zone
Two Zone_corr
Absolute flow angle
70
60
50
40
30
0.015
0.02
0.025
0.03
0.035
0.04
0.045
ϕ

Fig. 4-8 (cont'd)

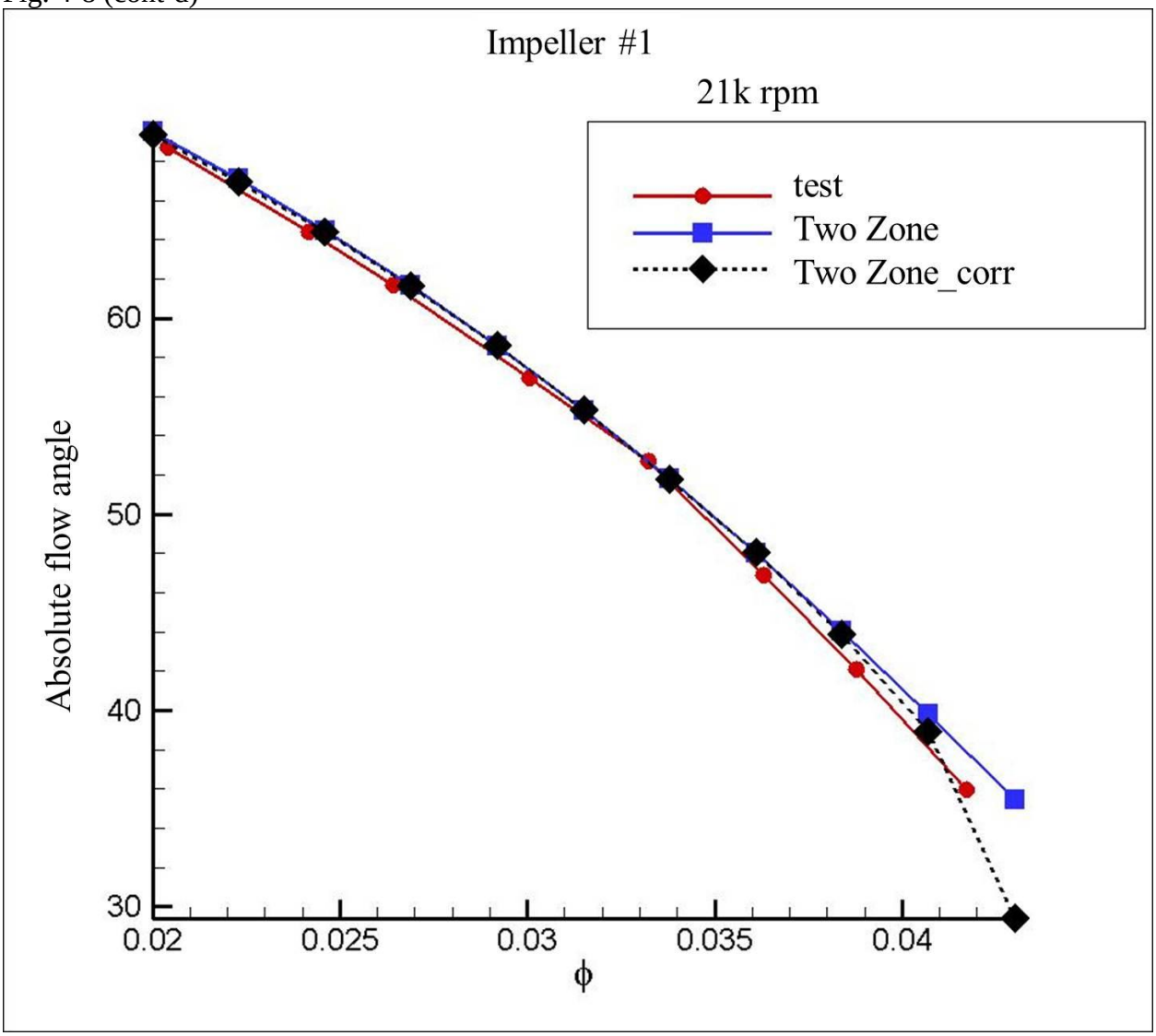
Impeller #1
21k rpm
test
Two Zone
Two Zone_corr
Absolute flow angle
60
50
40
30
0.02
0.025
0.03
0.035
0.04
ϕ

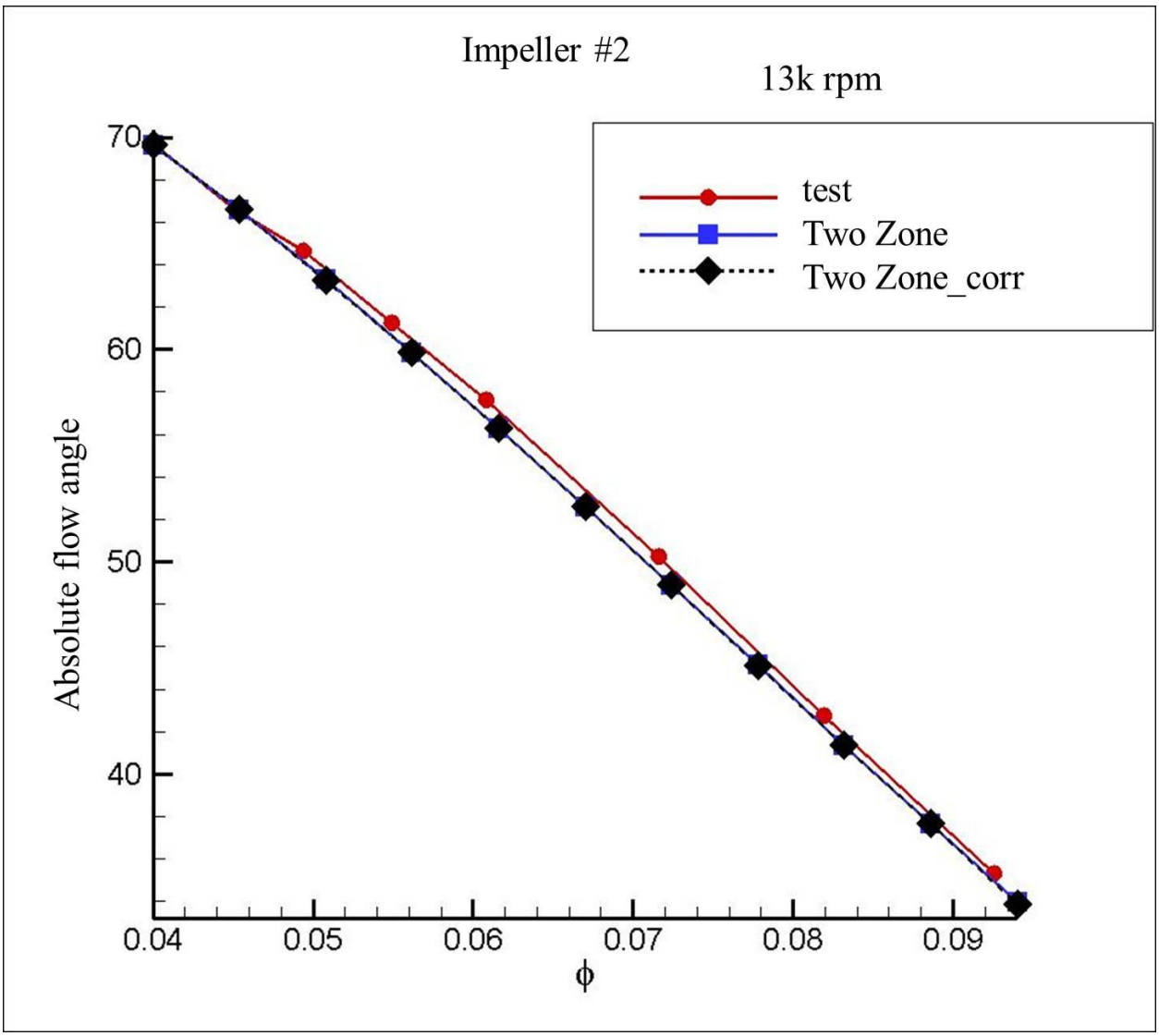

Fig.4- 9 Absolute flow angle calculated by the corrected diffusion model (impeller #2, 13k, 19k, 21k rpm)

Fig. 4-9 (cont'd)

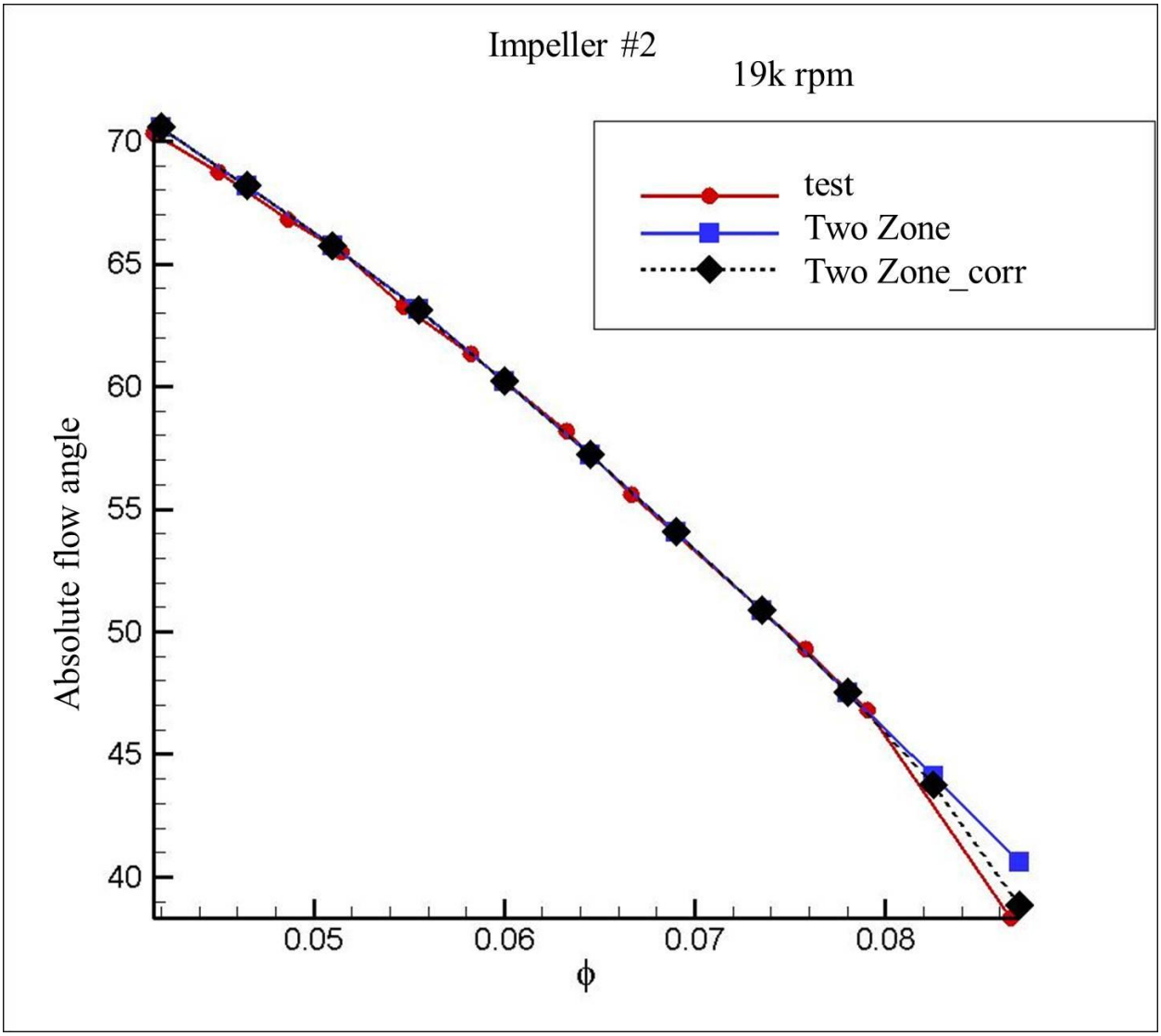
Impeller #2
19k rpm
test
Two Zone
Two Zone_corr
Absolute flow angle
70
65
60
55
50
45
40
0.05
0.06
0.07
0.08
ϕ

Fig.4-9 (cont'd)

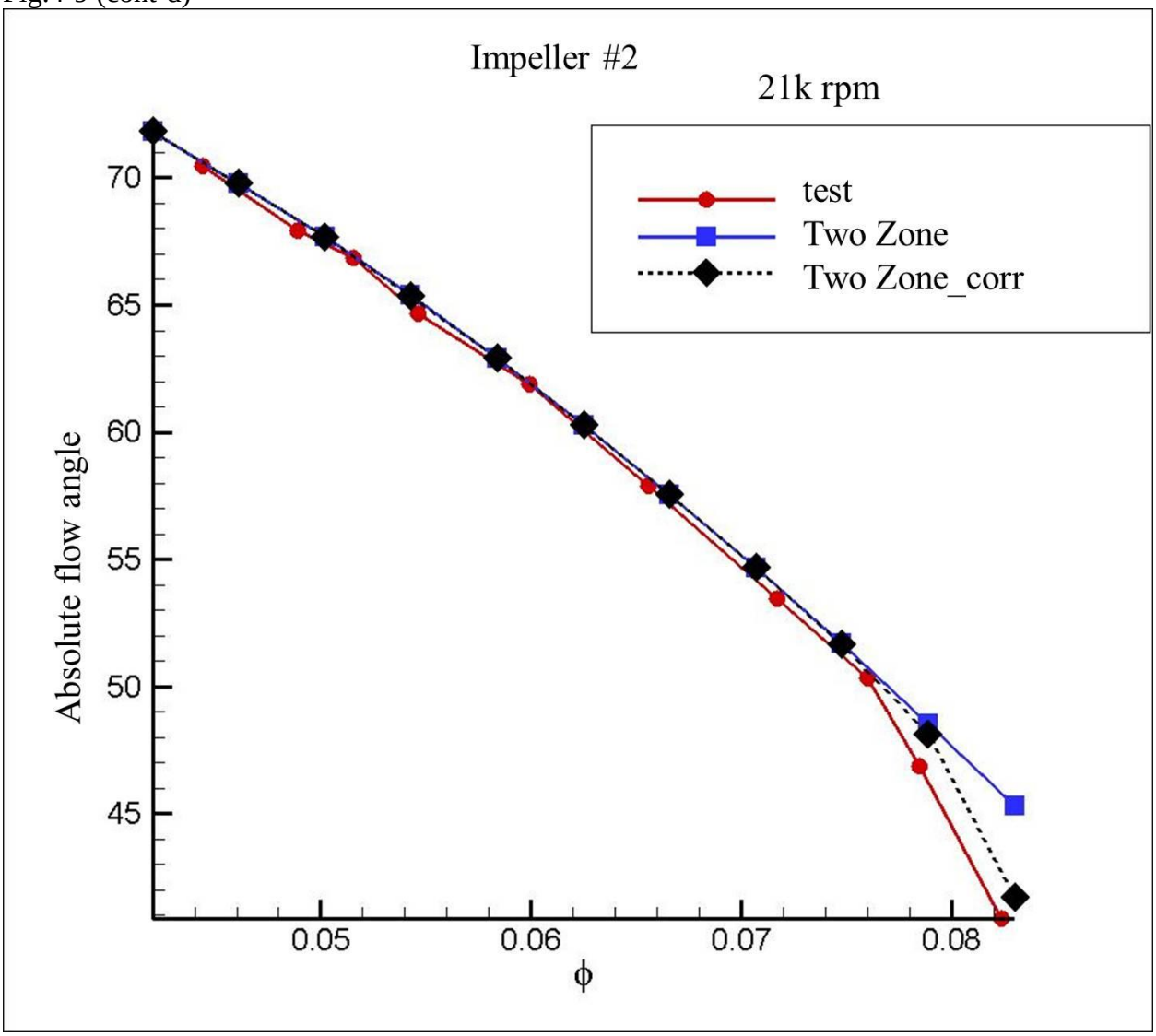

4.5. CONCLUSION

This chapter discussed the diffusion model in 1D analysis and showed a corrected diffusion model to improve the accuracy of the head coefficient prediction. The TEIS model, which is used for the diffusion model in the Two-Zone model, has two pressure recovery effectivenesses to predict relative velocity at the impeller exit. Generally, the pressure recovery effectivenesses are invariant parameter during off design calculation. However, fixed pressure recovery

effectiveness cannot predict an accurate diffusion ratio through the impeller. In order to improve the accuracy of the diffusion ratio, the study applies the impeller inlet loss model to element “a”, inlet portion. By applying impeller inlet loss, the inlet diffusion loss, to the existing diffusion model without other loss models, the accuracy of the Two-Zone model with TEIS is improved. This is because the inlet diffusion loss is changed significantly among total loss models in surge and choking losses.

5. RE-DESIGN IMPELLER

5.1. OBJECTIVE

1D performance analysis has been conducted for the previous chapters. This study showed accurate 1D analysis results and improved accuracy through the corrected model. This chapter is going to show how use 1D analysis when re-designing the existing impeller. The main purpose of the re-design impeller is to make a scaled impeller so that it shows better performance and efficiency than the existing impeller. This chapter shows an impeller re-design procedure using 1D performance analysis and a comparison of the results of 1D analysis and CFD results. Finally, this study compares the CFD results of the original impeller and the re-designed impeller. The requirements of re-design process maintain a machine Mach number of 0.7 and a design point flow coefficient of 0.025.

5.2. ORINAL IMPELLER

The characteristics of the original impellers, two different tip widths, are presented in Table 5-1. As shown in Table 5-1, the impeller with a wider tip width gives an additional surge margin. The head coefficient is decreased by 8.2% and diffusion ratio is increased by 24% because of a wider tip width condition. The corrected machine Mach numbers of 0.75 are same. Fig. 5-1 shows the meridional shape of impeller.

Table 5- 1 Information of the original impeller

b2/d2	0.0393	0.0294
Flow Coefficient, Φ	0.0245	0.0245
Head Coefficient, Ψ	1.22	1.12
Rotor efficiency	0.84	0.84
Work factor, q	0.73	0.675
Surge Margin	20%	40%
Diffusion ratio W_2/W_{1t}	0.62	0.77
Flow angle, α_2	79.5	79.5
Backsweep angle	45	45
Machine Mach #, Mn	0.75	0.75

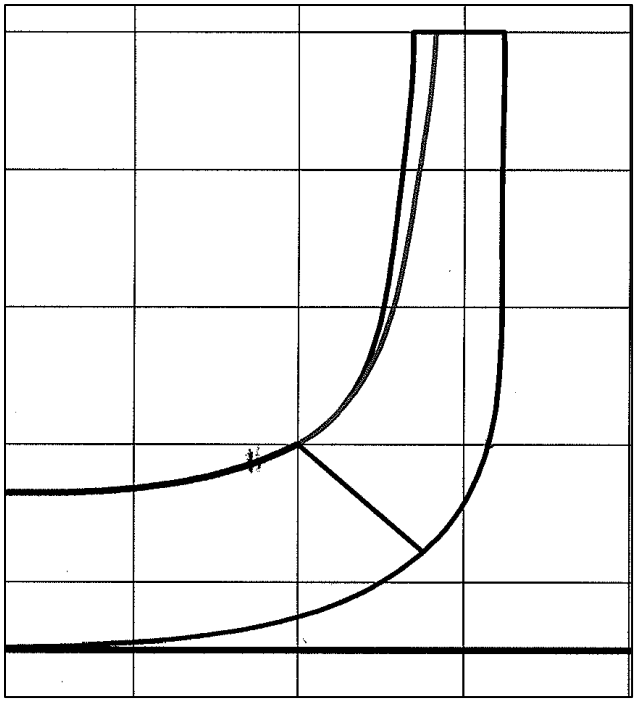

Fig. 5- 1 Meridional shape of the original impeller with wider and smaller tip width.

5.2.1. 1D PERFORMANCE ANALYSIS OF ORIGINAL IMPELLER

Before conducting the re-design procedure, this study performed a 1D analysis on the original impeller with a wider tip width. Fig. 5-2 shows the head coefficient, the work factor total to total efficiency, the results of 1D performance analysis of original impeller using the Ron Aungier's method, and the corrected Two-Zone model. As shown in the figure, Ron Aungier's method predicts these properties better than the Two Zone model. Fig. 5-3 and Fig. 5-4 show an absolute flow angle at the impeller exit and a diffusion ratio through the impeller passage, which are the result of two 1D analysis methods. As the figure shows, the results of the absolute flow angle at the impeller exit are fairly well predicted in both analysis methods. The results of the diffusion ratio show that Ron Aungier's method is more accurate in the diffusion ratio.

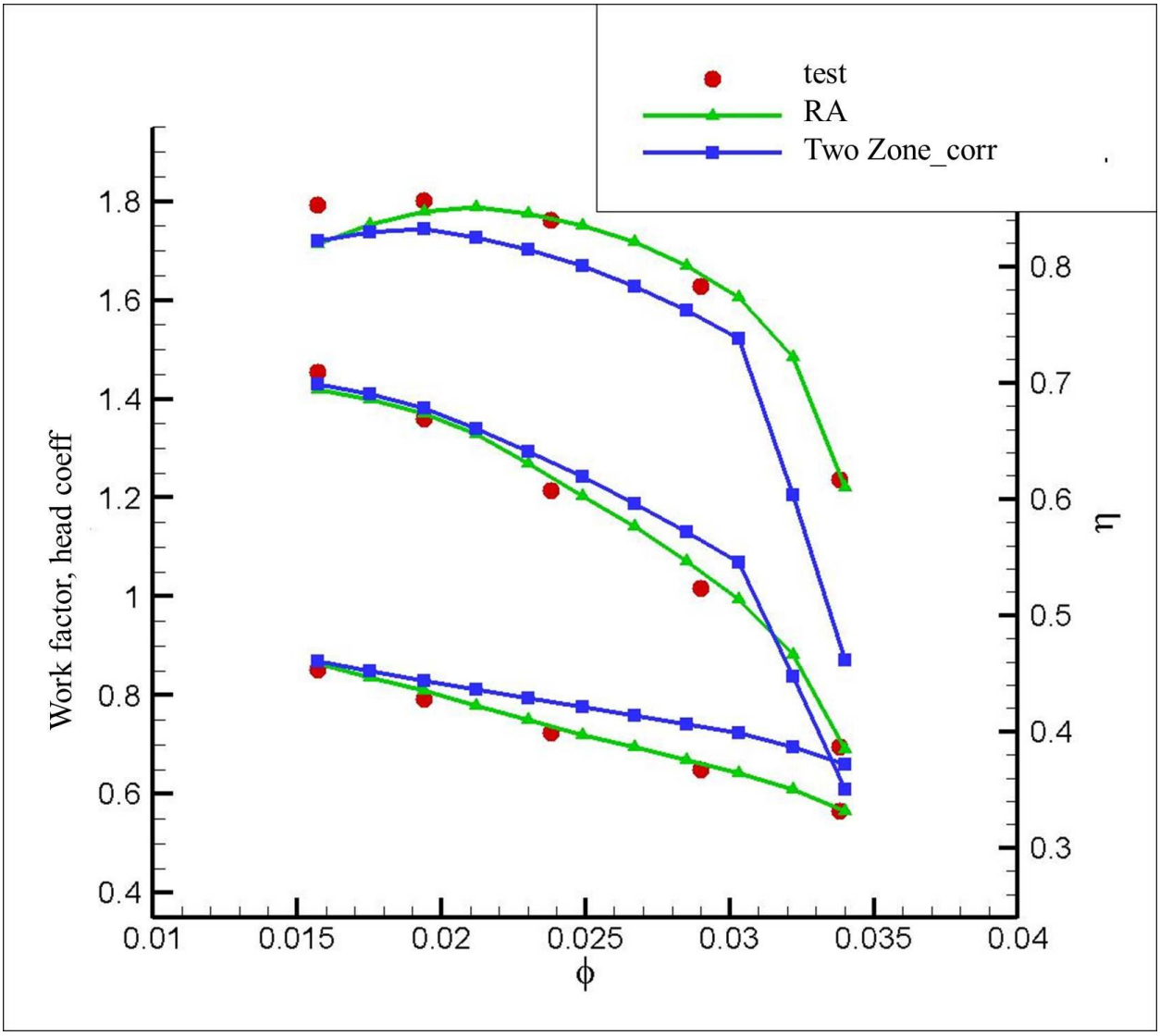

Fig. 5- 2 Comparing work factor, head coefficient and efficiency, the 1D analysis results, with test data (original impeller)

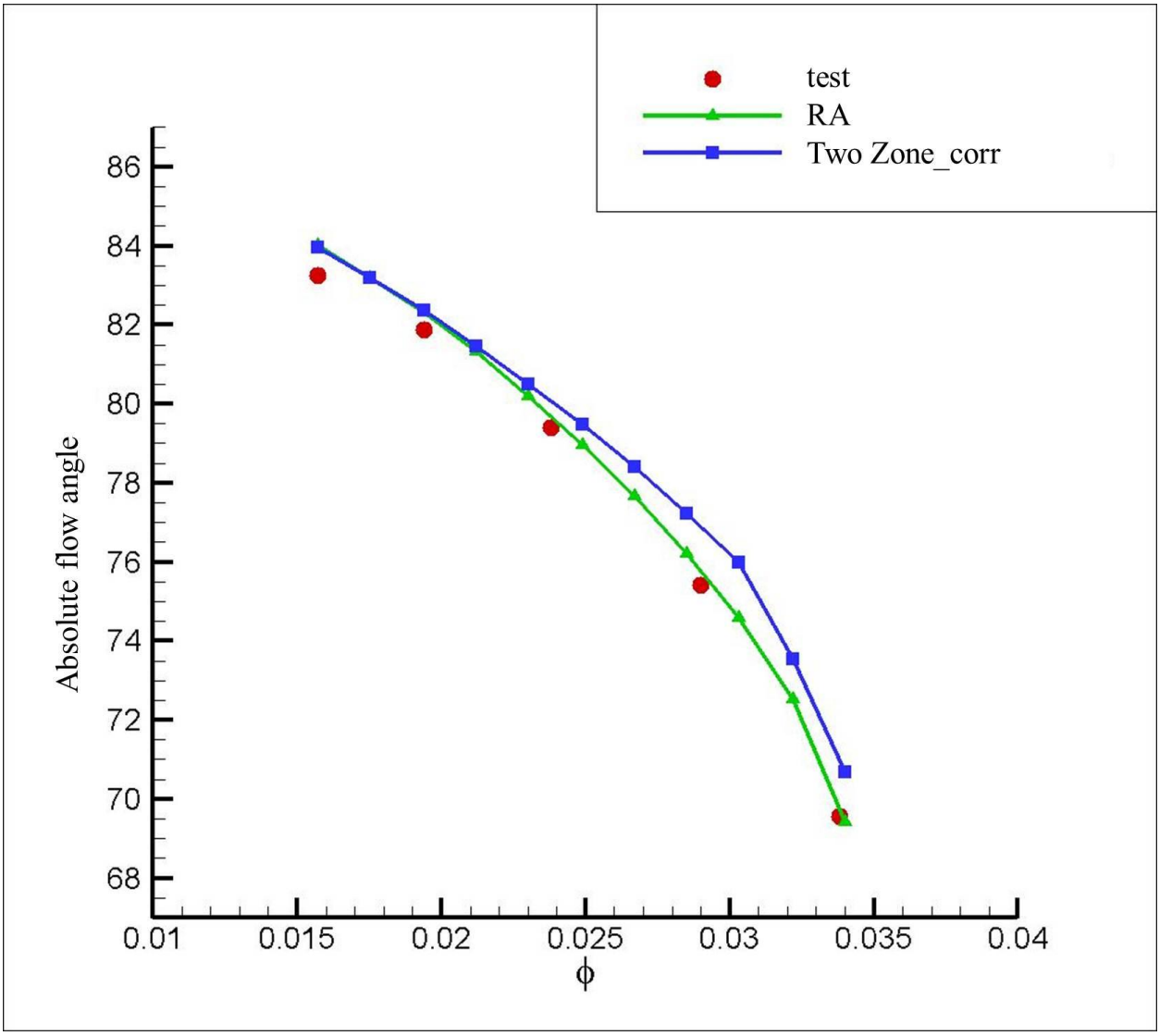

Fig. 5- 3 Comparing absolute flow angle, 1D analysis, with test data (original impeller)

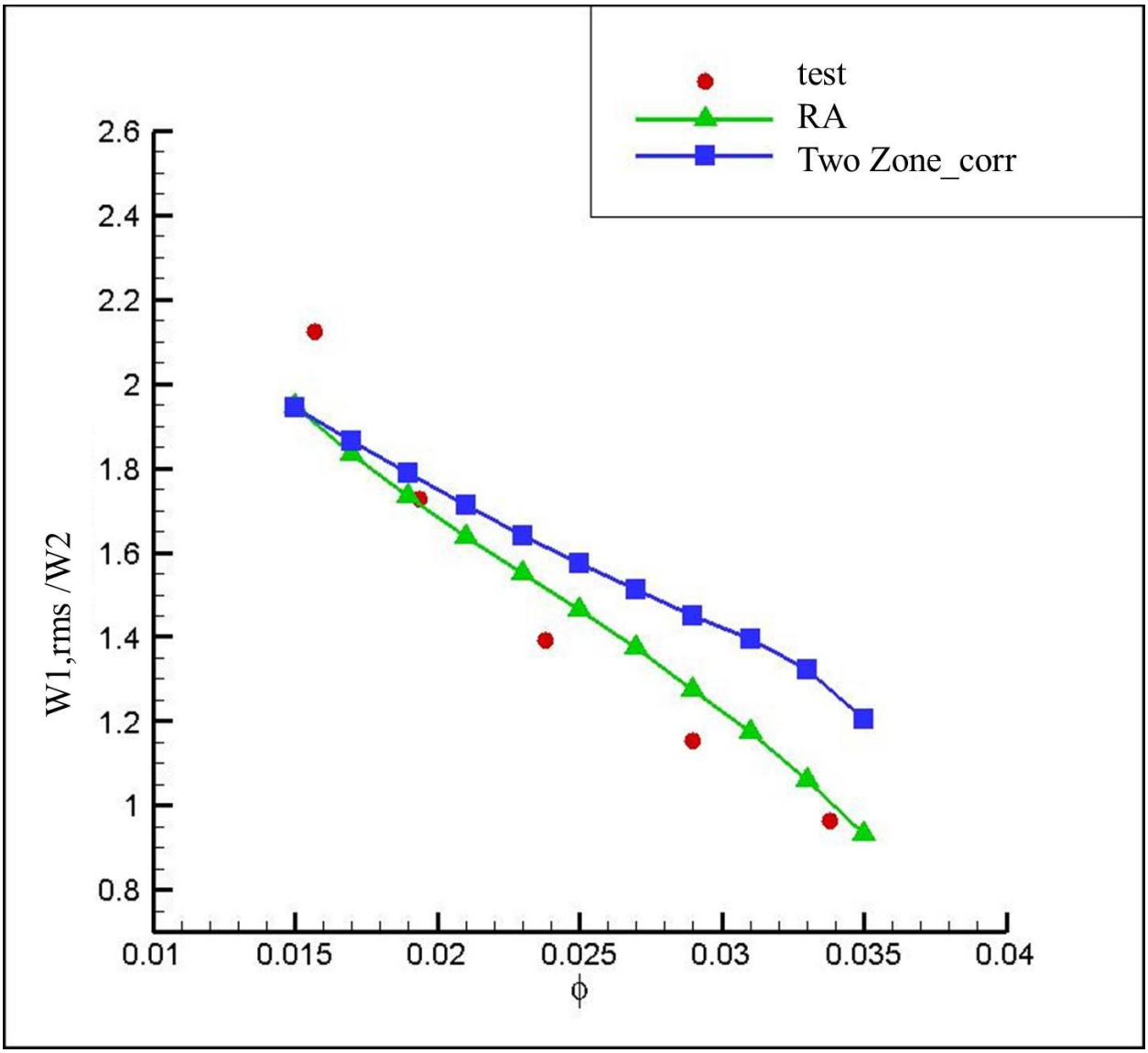

Fig. 5- 4 Comparing diffusion ratio, 1D analysis, with test data (original impeller)

5.3. INVERSE DESIGN USING 1D ANALYSIS CODE

This study shows the re-design procedure using the 1D analysis method. The centrifugal compressor design starts with a 1D preliminary design. However, when the new impeller characteristics were similar to the existing impeller or redesign, 1D performance analysis can be used instead of the preliminary design. This is beneficial to reduce the range of the variables, which is needed for the preliminary design procedure. A main issue of the redesign in this study

is finding trade-off points of the impeller tip width and the impeller blade exit angle. To make a better head increase, the blade exit angle (from radial) must decrease keeping with impeller tip width. However, as the blade exit angle decreases, impeller tip width needs to decrease to maintain efficiency. To find the trade-off point, this study conducted 1d performance analysis changing both blade exit angle, and impeller tip width keeping with other variables. Fig. 5-5 shows blade exit angle (from tangential) at the best efficiency point according to the flow coefficient [12]. As shown in Fig. 5-5, the blade exit angle near the designated impeller design point, at the best efficiency point is roughly from 40 to 50 degree.

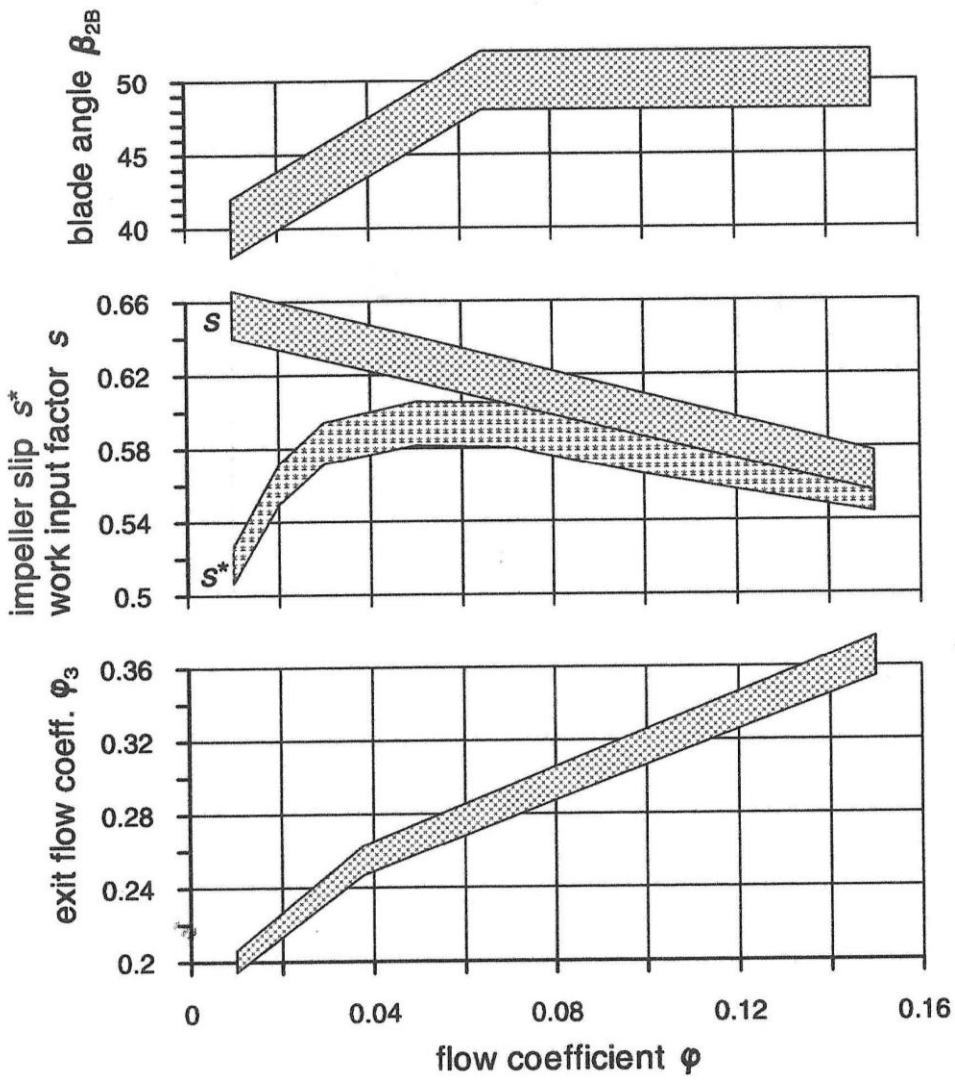

Fig. 5- 5 Impeller exit flow coefficient, impeller slip factor, work input factor and blade angle (from tangent) as functions of the inlet flow coefficient (empirically determined values for the best efficiency point) [12]

5.3.1. DIFFUSION RATIO

The diffusion ratio affects impeller efficiency and head rise. The lower diffusion ratio drops the impeller efficiency but brings on a head rise. Therefore, it is important to determine the diffusion ratio through the impeller. Generally, the diffusion ratio (W_2/W_{1t}) lies on between 0.55 and 0.70. In order to make a high performance impeller, the diffusion ratio approaches 0.55; and to make high efficiency impeller, the diffusion ratio becomes close to 0.70.

The diffusion ratio ($W_{1,rms}/W_2$) that resulted from the 1D performance analysis on the original impeller is shown in Fig. 5-4. Based on the 1D analysis results of the diffusion ratio, the diffusion ratio of the re-design impeller was determined. Fig. 5-6 shows the diffusion ratio according to impeller tip width (b_2) and impeller blade exit angle (β_2). As shown in the figure, the impeller tip width becomes larger as blade angle increases to keep the diffusion ratio. The cases used in this study are determined by Fig. 5-6. Four cases are selected by the diffusion ratio of 0.62, with considering both head rise and efficiency. Table 5-2 shows four cases used in this chapter.

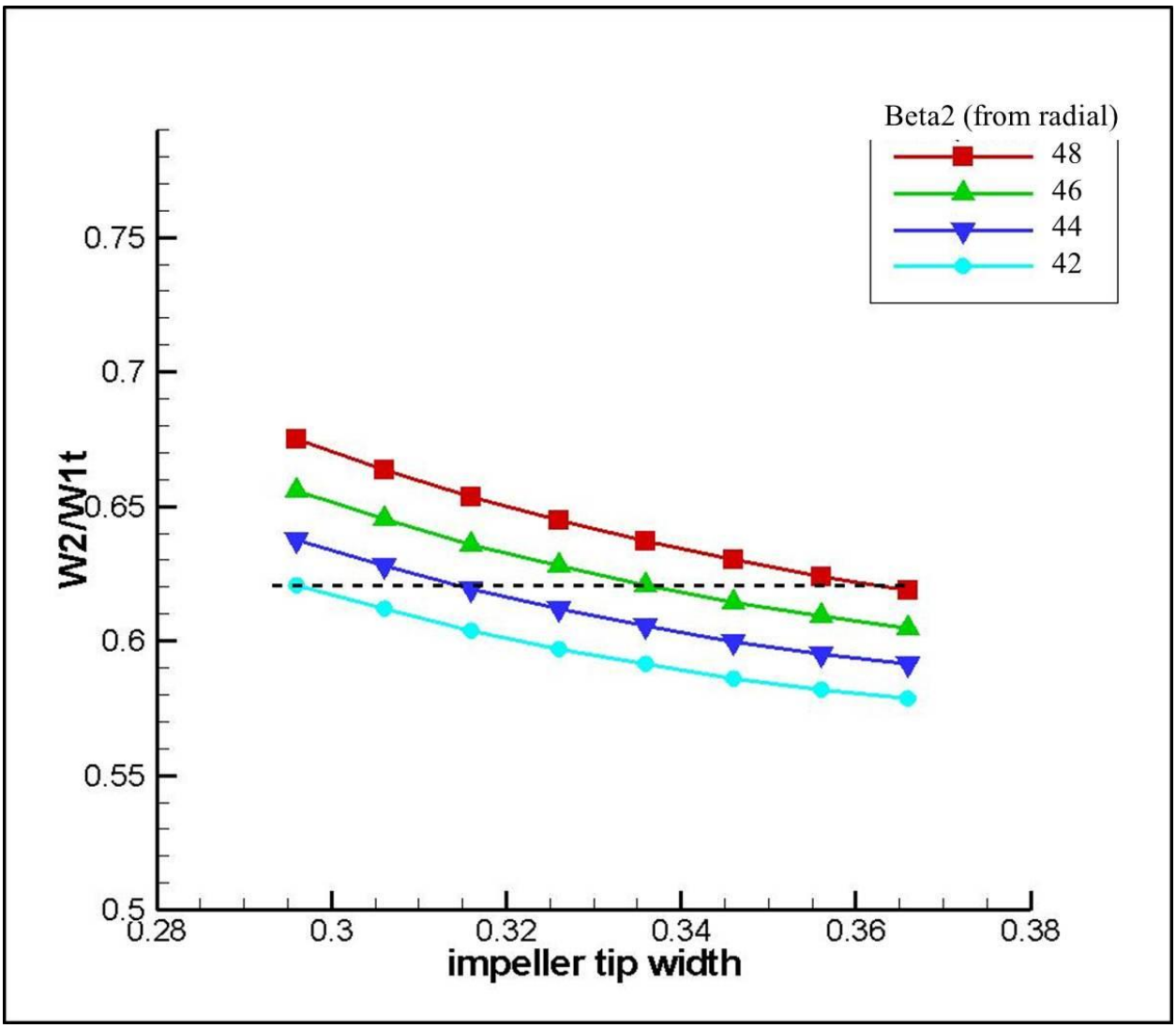

Fig. 5- 6 The diffusion ratio according to the impeller tip width and blade exit angle calculated by 1D analysis code using Ron Aungier's method.

Table 5- 2 Cases for impeller re-design designate diffusion ratio of 0.6

	Blade exit angle, β_2 (degree) (from radial)	Impeller tip width, b_2/d_2
Case1	48	0.0403
Case2	46	0.0373
Case3	44	0.0350
Case4	42	0.0329

5.3.2. MERIDIONAL AND BLADE CURVE DESIGN

After the 1D calculation, the impeller design procedure is on the blade design including meridional curve and blade curve design. This procedure determines the impeller 2D and 3D shape. Flow separation and blade loading to get total pressure rise within the impeller are determined by these 2D and 3D design procedures as well as the 1D design. Because of this, this procedure should be done carefully.

To complete the re-design and be independent on the 2D and 3D design, meridional shape changed as little as possible and blade angle distribution is determined by the same equation. Ron Aungier suggested an equation to be used to calculate the blade angle distribution [2].

$$\beta_s = \beta_{1s} + (\beta_{2b} - \beta_{1t})\left(3\xi^2 - 2\xi^3\right)$$

$$\beta_h = \beta_{1h} + A\xi + B\xi^2 + C\xi^3$$

$$\bar{\beta}_h = 90K + (1-K)(\beta_{2b} + \beta_{1h})/2$$

$$A = -4\left(\beta_{2b} - 2\bar{\beta}_h + \beta_{1h}\right)$$

$$B = 11\beta_{2b} - 16\bar{\beta}_h + 5\beta_{1h}$$

$$C = 16\beta_{2b} + 8\bar{\beta}_h - 2\beta_{1h} \qquad (5\text{-}1)$$

The parameter K is for a blade angle at the midpassage so that it determine maximum blade angle. Fig. 5-7 shows meridional curves for the cases used in this study. All cases have the same impeller tip diameter and different impeller blade exit angles and tip widths. Fig 5-8 shows blade angle distribution calculated by the equation Ron Aungier suggested, K=0.1. In order to be independent on exit lean angle, the lean angles of all the impellers are in the range of 0 to 5 degrees. Theta angle distributions of the impellers are presented in Fig 5-9. Theta angle at the impeller exit are around 55 degrees. Area distributions of the impeller passage are shown in Fig. 5-10. The area distributions have some difference because their areas are almost same until the meridional distance of 0.3, but after that the impeller passage areas are different because of impeller exit width.

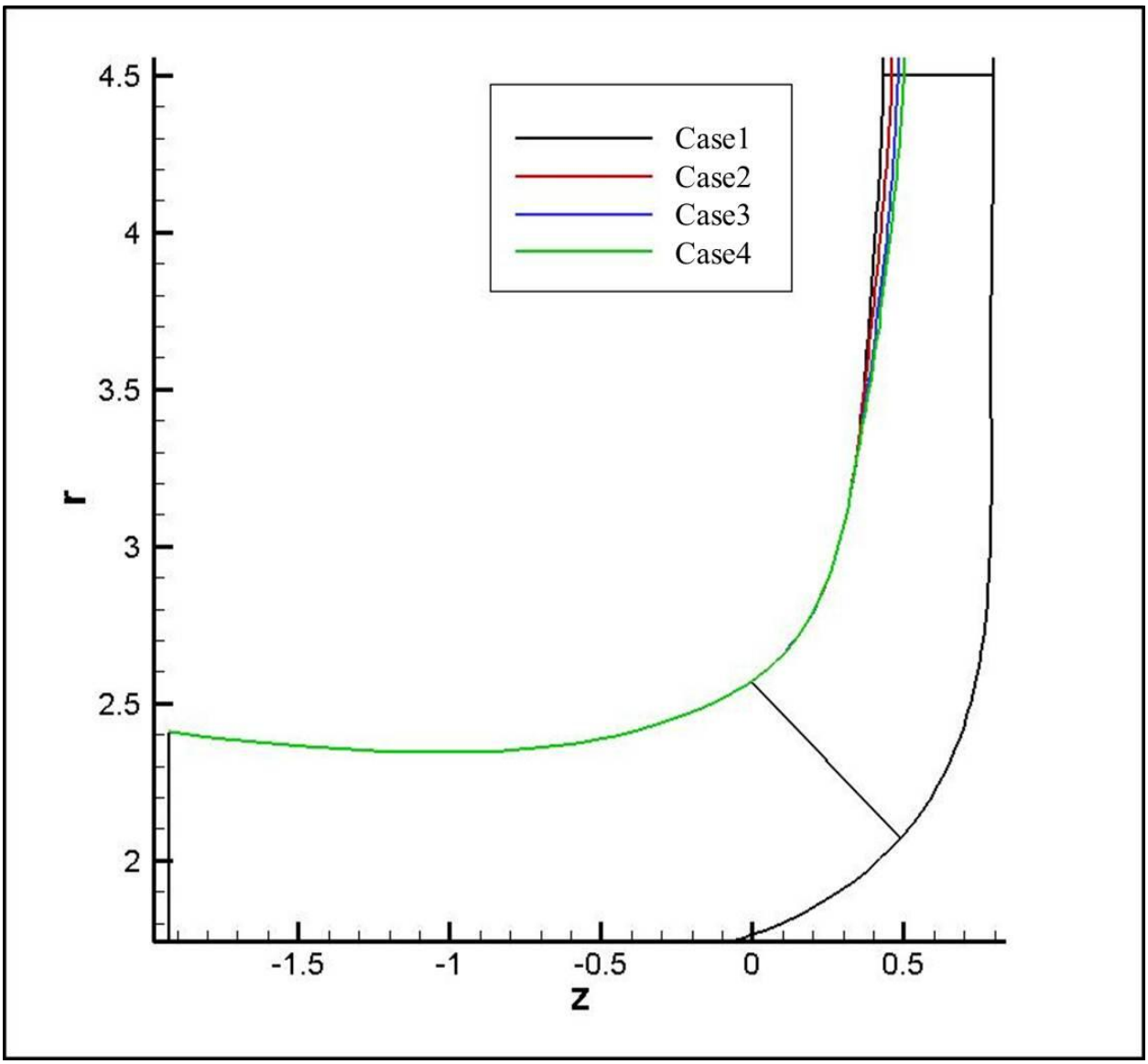

Fig. 5- 7 Meridional shape of all the cases

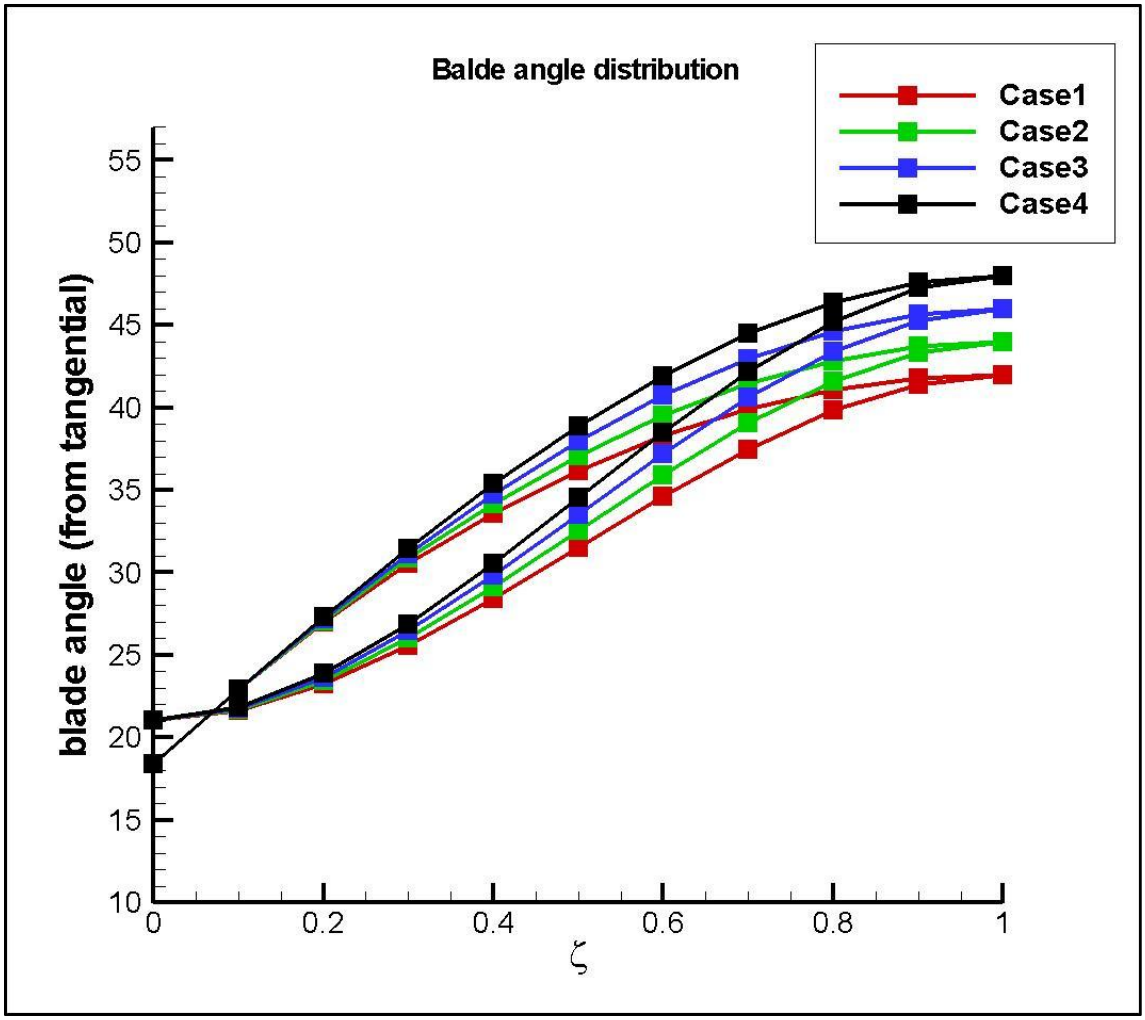

Fig. 5- 8 Blade angle distribution of all the cases according to m`%

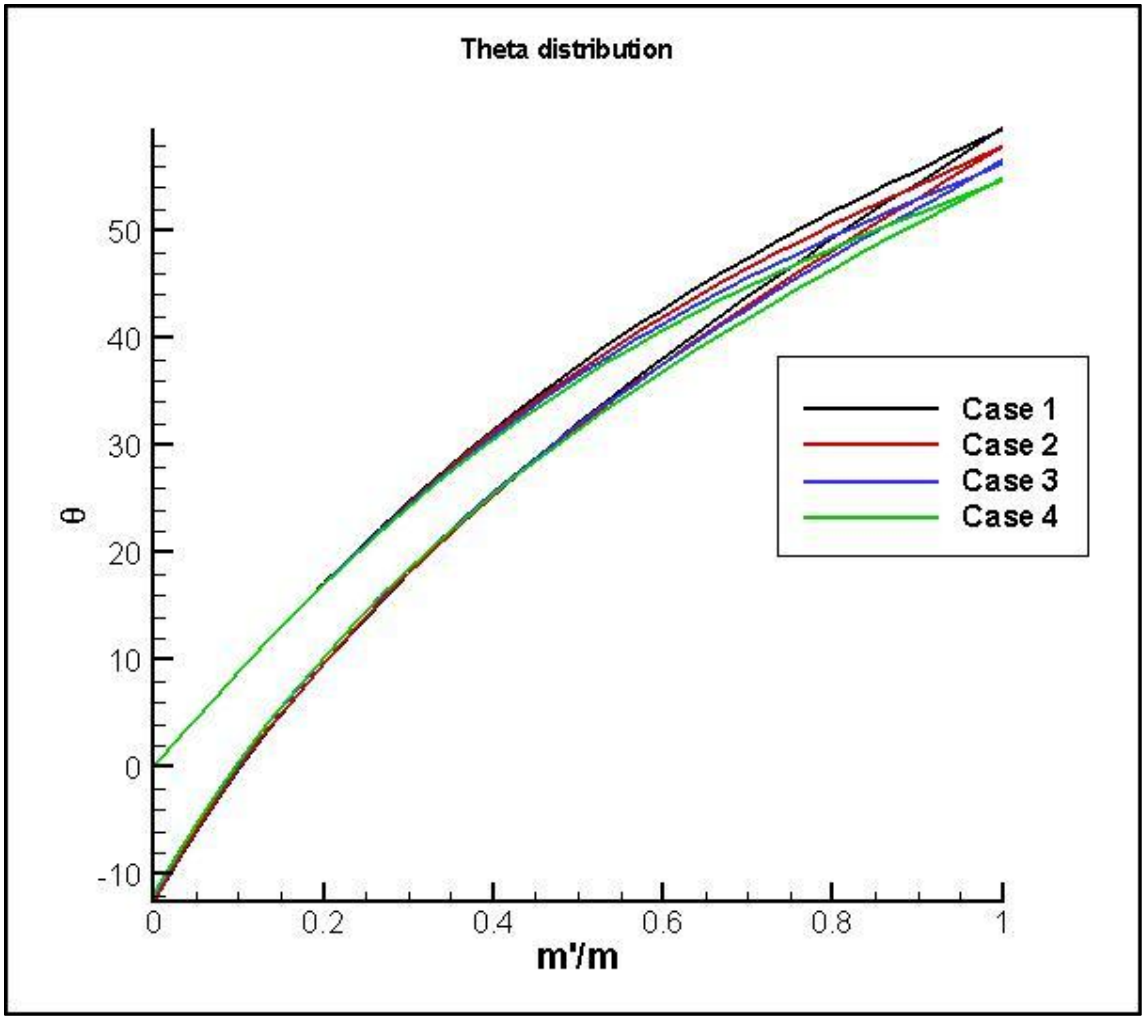

Fig. 5- 9 Blade theta angle distribution of all the cases according to m`%

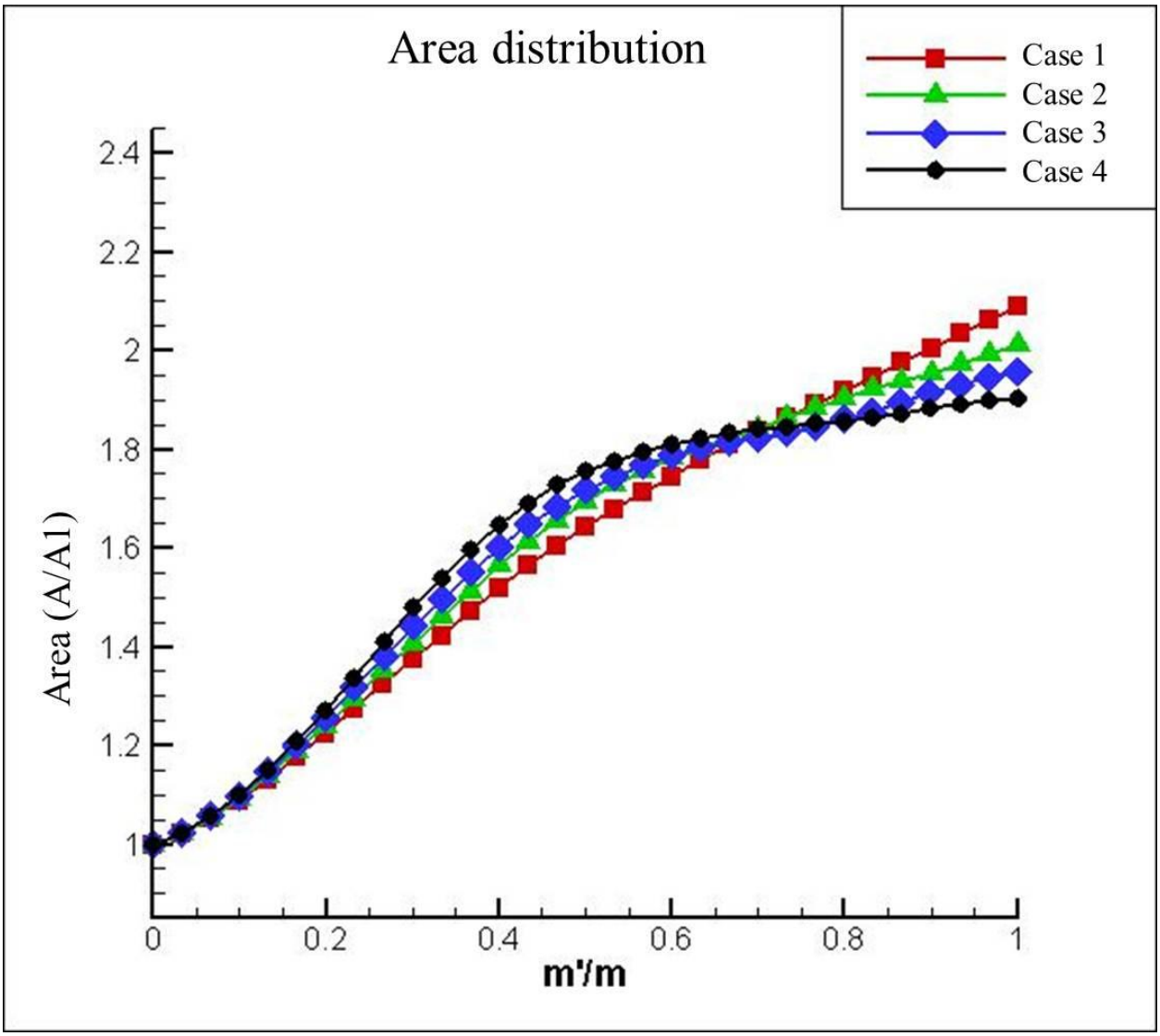

Fig. 5- 10 Area distribution (A/A1) of all the cases according to m`%

5.4. 1D PERFORMANCE ANALYSIS ON THE 4 CASES

Before CFD analysis on the cases, this study conducted a 1D performance analysis on the cases for predicting impeller performance. Fig 5-11 shows efficiency and head coefficient results using a 1D analysis code according to the flow rate of all cases. As shown in the Figure 5-11, all cases show almost the same results of head coefficient and efficiency at the impeller exit. At the

diffuser inlet, however, efficiencies are different between the cases and efficiency difference become larger around the surge region.

Fig 5-12 presents the absolute flow angle and diffusion ratio at the diffuser inlet. The figure shows that the diffusion ratio is almost the same along the whole flow rate and the absolute flow angles have some difference. Absolute flow angle is a very important property at the impeller exit because of high tangential flow results in backflow at the vaneless diffuser. As shown in the Fig. 5-11, over 78 degrees of the absolute flow angle at the impeller exit lead to a significant impeller efficiency drop. Among the cases, case 4 shows the best efficiency at the diffuser inlet because the absolute flow angles are the least along the whole flow range.

Fig 5-13 shows the work input parameter calculated by 1D analysis code. As discussed in chapter 2, the work input parameter consists of blade work, recirculation, leakage, and disk friction parameter. Among them, recirculation, leakage and disk friction are parasitic loss between the impeller exit and diffuser inlet and contribute to total loss. As shown in the figure, the recirculation occupies most of the parasitic work input parameter and other parasitic losses do not change largely as much as the recirculation parameter according to the flow rate.

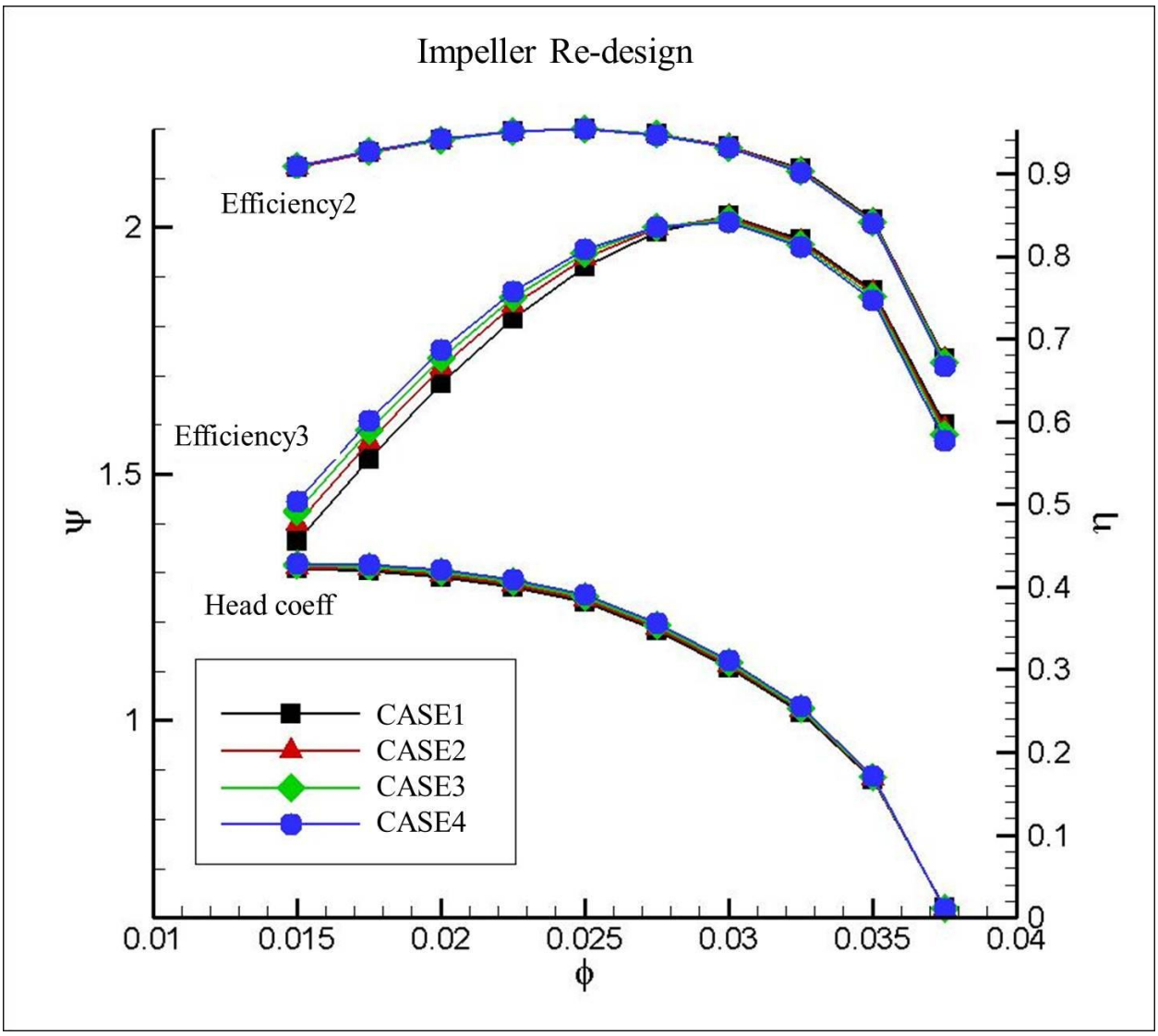

Fig. 5- 11 Efficiency and head coefficient according to the flow rate (Case1, Case2, Case3, Case4)

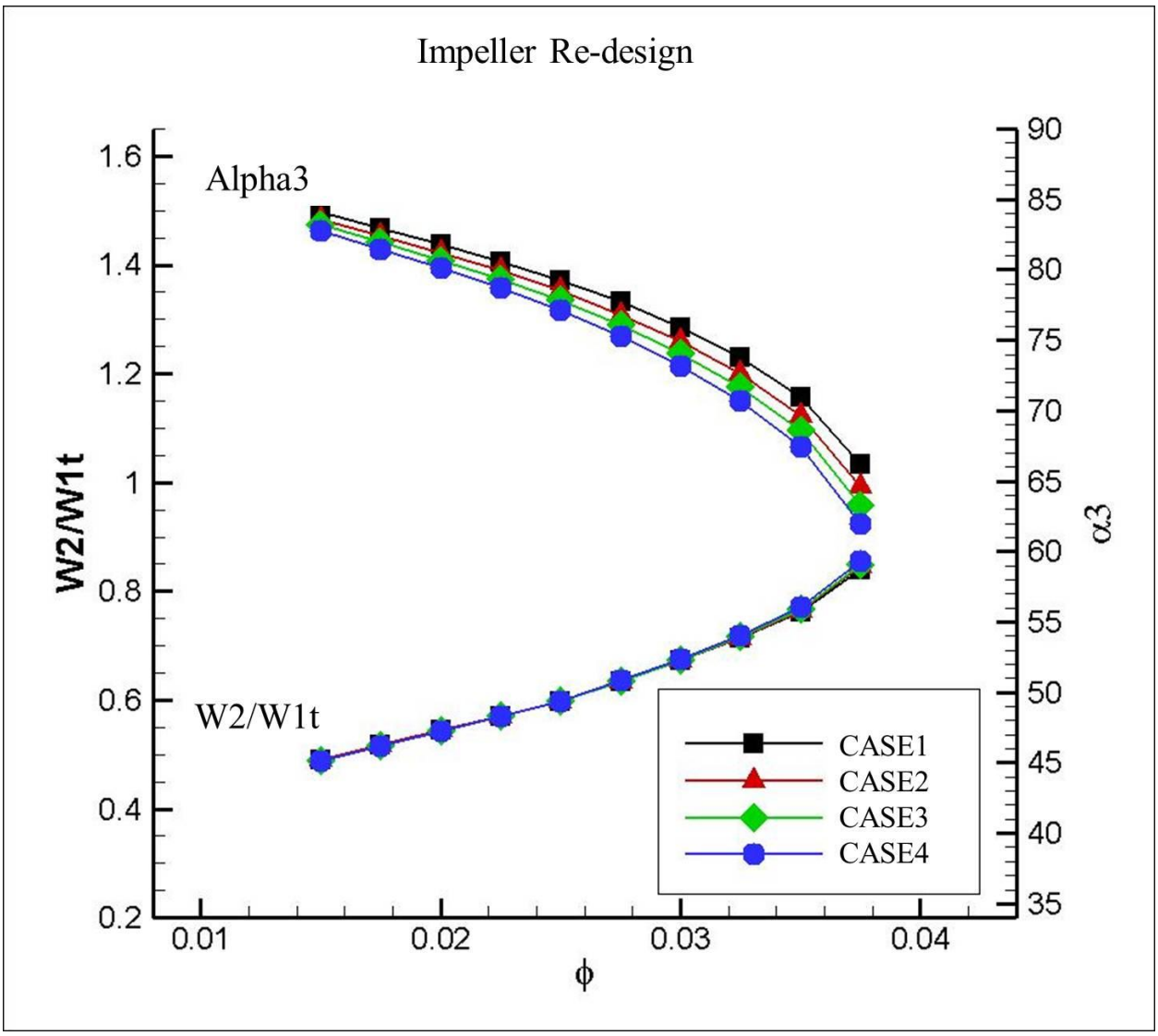

Fig. 5- 12 Diffusion ratio and Absolute flow angle at the diffuser inlet.

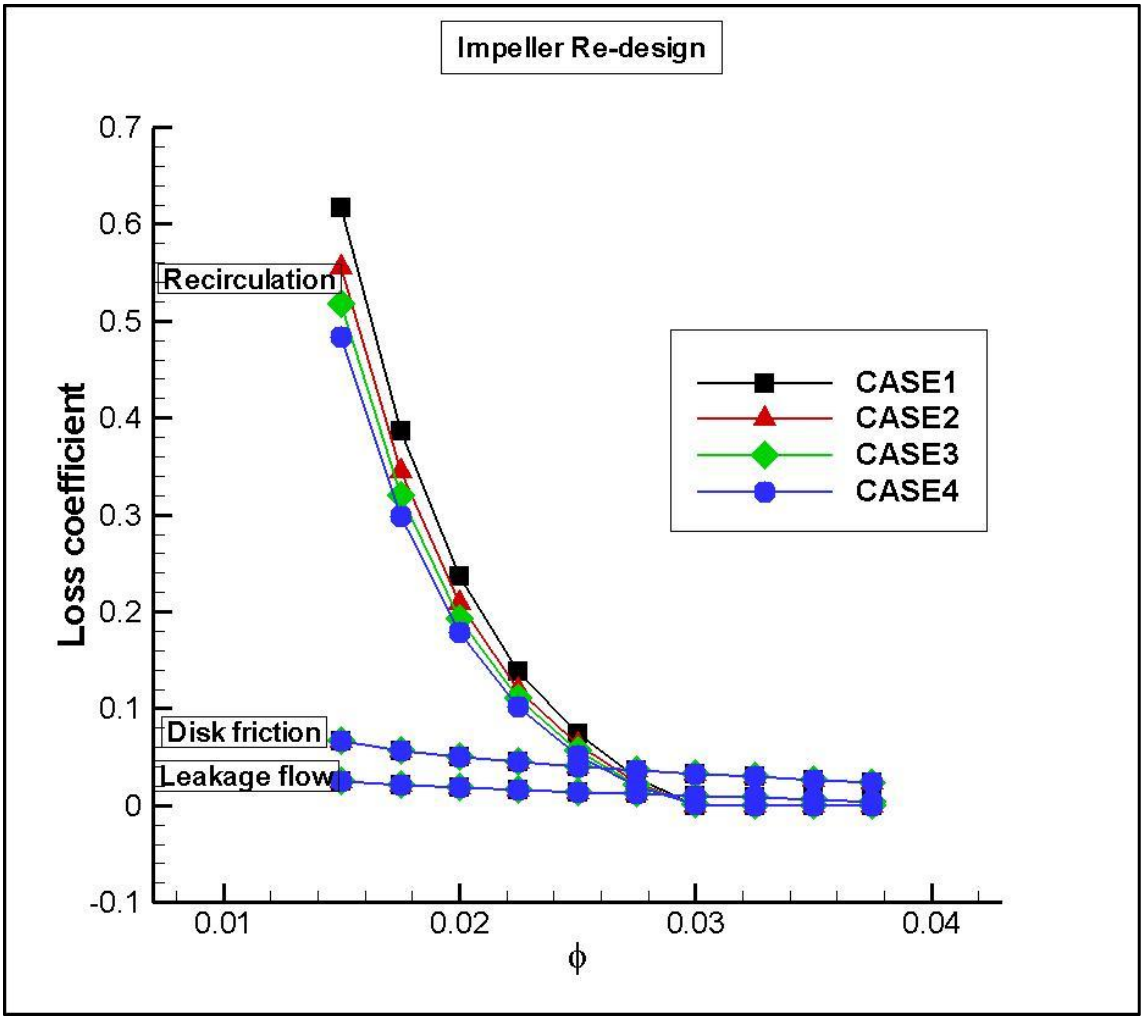

Fig. 5- 13 Parastic work input (Recirculation, Disk friction and Leakage loss)

5.5. CFD ANALYSIS AND COMPARE WITH 1D ANALYSIS

It is important for the impeller design process to do the CFD analysis that predicts impeller performance. The impeller design program, Bladegen, for the CFD analysis is used in the simulation. TurboGrid is used for the grid generation. Fig. 5-14 and Fig. 5-15 show 3D impeller shape and grid generated for the simulation respectively. Total grid points are 350000 to 400000 according to the cases and all grids in the cases have almost the same grid points and shape to reduce uncertainty from the mesh. Grid generation is conducted on one passage and a periodic condition is used in the simulation. ANSYS CFX is used for CFD analysis. The

domains for the simulation consist of rotating inlet domain, rotating main passage domain, and stationary outlet domain. Inlet boundary conditions are set as total pressure, total temperature, and velocity direction; outlet boundary conditions are set as mass flow rate. A frozen – rotor interface was used between the stationary and rotating blocks.

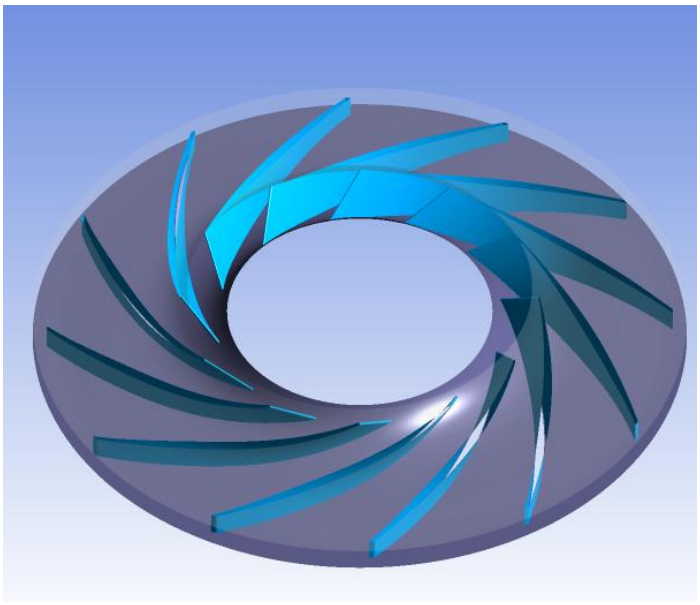

Fig. 5- 14 3D shape of redesigned impeller

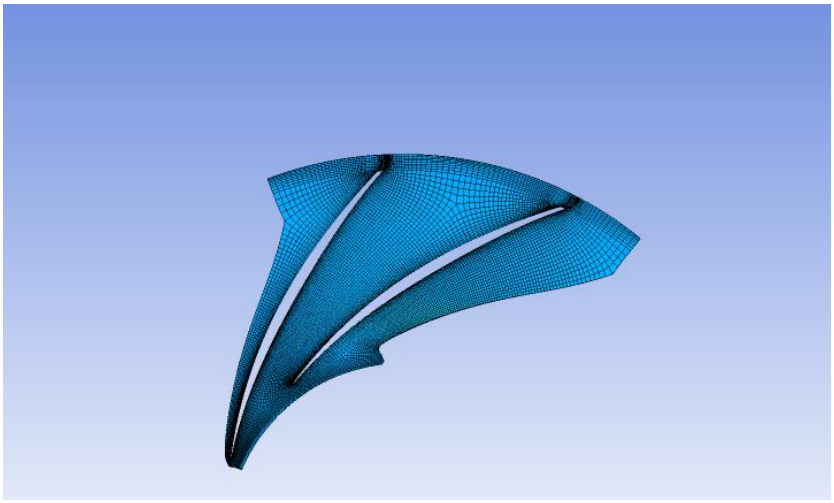

Fig. 5- 15 Grid generated for re-design impeller

At the design point, flow coefficient of 0.025, 1D analysis and CFD analysis are conducted. Fig. 5-16 shows efficiency and head coefficient for all cases. As shown in the figure, both efficiency and head coefficient of CFD results are bigger than the results of 1D analysis. Efficiencies in CFD and 1D analysis are around 0.962 and 0.958 respectively. Head coefficients in CFD and 1D analysis are around 1.35 and 1.25 respectively. Fig. 5-17 shows the diffusion ratio (W_2/W_{1t}) and absolute flow angle results of 1D analysis and CFD of all cases. Absolute flow angle and diffusion ratio are very close between 1D analysis and CFD results. As blade exit angle increases, absolute flow angle increases. It means that blade exit angle affects the diffuser inlet condition at the same diffusion ratio. The diffusion ratios are close to 0.6. All cases show almost same result.

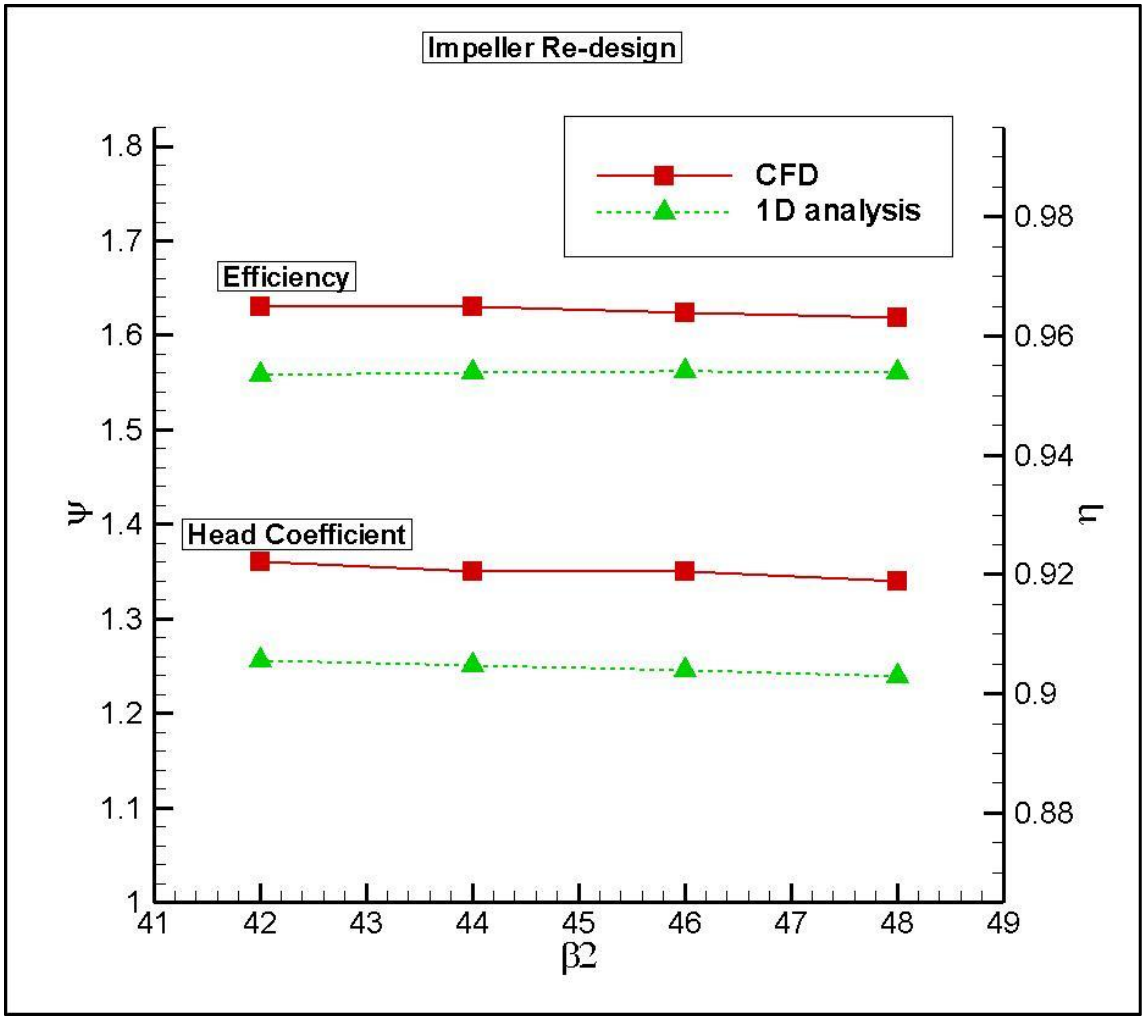

Fig. 5- 16 Comparison of Head coefficient and efficiency of 1D analysis and CFD result

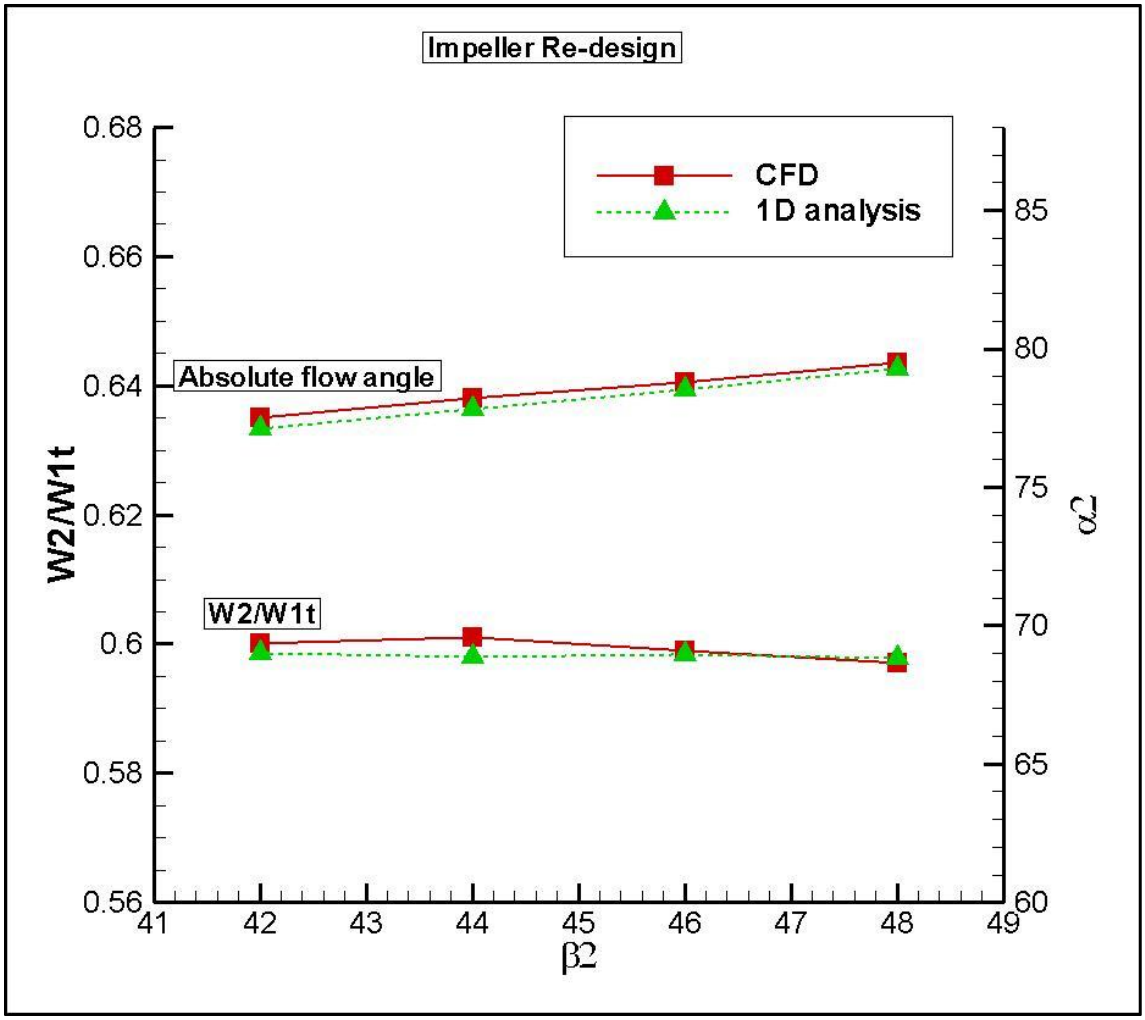

Fig. 5- 17 Comparison of the diffusion ratio and absolute flow angle, results of 1D analysis and CFD

5.6. CONCLUSION

Impeller re-design using 1D analysis code is conducted in this chapter. 1D analysis code is used for the diffusion ratio, which is important to start the impeller design and affect its performance and efficiency. The impeller re-design targeted the diffusion ratio of 0.6 and better efficiency and head coefficient than those of original impeller. 1D analysis found a trade-off point between the blade tip width (b_2) and the blade exit angle (β_2). This study made four different speeds and conducted CFD analysis.

As results of the 1D analysis and CFD, the results of efficiency, diffusion ratio, and absolute flow angle in 1D analysis are almost the same as the CFD result. However, 1D analysis predicts head coefficient and efficiency less than the results of the CFD results. The results could be compared with test results because wall condition in CFD analysis is a smooth condition that affects skin friction loss.

6. CONSIDERATION OF AXIAL LENGTH FOR IMPELLER DESIGN

In the definition of an initial meridional profile, building on the 1-D parameters and design process, the first task is to select the axial length-diameter ratio, L_{ax}/d_2. The impeller length affects a number of significant design issues, including the overall length of the machine, the shaft dynamics, the impeller bore stresses, and the aerodynamic performance. The curvature along the shroud is driven by the need to turn the flow from an axial direction at the leading edge to a radially oriented flow at the exit. The length over which this turning takes place becomes a critical factor. The most effective way to reduce the curvature is to increase the distance over which the turning takes place; i.e. ,make the impeller longer. So wide is the impeller axial length, L_{ax}, impact, in fact, that L_{ax}/d_2 cannot sensibly be included as a varying parameter in the iterative aerodynamic design procedure; it is better to select a value at the outset with guidance from empirical rules or established custom and practice. From an aerodynamic standpoint, Birdi [13] has suggested

$$\frac{L_{ax}}{d_2} = \sqrt{\left[K_1 \left(M_{w1s} + K_2 \right) \left(1 - \frac{d_{1m}}{d_2} \right) \frac{d_{1s} - d_{1h}}{d_2} \right]} \qquad (6\text{-}1)$$

where, K_1 = 0.28 and K_2=2 0.8. Equation (6-1) yields L_{ax}/d_2 values of 0.32 - 0.37 for inlet Mach numbers of 0.9 - 1.2 for typical ranges of diameter ratios in the expression. The physical basis for equation (6-1) lies in the balance of reduced skin friction, prompting low L_{ax}/d_2 especially at low d_{1m}/d_2, against the need to allow adequately gentle turning from axial to radial, particularly at high M_{w1t} which prompts higher L_{ax}/d_2. For a single-stage compressor there is usually freedom to choose an aerodynamically optimum axial length, in contrast to

multistage designs in which the axial length of the rotor tends to be limited by overall shaft length considerations.

Similarly Aungier[14] developed a correlation for optimum L_{ax}/d_2 based on his experience and wide sources of data a function of diameter ratio (d_2/d_{1t}) and flow coefficient (Φ) as

$$\frac{L_{ax}}{d_2} = 0.014 + 0.023\frac{d_2}{d_{1s}} + \phi \qquad (6\text{-}2)$$

Sorokes et al.[15] carried out an extensive work to determine the impact of shroud curvature on the performance of a centrifugal impeller or stage. They showed that the value of L_{ax}/d_2 and related curvature geometry are especially important in the design of high inlet relative Mach number centrifugal compressor impellers. They showed that if the impeller has rapid curvature or tight turning in the leading edge region, the inlet relative Mach number will be unacceptably high. Conversely, efforts to reduce the curvature typically result in longer impellers that can lead to rotor-dynamics concerns in multi-stage compressors.

Brammert et al [16] investigated three centrifugal impellers having an elliptic blade shape and identical blade geometry at inlet and exit but different shapes of the meridional contours (L_{ax}/d_2 = 0.325 – 0.5). They showed that with increasing impeller length, the wake zone at the suction side of the blades can be only partially influenced and friction losses become dominant. A smooth curvature of the meridional cross section of the impeller channel leads to a better jet-wake ratio at impeller exit.

Al-Zubaidy [17] developed a general direct-design method for radial flow impellers (based on a prescribed relative velocity schedule). He varied the axial length, L_{ax}, of each

impeller systematically in order to assess its impact on the efficiency. The results showed that there is a specific region of axial length band where the highest efficiency for all designs occurred.

With the above background information, the design was carried out varying axial length based on difference in length between radii, impeller exit and impeller inlet shroud (r_2-r_1). The study presents axial length ratio L_{ax} to d_2 of 0.30 to 0.45.

6.1. DESIGN CASES

In terms of flow stability at the impeller exit and diffuser inlet, high Mach number and high swirl flow should be avoided. In such conditions, axial length could be one of the design considerations. To make the instability condition, a high Mach number and high swirl condition are defined in Table 6-1. High Mach number and high swirl defined between 0.8 and 1.1 and 78 and 85 degree respectively. With these requirements 1D design results are shown as table 6-2.

Table 6- 1 Mach number and absolute flow angle range for unstable flow condition

	Value
Mach number	0.8~1.1
α_2	78^o~85^o

Table 6- 2 1D geometry conditions for the cases

Inlet shroud diameter (D_{s1})	83.15 mm
Inlet hub diameter (D_{h1})	40 mm
Inlet shroud blade angle (β_{h1})	53.89^{o}
Inlet hub blade angle (β_{s1})	33.40^{o}
Exit diameter (D_2)	210.407 mm
Exit blade angle (β_{2b})	60^{o}
Exit flow angle (α_{2b})	10^{o}
Blade number	16
Rotational speed	40000 rpm
Blade exit width	6.137 mm
Mass flow rate ($\dot{m}$)	0.5 kg/s

To make meridional curves, an elliptic equation was used and a 3D camber line was made by Casey's method[18]. The study considered six cases of varying axial length based on the difference between r_2 and r_1 to determine proper axial length using equation (6-3). The cases are shown in Table. 6-3. Meridional curves are presented in Fig. 1. And a is used as normalized value in each case.

$$Lax = a(r_2 - r_1) \quad (6\text{-}3)$$

Table 6- 3 Axial length along with respect to factor a

A	L_{ax}
1.0	63.63mm
1.1	69.99mm
1.2	76.35mm
1.3	83.71mm
1.4	89.08mm
1.5	95.44mm

And hub and shroud camber lines are determined by cubic equation (6-4). Boundary conditions of this equation are determined by blade angles, θ_2 and angles between axial coordinate and meridional curve so as to determine constants in the equation. Camber lines in the study are shown in Fig. 6-2.

$$c=r\theta=Am^3+Bm^2+Cm+D \quad (6\text{-}4)$$

After determine all curves to make 3D impeller geometry impeller shape is presented in Figure 6-3.

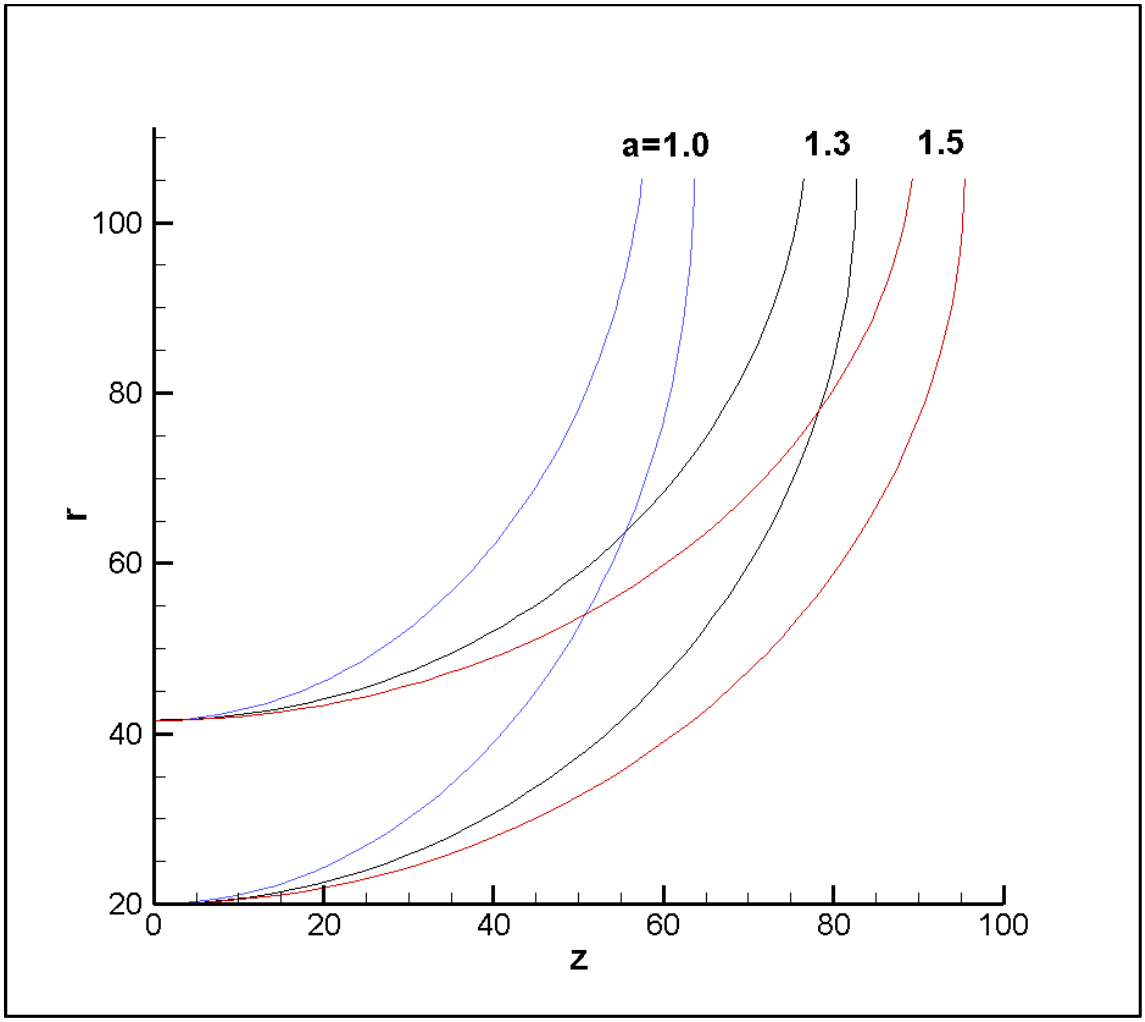

Fig. 6- 1 Meridional curves of the all cases

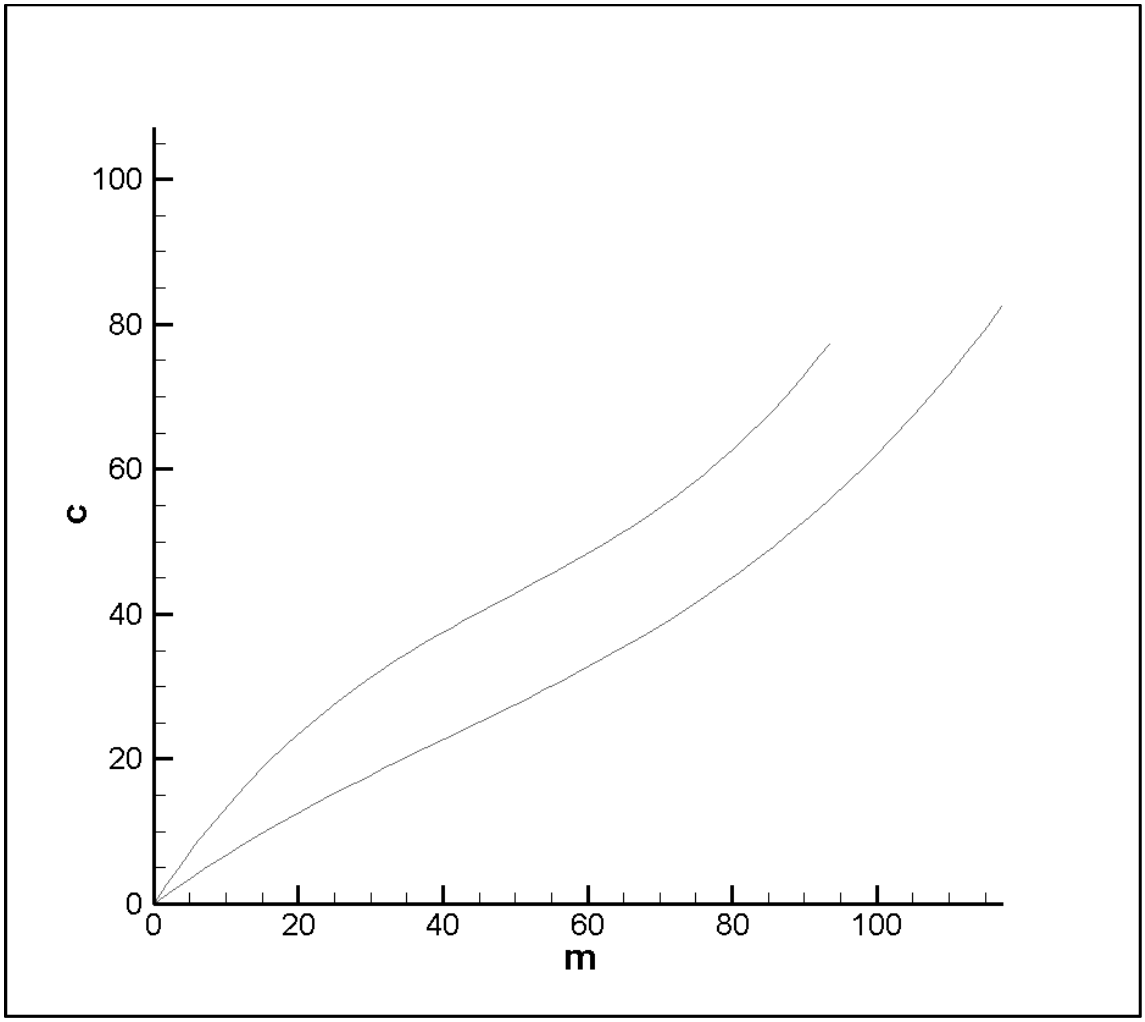

Fig. 6- 2 Camber line vs. Meridional distance

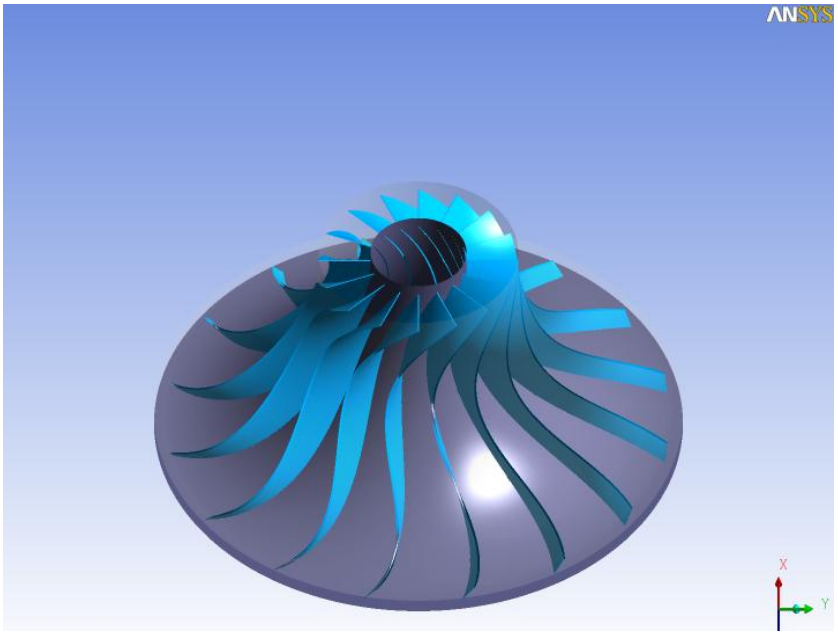

Fig. 6- 3 3D Impeller shape

6.2. CFD ANALYSIS

In the study, CFD analysis was conducted using ANSYS CFX. The impeller grid nodes account is 300K-330K. Fig 6-4 shows mesh element shape. The domains for the study are consisted of stationary inlet domain, rotating main passage domain, and stationary outlet domain. Inlet boundary conditions are set as total pressure, total temperature, and velocity direction; and outlet boundary conditions are set as mass flow rate.

A high resolution scheme has been used as an advection scheme. A k-ε model was employed as a turbulent model. A frozen – rotor interface was used between the stationary and rotating blocks. The domains in the study consisted of stationary inlet domain, rotating main passage domain, and stationary diffuser domain.

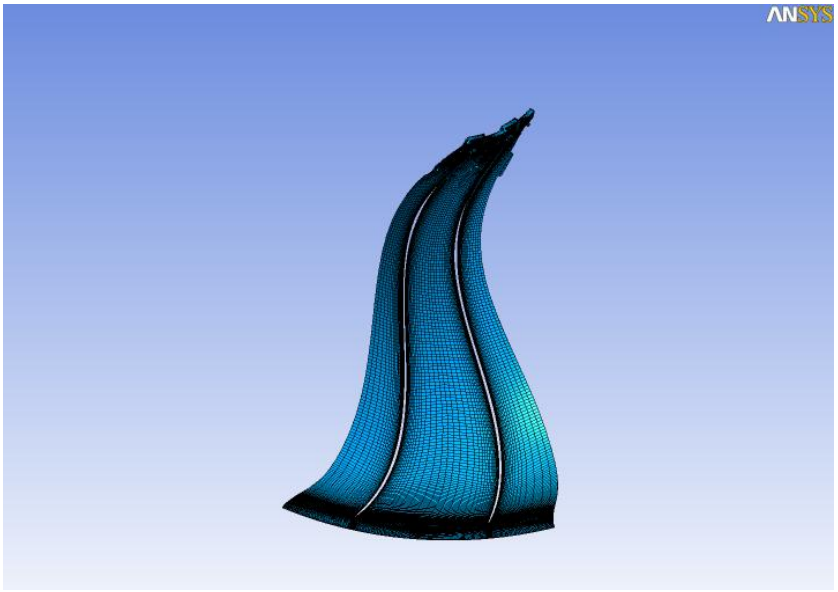

Fig. 6- 4 Mesh elements at 50% span

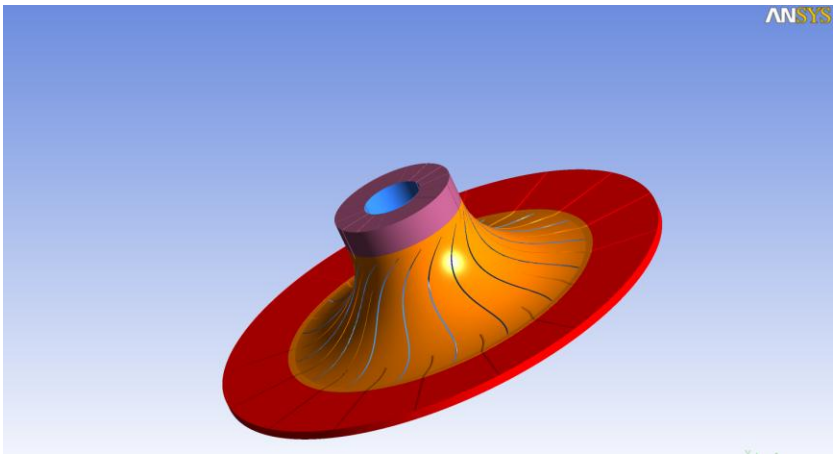

Fig. 6- 5 Domains used in the analysis

6.3. RESULTS

The performance of the impeller has been carried out for all cases. The Mach number, absolute velocity flow angle, and static pressure at 0%, 3%, 6%, and 9% from the impeller exit are given in Fig. 6-6 to Fig. 6-17 respectively.

As shown in the absolute velocity flow angle contour, the case of a=1.5 has the most uniform flow at 0%; and all cases show that the absolute flow angle decreases as going to the shroud from the hub. Also, it is observed that the absolute flow angle is higher at the pressure side near the hub. Generally over the whole region, impeller, a=1.5, has a high tangential flow at the impeller exit.

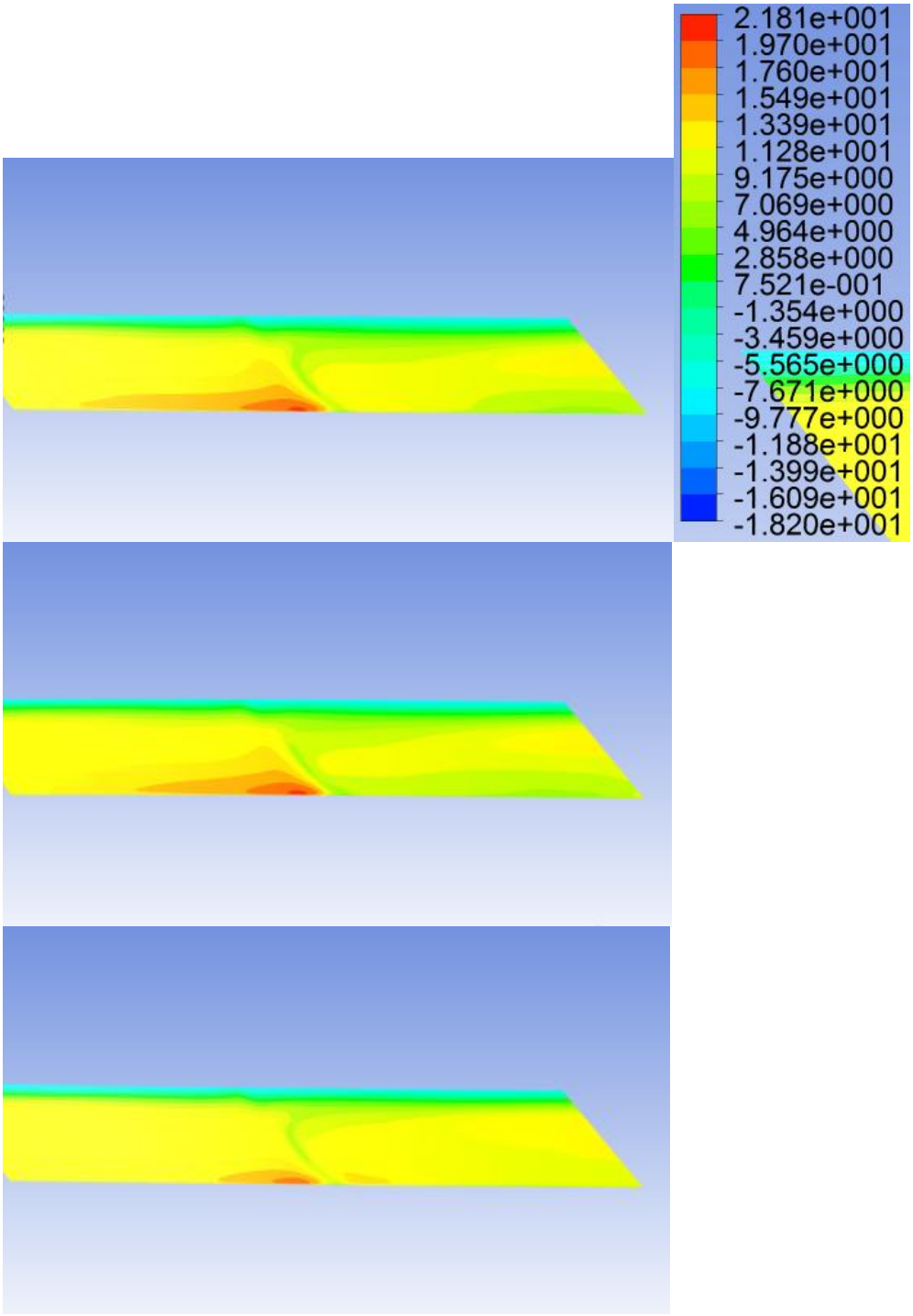

Fig. 6- 6 Absolute flow angle contour at 0% from the impeller exit (a=1.0, a=1.3, a=1.5)

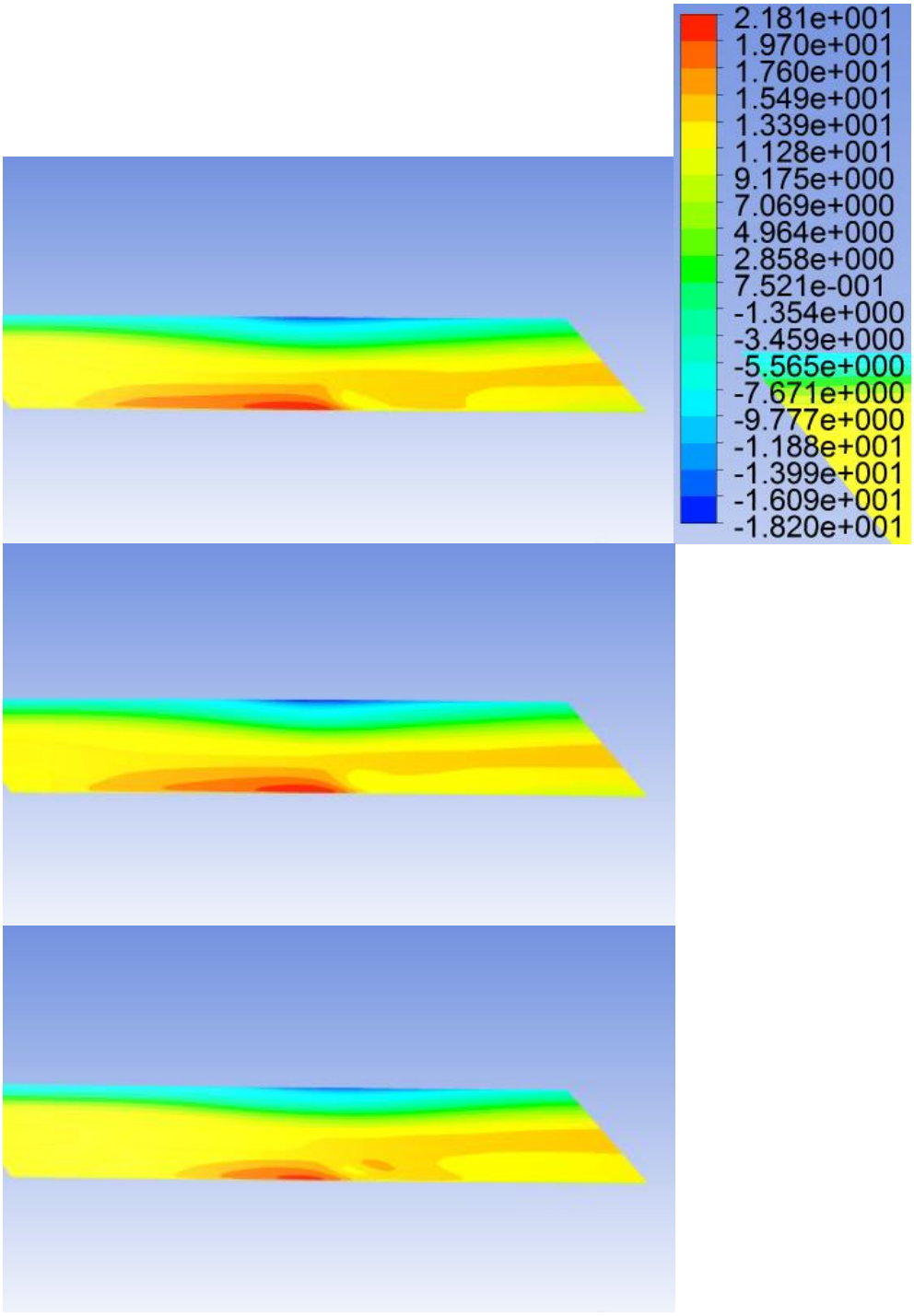

Fig. 6- 7 Absolute flow angle contour at 3% from the impeller exit (a=1.0, a=1.3, a=1.5)

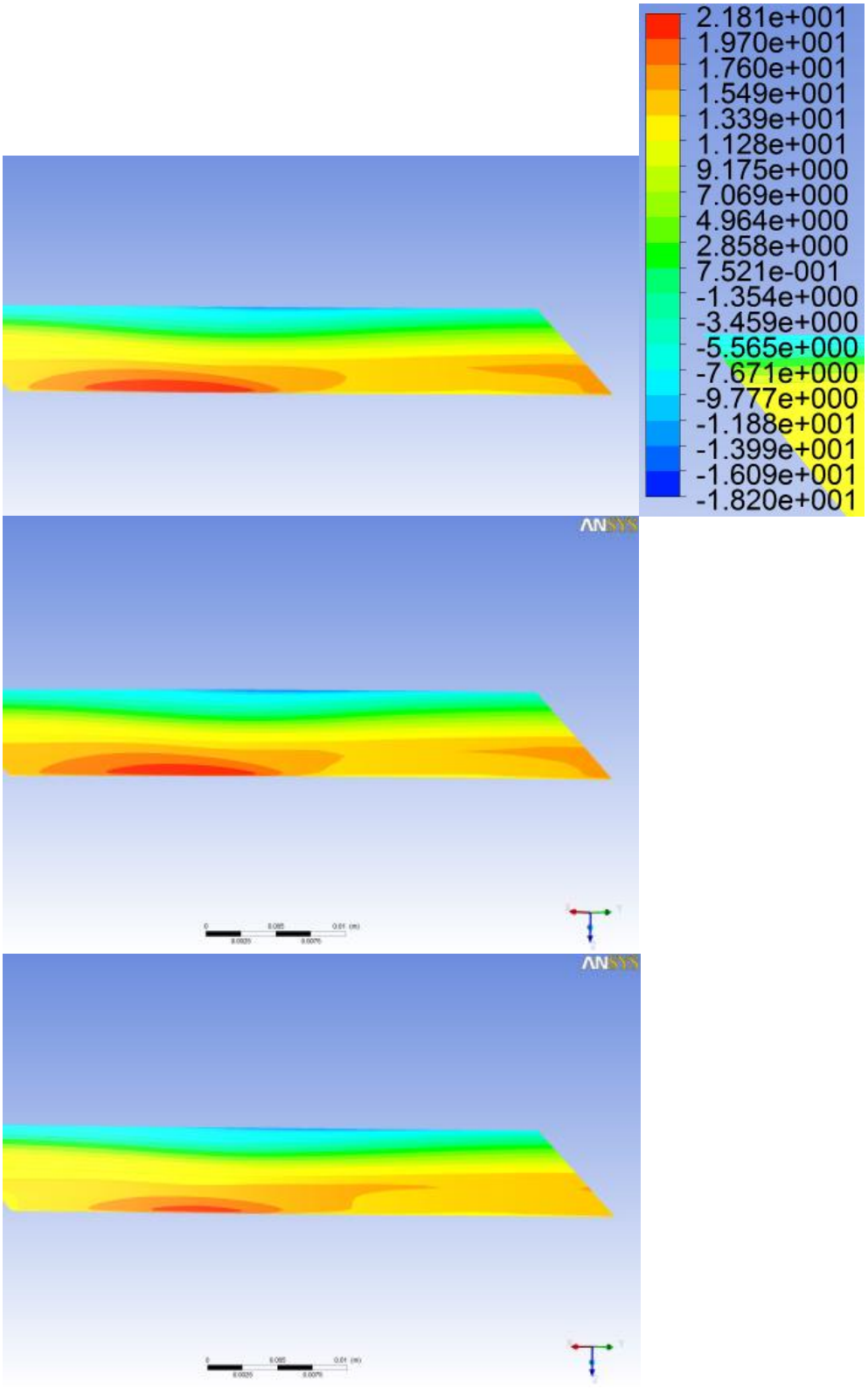

Fig. 6- 8 Absolute flow angle contour at 6% from the impeller exit (a=1.0, a=1.3, a=1.5)

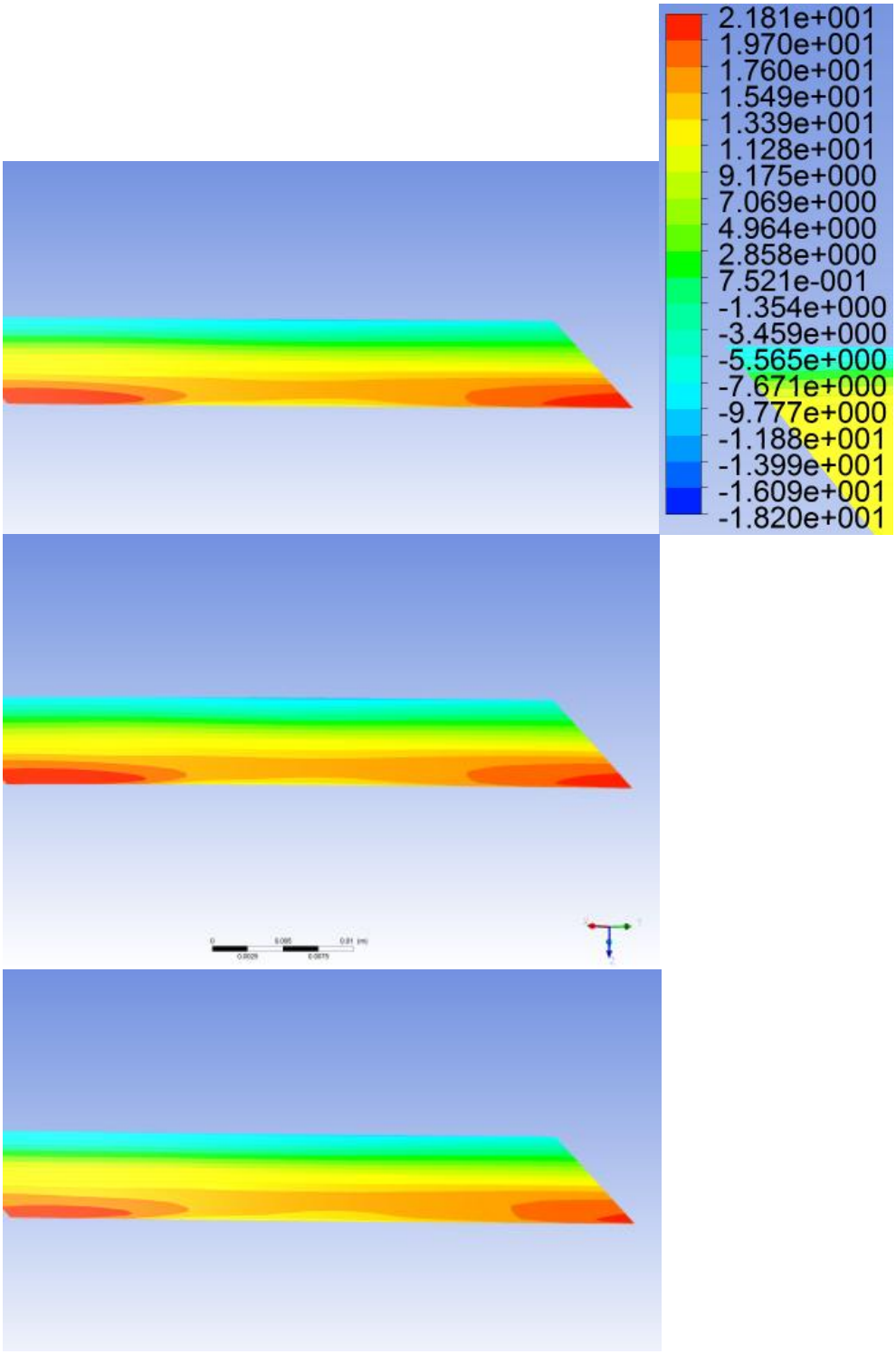

Fig. 6- 9 Absolute flow angle contour at 9% from the impeller exit (a=1.0, a=1.3, a=1.5)

Similar to the absolute flow angle, in Mach number contour, Mach number distribution shows the most uniform flow at the case of a=1.5. In particular, the case of 1.0 and 1.3 at 9% in Figure 13, there is still not uniform region near the hub. But throughout the check point, 0%, 3%, 6%, and 9%, the case of a=1.5 shows that the Mach number is smaller than the other cases.

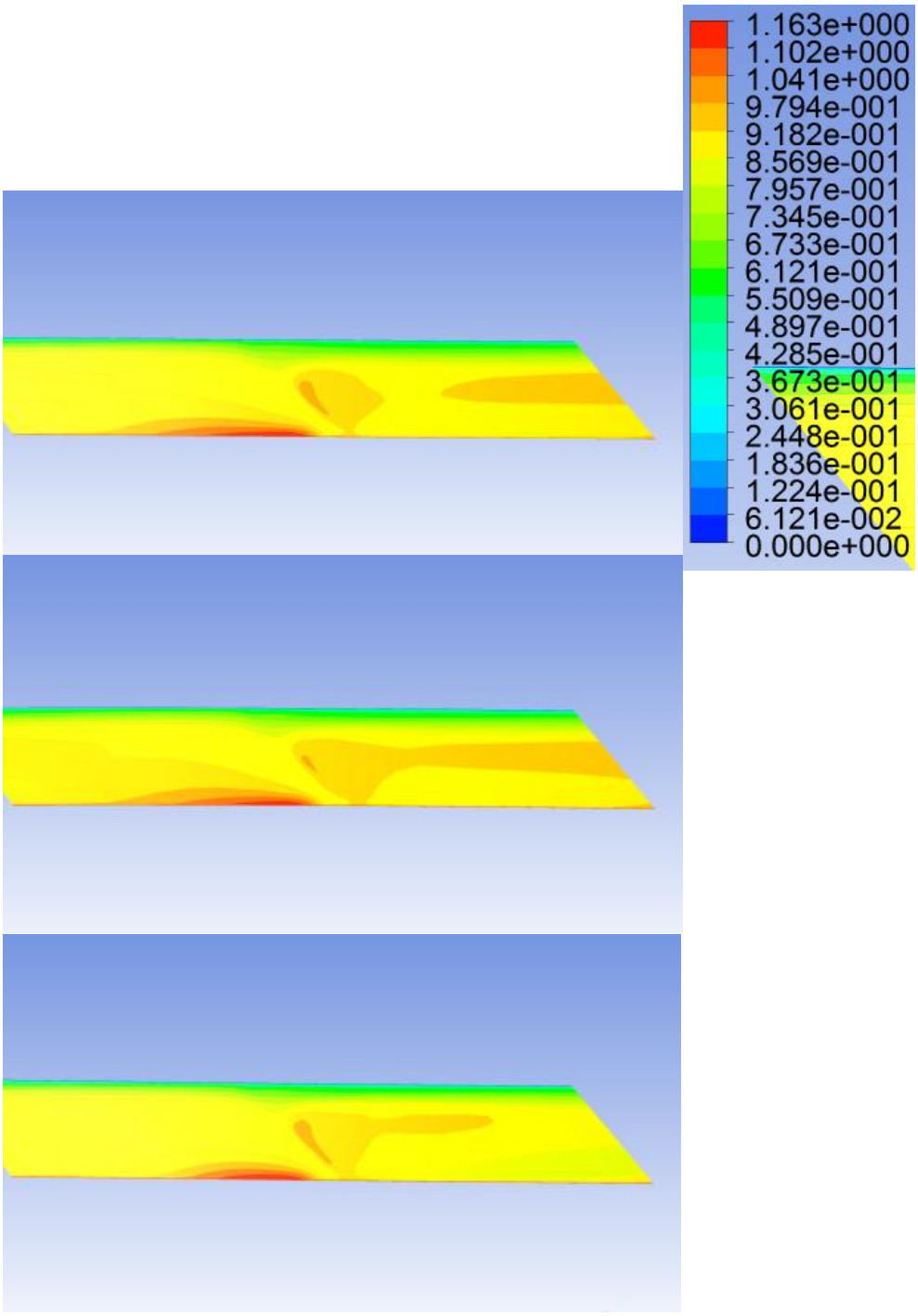

Fig. 6- 10 Absolute Mach number contour at 0% from impeller exit (a=1.0, a=1.3, a=1.5)

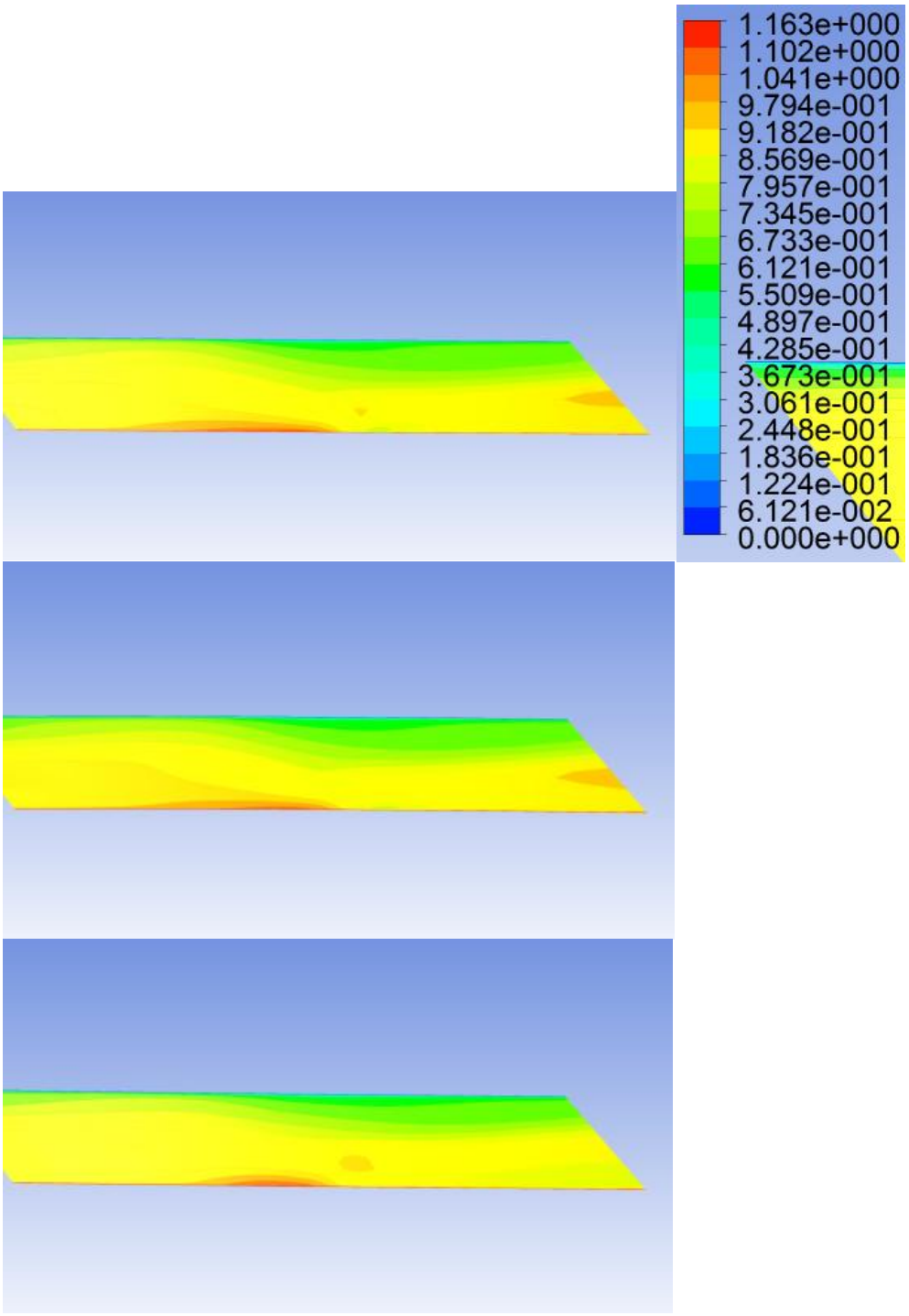

Fig. 6- 11 Absolute Mach number contour at 3% from impeller exit (a=1.0, a=1.3, a=1.5)

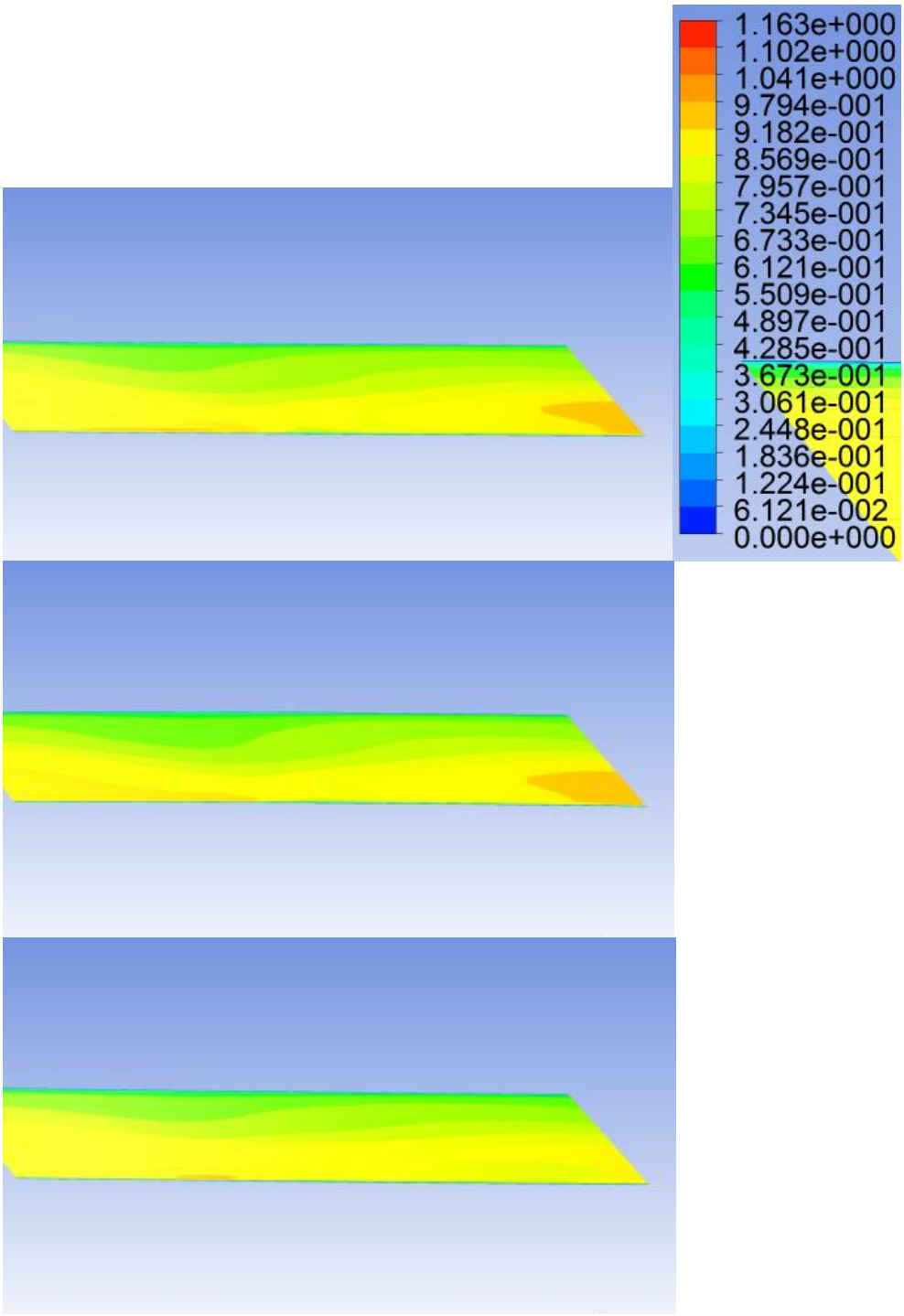

Fig. 6- 12 Absolute Mach number contour at 6% from impeller exit (a=1.0, a=1.3, a=1.5)

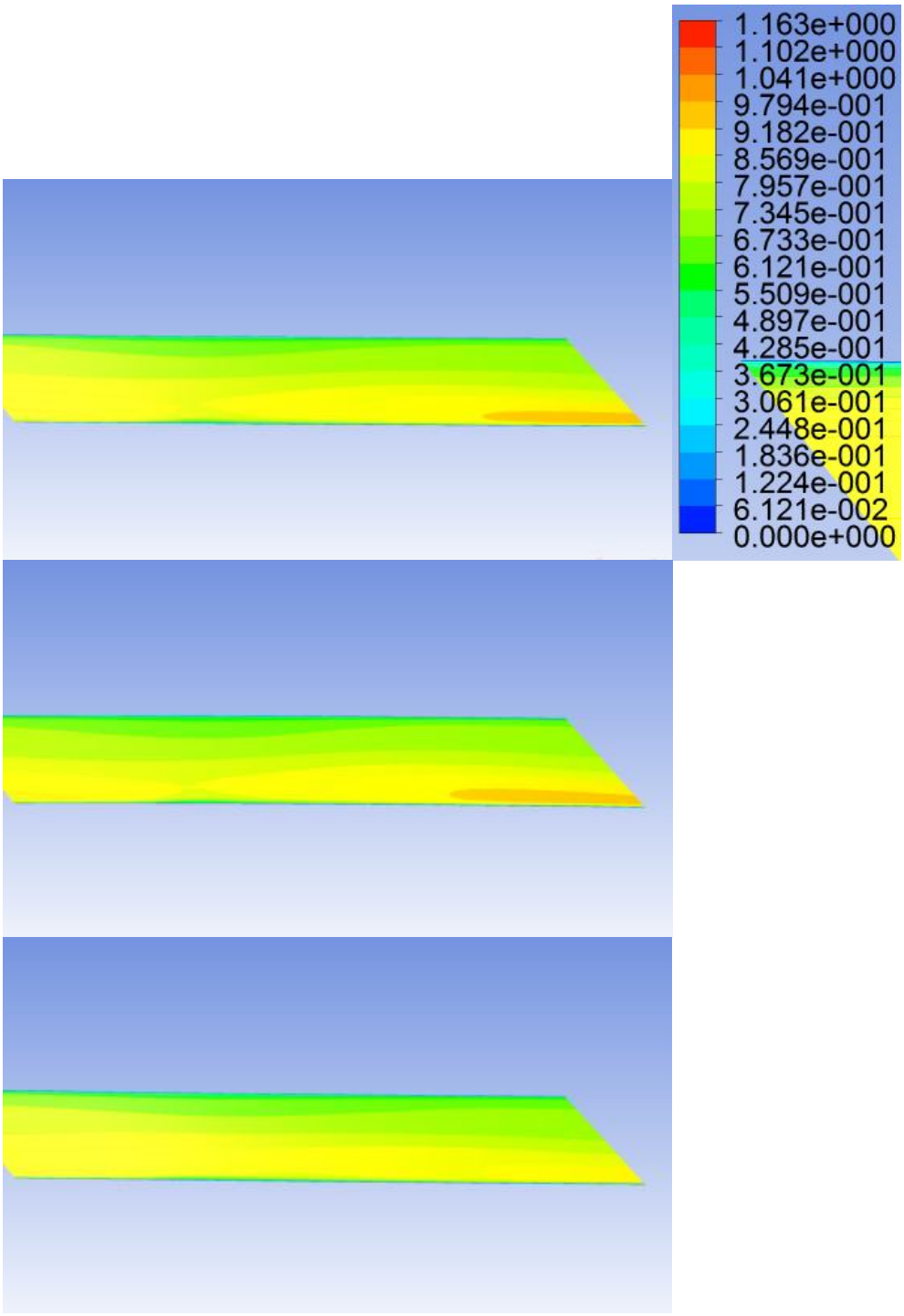

Fig. 6- 13 Absolute Mach number contour at 9% from impeller exit (a=1.0, a=1.3, a=1.5)

The static pressure contours are shown in Fig. 6-12 to 6-17. It can be shown in pressure contour that at the case of a=1.5, difference between suction side and pressure side is smaller than a=1.0 and a=1.3.

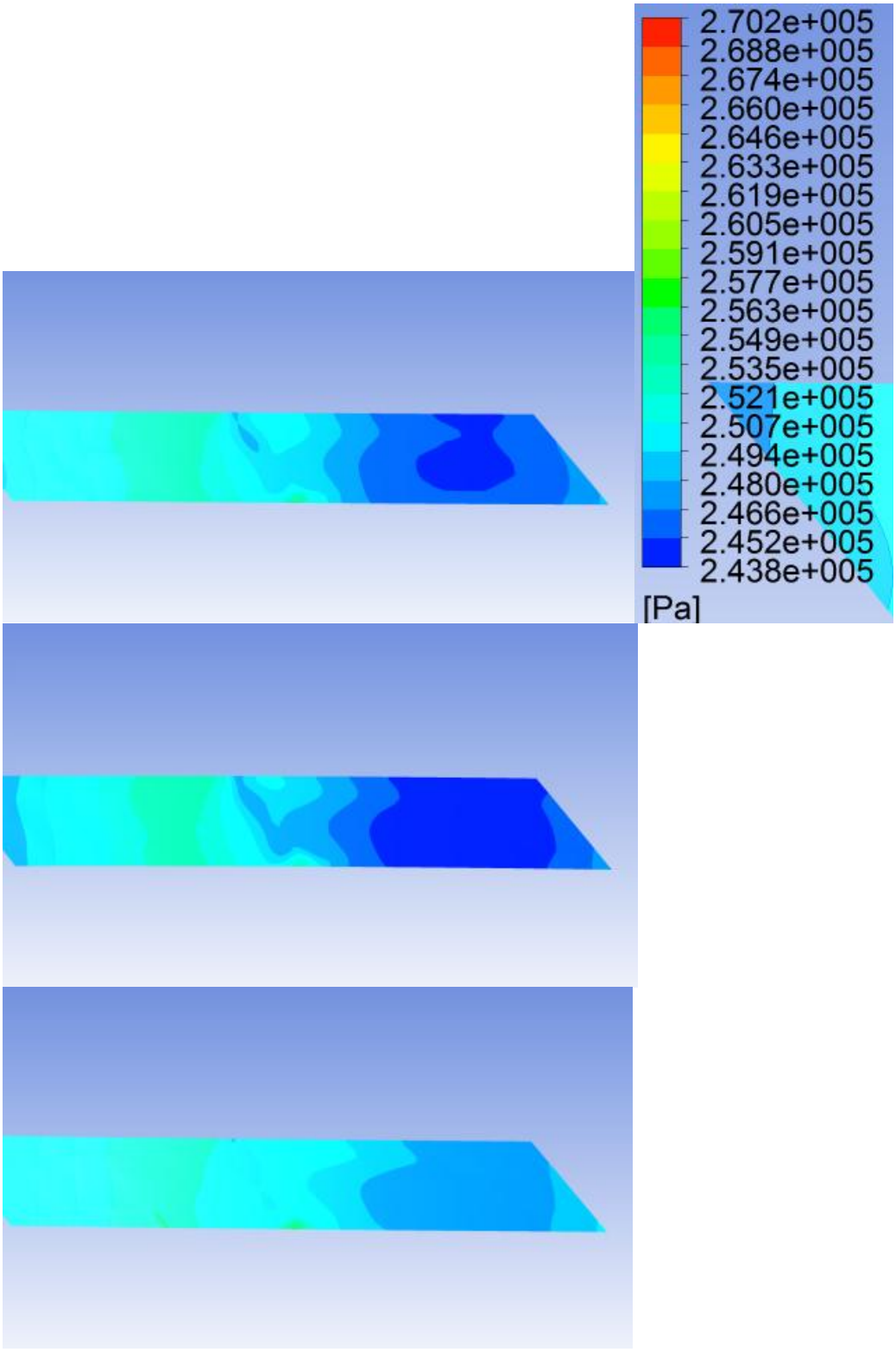

Fig. 6- 14 Static pressure contour at 0% from the impeller exit (a=1.0, a=1.3, a=1.5)

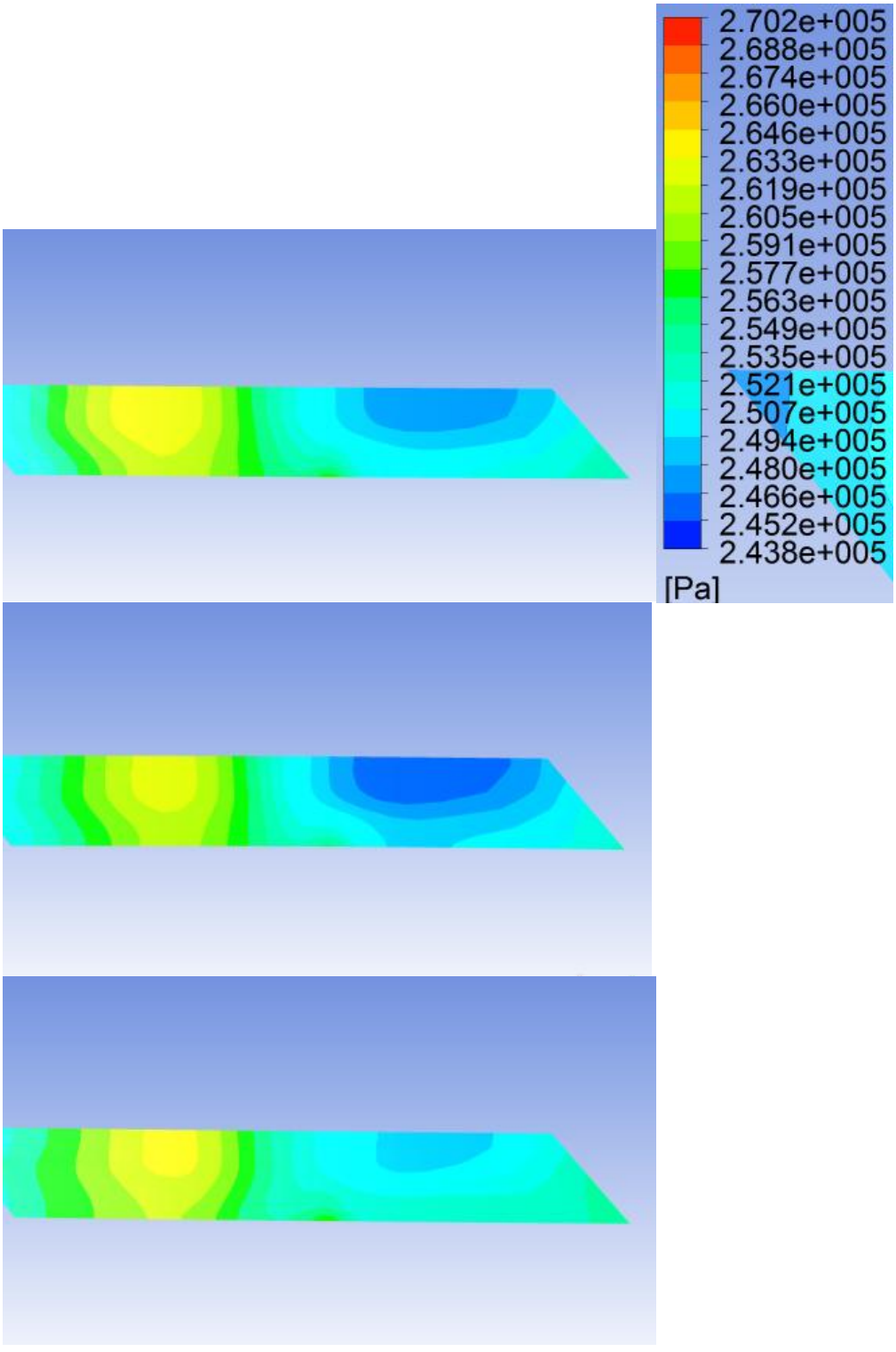

Fig. 6- 15 Static pressure contour at 3% from the impeller exit (a=1.0, a=1.3, a=1.5)

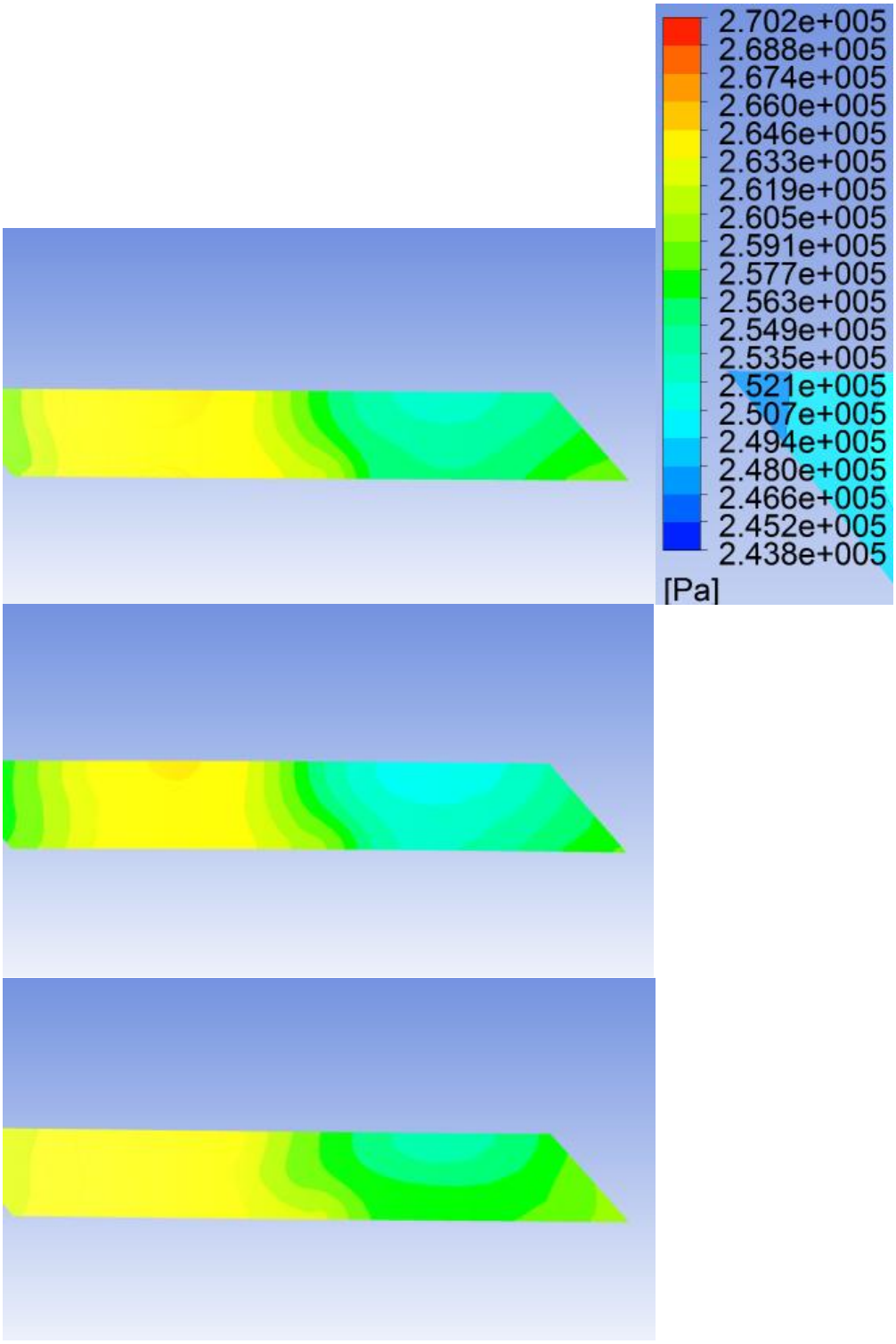

Fig. 6- 16 Static pressure contour at 6% from the impeller exit (a=1.0, a=1.3, a=1.5)

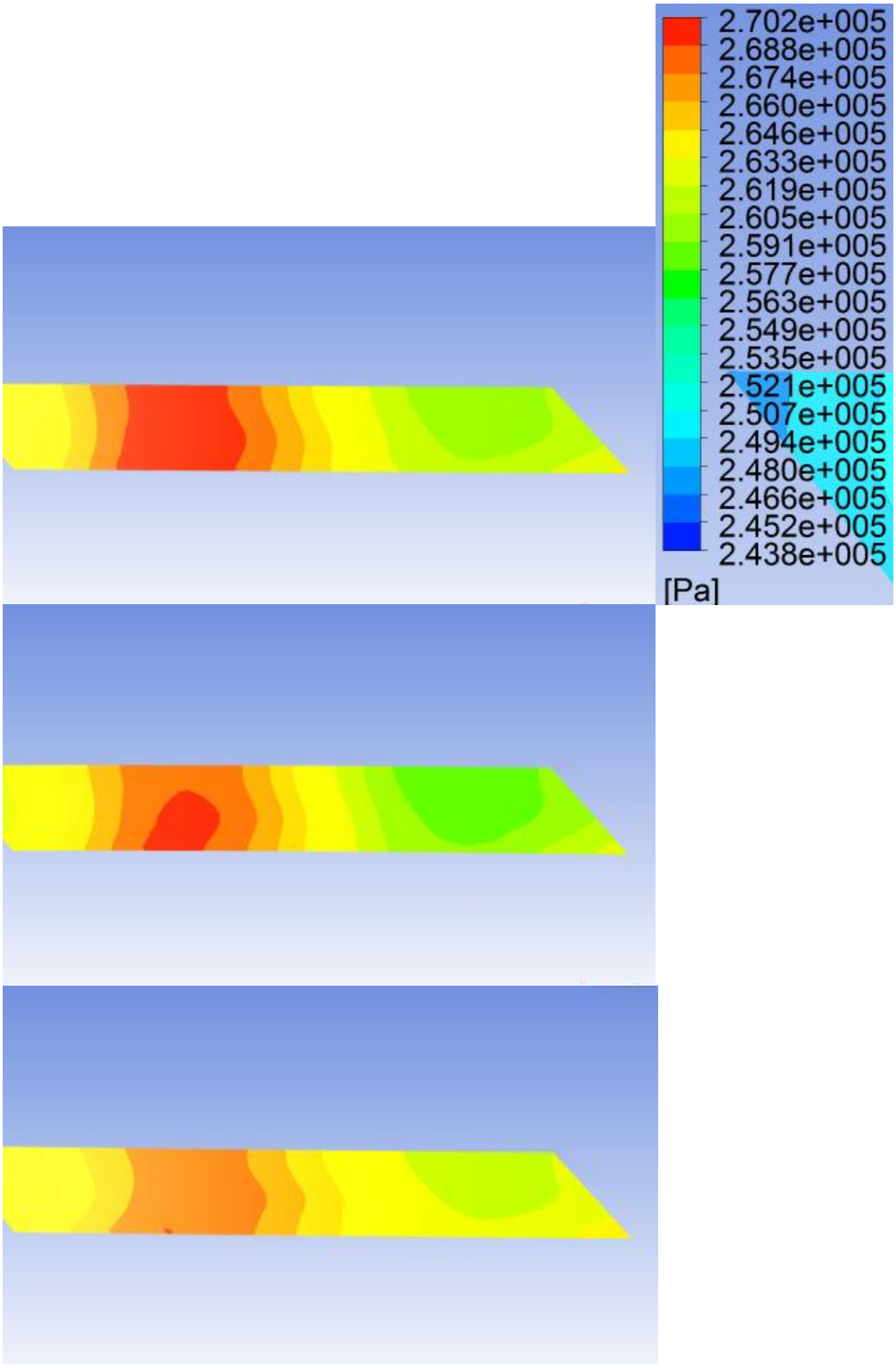

Fig. 6- 17 Static pressure contour at 9% from the impeller exit (a=1.0, a=1.3, a=1.5)

Fig. 6-18 presents mass averaged flow angle, Mach number, and static pressure distribution along the radius after impeller exit. First, in the flow angle chart, the absolute flow angle is about 10 degree right after impeller exit in the case of a=1.5; and as flow goes downstream, differences in flow angle between the cases goes down. Second, in the chart for Mach number, the cases of 1.0 and 1.3 are almost the same and have a maximum Mach number of 0.9 at the impeller exit. The case of a=1.5 shows that Mach number is a little smaller than other cases. Finally, the pressure distribution shows that static pressure can be observed the case of a=1.5 has maximum value throughout the impeller exit region.

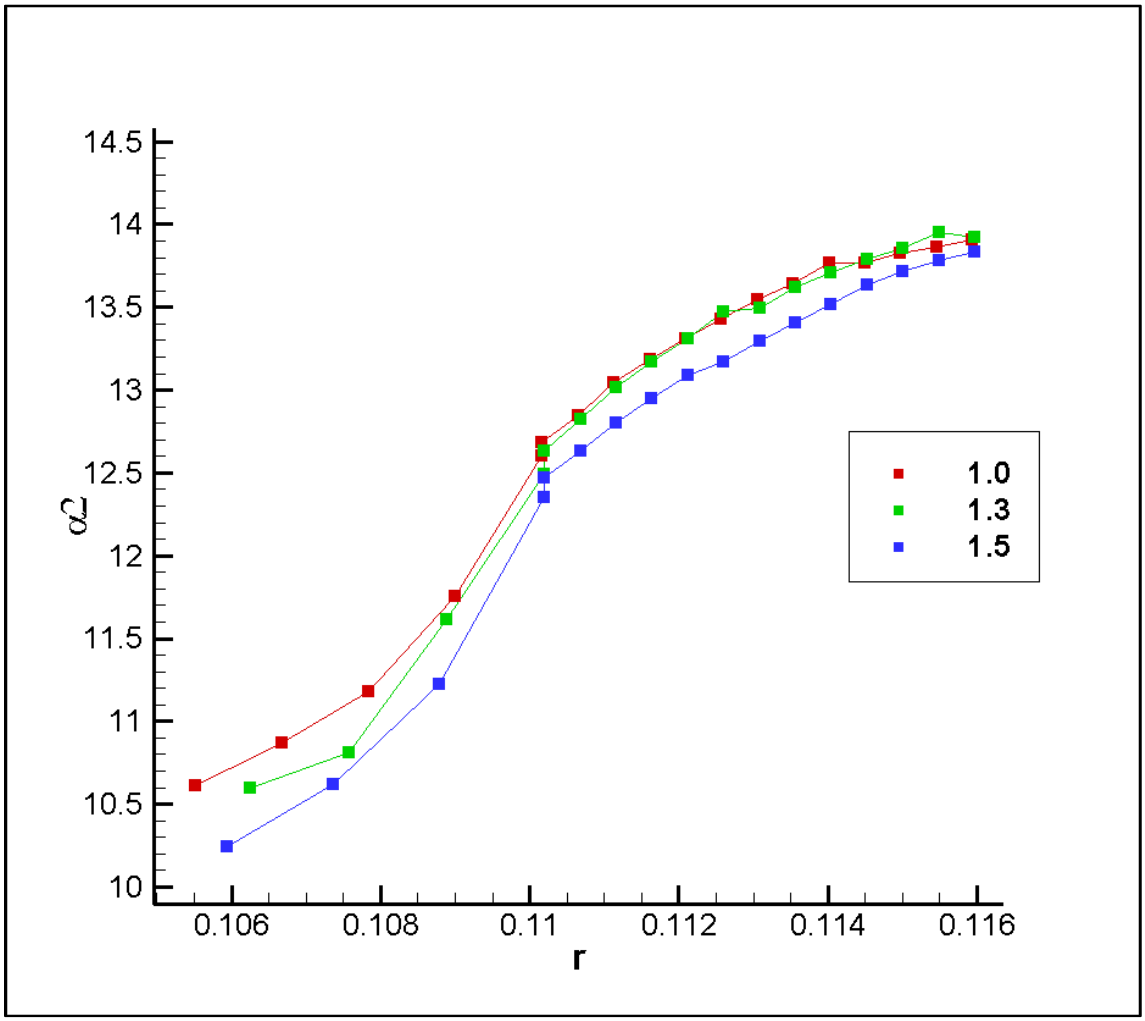

Fig. 6- 18 Mass flow averaged absolute flow angle, Mach number and static pressure after impeller exit

Fig.6-18 (cont'd)

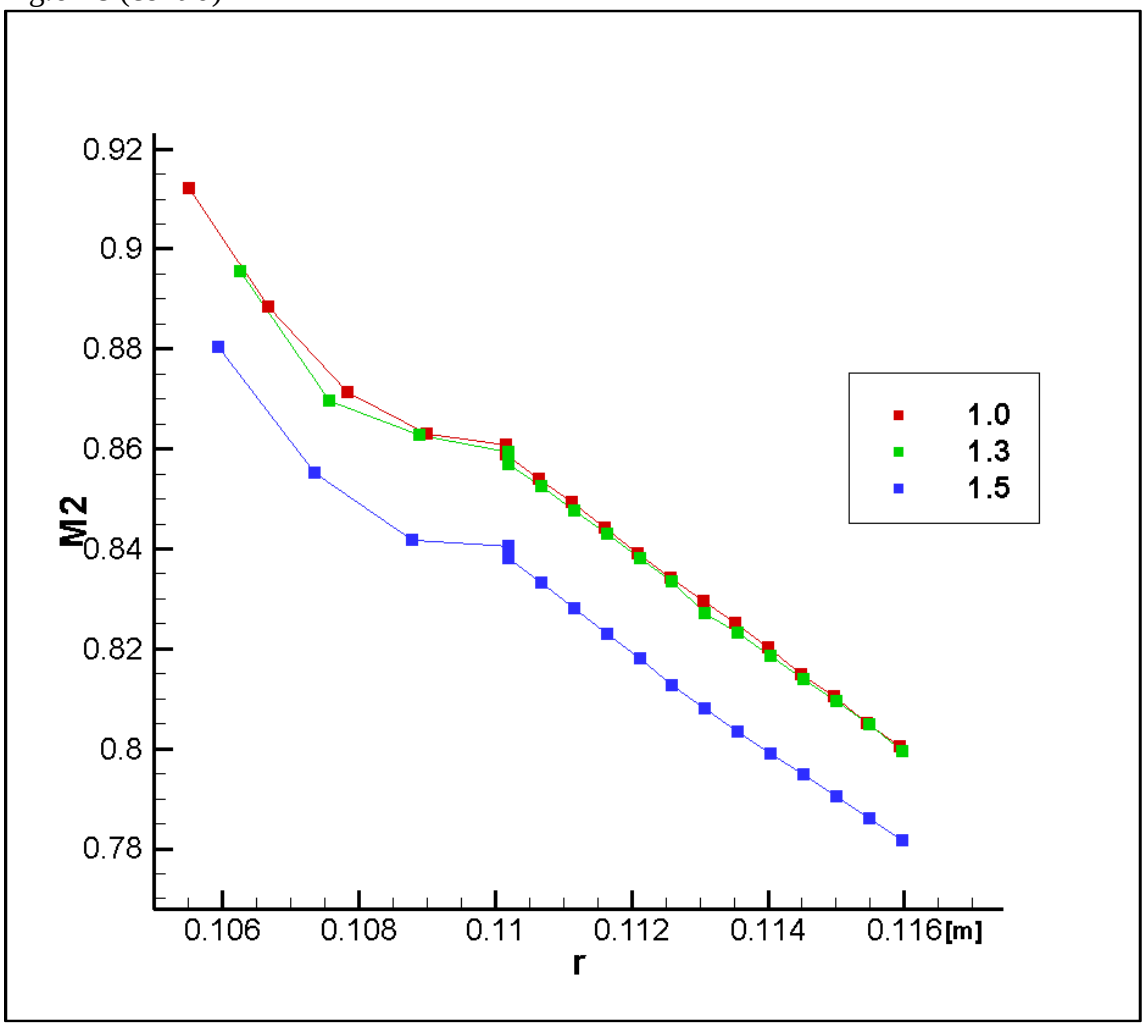

Fig.6-18 (cont'd)

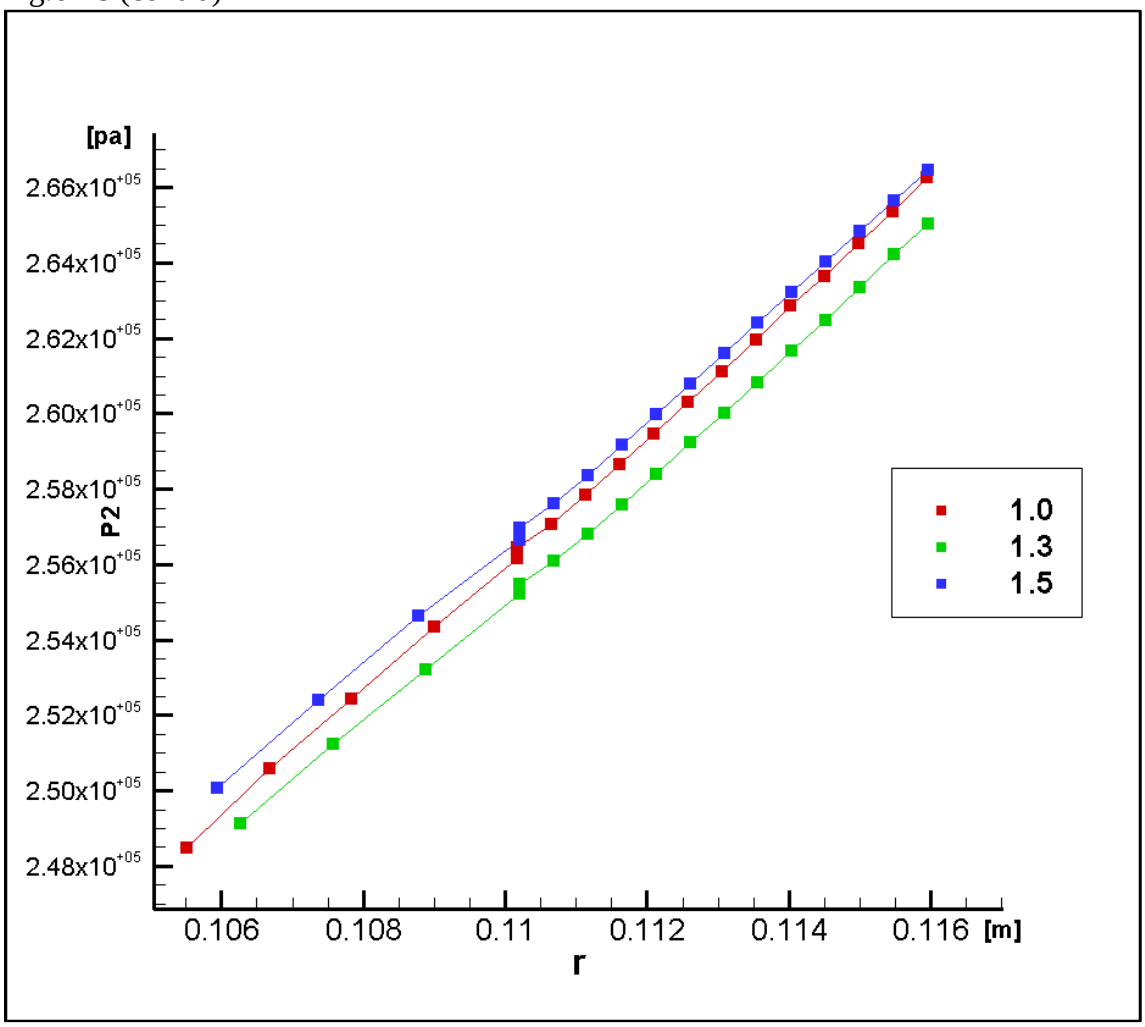

Fig6-19 presents the mass averaged flow angle distribution at the impeller exit (0%) along the hub to shroud. The chart shows that the flow angle of the case of a=1.5 is more uniform in the span-wise direction as increase axial length.

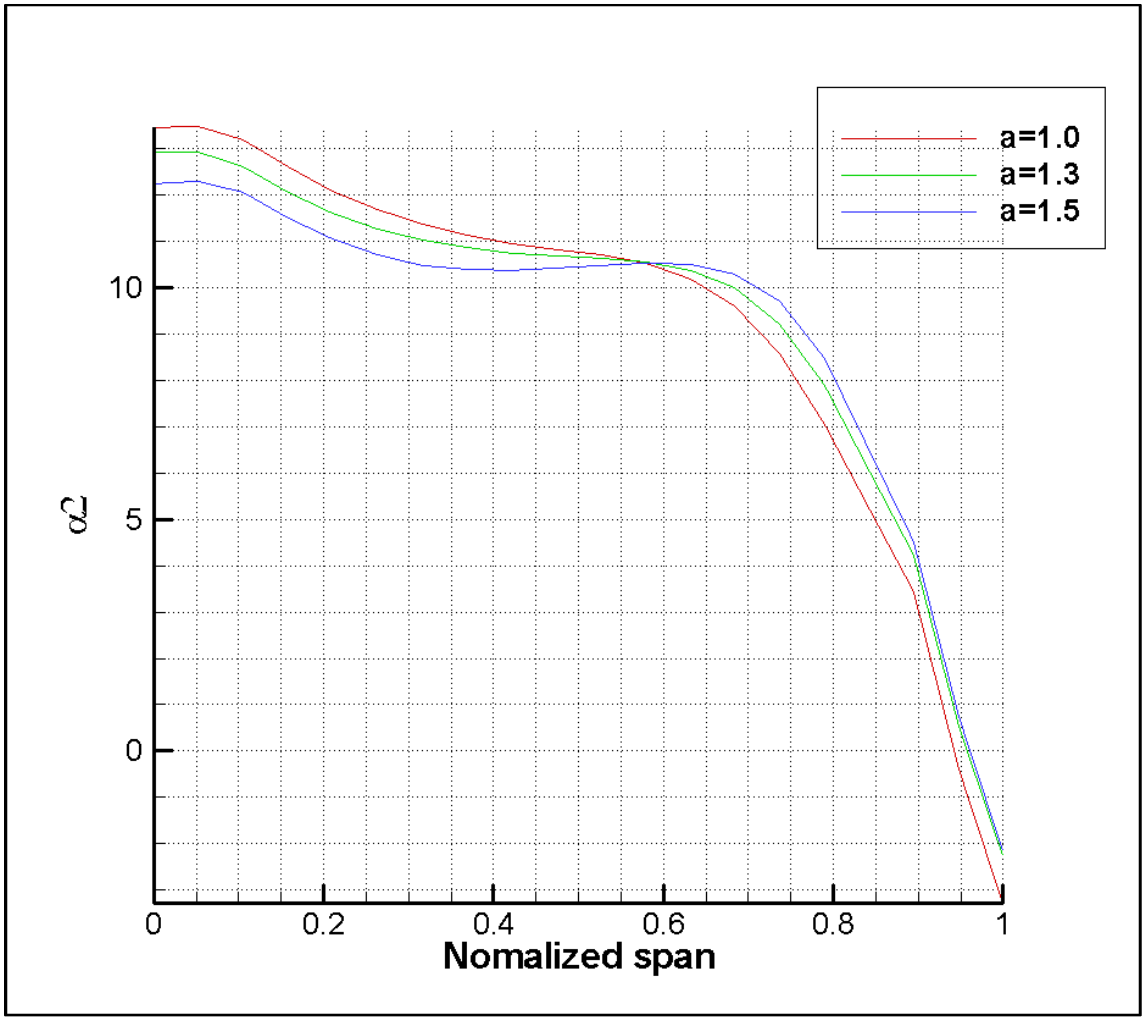

Fig. 6- 19 Hub to shroud mass averaged absolute flow angle distribution at the impeller exit

7. CONCLUSION

This study has presented flow characteristics, Mach number, flow angle and pressure, at the impeller exit varying axial length based on length difference between impeller exit and impeller inlet shroud radius. This study is focused on the effect of impeller axial length when the flow is unstable at the impeller exit. For such a condition, the cases, which have high Mach number and high swirl at the impeller exit, are designed. The effect of axial length on flow conditions at impeller exit is difficult to predict. Also, it is important to check flow uniformity at the impeller exit in order to make proper experiment conditions.

Although the flow characteristic within the impeller, especially the relative Mach number contour, shows that the flow is unstable near the shroud, proper flow angle and Mach number at the exit, the goal of the study, are obtained.

As a result of the cases varying axial length, the case of a=1.5 is the most stable at the impeller exit because absolute flow angle and Mach number are uniform, although absolute flow angle is more tangential.

7.1. 1D PERFORMANCE ANALYSIS ON TESTED IMPELLER

This study made 1D analysis code based on Ron Aungier's model, which is empirical based, and a Two-Zone model with TEIS model, which is physics based, and applied it to the tested impeller. Two different 1D analysis methods are tested and compared with test data. While Ron Aungier's method shows better performance prediction in whole passage, Two-Zone model shows an accurate prediction in the narrow flow range, especially around design points.

This study shows the relative pressure loss models in Ron Aungier's model. They predict that relative total pressure drop affects head rise through the impeller. It captures head coefficient

around the choking and surge region better than the Two-Zone model. Most of the total pressure losses are affected by diffusion loss, which is a function of the relative velocity ratio across the impeller inlet and impeller throat.

7.2. TWO ZONE MODEL WITH CORRECTED DIFFUSION MODEL

This study shows that a Two-Zone model can capture the head coefficient well around the design point. However, because of its characteristics of predicting the diffusion ratio, this study shows a Two-Zone model can predict a very narrow flow range. As rotational speed increases, the differences in head coefficient around the choking point are increased. Japikse suggested the TEIS model, which is a diffusion model, in a Two-Zone model. The TEIS model predicts the diffusion ratio accurately. However, in every single flow rate, TEIS model uses invariant pressure recovery effectiveness during the whole flow range so that it needs to be changed as a function of the loss model. This study focused on pressure recovery effectiveness in the inlet portion of the impeller. This is because the differences in head coefficient are mainly affected by the inlet diffusion loss model in Ron Aungier's model.

This study applies inlet diffusion loss model to the diffusion model in the Two-Zone model. After applying the corrected diffusion model in the Two-Zone model, the 1D performance analysis result shows a better prediction in the choking and surge region.

7.3. RE-DESIGN IMPELLER

This study showed a re-design impeller procedure and performed a 1D impeller design using a 1D analysis code. The impeller design procedure usually starts with a 1D preliminary design. However, if the designer could reduce variables such as the machine Mach number,

impeller diameter and flow rate, the 1D analysis code can replace the 1D preliminary design code. Especially in re-design impeller work, 1D analysis code plays an important role in the design procedure because the designer could expect impeller performance. This study made four cases that have the same diffusion ratio, which is predicted by the 1D analysis code and conducted CFD analysis. CFD results are compared with the 1D analysis results.

7.4. CONSIDERATION OF AXIAL LENGTH FOR IMPELLER DESIGN

With the 1D design procedure, an axial length of the impeller is determined. Impeller axial length affects impeller curvature and blade length and theta angle. When the impeller exit flow is unstable (high Mach number and high swirl at the impeller exit), the effect of axial length is studied.

CFD analysis shows that the flow condition at the impeller exit is stable as the axial length increases, although the impeller exit flow is the most tangential flow.

7.5. CONTRIBUTION

This study made two different 1D analysis codes using Ron Aungier's method and Two-Zone modeling. Two 1D analysis codes conducted a 1D analysis on the tested impeller and showed its results, which are compared to each other. Relative loss models in Ron Aungier model showed how much the relative pressure loss changes according to the flow rate and the impeller rotational speeds.

A method that determines the diffusion ratio in the Two-Zone model is corrected based on the inlet loss model in Ron Aungier's model. By applying corrected inlet diffusion model, the accuracy of Two Zone model has been improved.

This study also showed an impeller re-design procedure. The 1D analysis code finds a trade-off point, keeping the diffusion ratio between impeller tip widths and impeller blade exit angles. CFD results and 1D analysis results of re-designed impeller are compared and showed similar tendency.

7.6. RECOMMENDATION

The corrected diffusion ratio used in the Two-Zone model in this study does not consider the element “b”, which determines the diffusion ratio across the impeller throat to the exit. The study assumed other losses do not vary with impeller rotational speed. And it is difficult to consider all the relative total pressure losses because they are calculated in the iteration except inlet diffusion loss and incidence loss. However, the corrected diffusion model could be more accurate if other loss models were properly applied to element “b”.

Impeller re-design using 1D analysis code shows that 1D analysis code is useful for finding a trade-off point between an impeller tip width and a blade exit angle. In the meridional curve and blade angle distribution design process, it is necessary to consider changing area distribution at mid-passage, which mainly affects velocity diffusion.

Assuming impeller slip factor is very important when starting an impeller design. Although there are many empirical correlations for slip factor, slip factor used in the 1D analysis is changed for the 1D analysis method. The 1D analysis method based on empirical correlations, such as Ron Aungier’s method used in this study calculates aerodynamic blockage. However, the Two Zone model, which is based on physics, does not calculate aerodynamic blockage. Because of blockage problem, meridional velocities at the impeller exit are different according to 1D

analysis method. Therefore, in order to use both of the 1D analysis methods, a slip factor model correlation, which is a function of blockage, is recommended between them.

This study does not include testing the re-designed impeller. Through the testing of the re-designed impeller, the difference in performance between 1D analysis and CFD results is understood and parasitic work that is not included in CFD analysis can be verified. For better performance prediction, impeller slip factor can be found through the test.

REFERENCES

REFERENCES

[1] D. Japikse, *Centrifugal compressor design and performance*. Wilder, Vt.: Concepts ETI, 1996.

[2] R. H. Aungier, *Centrifugal compressors : a strategy for aerodynamic design and analysis*. New York: ASME Press, 2000.

[3] J. Robert C. Dean and Y. Senoo, "Rotating Wakes in Vaneless Diffusers.," *Journal of Basic Engineering,* vol. 82, pp. 563-570, 1960.

[4] D. Eckardt, "Instantaneous Measurements in the Jet-Wake Discharge Flow of a Centrifugal Compressor Impeller," *Trans ASME Journal of Engineering for Power,* vol. 97, p. 337, 1975.

[5] M. W. Johnson and J. Moore, "The Development of Wake Flow in a Centrifugal Impeller," *Journal of Engineering for Power,* vol. 102, pp. 382-389, 1980.

[6] Z. M. Moussa, "Impeller Casing Clearance Gap Flow Prediction Program," Carrier Corporation1978.

[7] R. E. Nece and J. W. Daily, "Roughness Effects on Frictional Resistance of Enclosed Rotating Disks," *Journal of Basic Engineering,* vol. 82, pp. 553-560, 1960.

[8] J. W. Daily and R. E. Nece, "Chamber Dimension Effects on Induced Flow and Frictional Resistance of Enclosed Rotating Disks," *Journal of Basic Engineering,* vol. 82, pp. 217-230, 1960.

[9] A. Egli, "The Leakage of Steam Through Labyrinth Glands," *Transactions ASME,* vol. 57, pp. 115-122, 1935.

[10] S. Lieblein, "Loss and Stall Analysis of Compressor Cascade," *Trans ASME Journal of Basic Engineering,* pp. 387-400, 1959.

[11] J. P. Johnston and J. R. C. Dean, "Losses in Vaneless Diffusers of Centrifugal Compressors and Pumps: Analysis, Experiment, and Design," *Journal of Engineering for Power,* vol. 88, pp. 49-60, 1966.

[12] K. H. Lüdtke, *Process centrifugal compressors : basics, functions, operation, design, application*. Berlin ; New York: Springer, 2004.

[13] P. M. Came and C. J. Robinson, "Centrifugal compressor design," *Proceedings of the Institution of Mechanical Engineers, Part C: Journal of Mechanical Engineering Science,* vol. 213, pp. 139-155, February 1, 1998 1998.

[14] R. H. Aungier, "Mean Streamline Aerodynamic Performance Analysis of Centrifugal Compressors," *Journal of Turbomachinery*, vol. 117, pp. 360-366, 1995.

[15] J. M. Sorokes, J. A. Kopko, P. R. Geise, and A. L. Hinklein, "The Influence of Shroud Curvature and Other Related Factors on Impeller Performance Characteristics," *ASME Conference Proceedings*, vol. 2009, pp. 1397-1406, 2009.

[16] K. Bammert, M. Rautenberg, and P. Knapp, "The influence of the meridional impeller shape on the energy-transfer in centrifugal compressors," *ASME, IGTI*, p. 9, 1980.

[17] Al-Zubaidy and S. N. J., "Axial length influence on the performance of centrifugal impellers," *Journal of Propulsion and Power*, vol. 8, pp. 1245-1251, 1992.

[18] M. V. Casey, "A Computational Geometry for the Blades and Internal Flow Channels of Centrifugal Compressors," *Journal of Engineering for Power*, vol. 105, pp. 288-295, 1983.